Tests of Subsurface Storage of Freshwater at Hialeah, Dade County, Florida, and Numerical Simulation of the Salinity of Recovered Water

AVAILABILITY OF BOOKS AND MAPS OF THE U.S. GEOLOGICAL SURVEY

Instructions on ordering publications of the U.S. Geological Survey, along with prices of the last offerings, are given in the current-year issues of the monthly catalog "New Publications of the U.S. Geological Survey." Prices of available U.S. Geological Survey publications released prior to the current year are listed in the most recent annual "Price and Availability List." Publications that may be listed in various U.S. Geological Survey catalogs (**see back inside cover**) but not listed in the most recent annual "Price and Availability List" may be no longer available.

Reports released through the NTIS may be obtained by writing to the National Technical Information Service, U.S. Department of Commerce, Springfield, VA 22161; please include NTIS report number with inquiry.

Order U.S. Geological Survey publications **by mail** or **over the counter** from the offices given below.

BY MAIL

Books

Professional Papers, Bulletins, Water-Supply Papers, Techniques of Water-Resources Investigations, Circulars, publications of general interest (such as leaflets, pamphlets, booklets), single copies of Earthquakes & Volcanoes, Preliminary Determination of Epicenters, and some miscellaneous reports, including some of the foregoing series that have gone out of print at the Superintendent of Documents, are obtainable by mail from

U.S. Geological Survey, Map Distribution
Box 25286, MS 306, Federal Center
Denver, CO 80225

Subscriptions to periodicals (Earthquakes & Volcanoes and Preliminary Determination of Epicenters) can be obtained ONLY from the

Superintendent of Documents
Government Printing Office
Washington, DC 20402

(Check or money order must be payable to Superintendent of Documents.)

Maps

For maps, address mail orders to

U.S. Geological Survey, Map Distribution
Box 25286, Bldg. 810, Federal Center
Denver, CO 80225

Residents of Alaska may order maps from

U.S. Geological Survey, Earth Science Information Center
101 Twelfth Ave. - Box 12
Fairbanks, AK 99701

OVER THE COUNTER

Books and Maps

Books and maps of the U.S. Geological Survey are available over the counter at the following U.S. Geological Survey offices, all of which are authorized agents of the Superintendent of Documents:

- **ANCHORAGE, Alaska**—Rm. 101, 4230 University Dr.
- **LAKEOOD, Colorado**—Federal Center, Bldg. 810
- **MENLO PARK, California**—Bldg. 3, Rm. 3128, 345 Middlefield Rd.
- **RESTON, Virginia**—USGS National Center, Rm. 1C402, 12201 Sunrise Valley Dr.
- **SALT LAKE CITY, Utah**—Federal Bldg., Rm. 8105, 125 South State St.
- **SPOKANE, Washington**—U.S. Post Office Bldg., Rm. 135, West 904 Riverside Ave.
- **WASHINGTON, D.C.**—Main Interior Bldg., Rm. 2650, 18th and C Sts., NW.

Maps Only

Maps may be purchased over the counter at the following U.S. Geological Survey offices:

- **FAIRBANKS, Alaska**—New Federal Bldg., 101 Twelfth Ave.
- **ROLLA, Missouri**—1400 Independence Rd.
- **STENNIS SPACE CENTER, Mississippi**—Bldg. 3101

Tests of Subsurface Storage of Freshwater at Hialeah, Dade County, Florida, and Numerical Simulation of the Salinity of Recovered Water

By MICHAEL L. MERRITT

U.S. DEPARTMENT OF THE INTERIOR

BRUCE BABBITT, Secretary

U.S. GEOLOGICAL SURVEY

Gordon P. Eaton, Director

CONTENTS

PLATES

[Plates are in pocket]

FIGURES

TABLES

CONVERSION FACTORS, VERTICAL DATUM, AND ACRONYMS

Multiply	By	To obtain
inch (in.)	25.4	millimeter
foot (ft)	0.3048	meter
mile (mi)	1.609	kilometer
foot per day (ft/d)	0.3048	meter per day
foot per mile (ft/mi)	0.1894	meter per kilometer
foot per year (ft/yr)	0.3048	meter per year
square foot per day (ft^2/d)	0.09290	meter squared per day
cubic foot (ft^3)	0.02832	cubic meter
cubic foot per day (ft^3/d)	0.02832	cubic meter per day
gallon (gal)	3.785	liter
gallon per minute (gal/min)	0.06309	liter per second
pound per cubic foot (lb/ft^3)	16.02	kilogram per cubic meter
pound per square inch (lb/in^2)	6.895	kilopascal
inverse pound per square inch (lb/in^2)$^{-1}$	0.1450	(kilopascal)$^{-1}$

Temperature, given in degrees Fahrenheit (°F), can be converted to degrees Celsius (°C) by the following equation:

$$°C = 5/9 \, (°F − 32)$$

Temperature, given in degrees Celsius (°C), can be converted to degrees Fahrenheit (°F) by the following equation:

$$°F = 9/5 \, (°C) + 32$$

Milligrams per liter (mg/L) is a unit expressing the concentration of chemical constituents in solution as weight (milligrams) of solute per unit volume (liter) of water. For concentrations less than 7,000 mg/L, the numerical value is the same as for concentrations in parts per million.

Sea level: In this report, "sea level" refers to the National Geodetic Vertical Datum of 1929 —a geodetic datum derived from a general adjustment of the first-order level nets of both the United States and Canada, formerly called Sea Level Datum of 1929.

ACRONYMS USED IN REPORT

ASR	aquifer storage and recovery
FGS	Florida Geological Survey
ID	inside diameter
MDWSA	Miami-Dade Water and Sewer Authority
OD	outside diameter
PVC	polyvinyl chloride
SFWMD	South Florida Water Management District
SWIP	Subsurface Waste Injection Program
USGS	U.S. Geological Survey

Tests of Subsurface Storage of Freshwater at Hialeah, Dade County, Florida, and Numerical Simulation of the Salinity of Recovered Water

By Michael L. Merritt

Abstract

Injection and observation wells were drilled in late 1974 for the purpose of conducting tests of storage and recovery of potable water in the brackish Upper Floridan aquifer. Three tests, involving storage and recovery cycles of varying volumes and storage period lengths, were performed between July 1975 and January 1980. Recovery was by natural artesian flow, and recovery efficiencies were 32.9, 47.8, and 38.5 percent. Wellbore plugging occurred during the injection stages, but injectivity was restored by periodic 2- to 3-hour backflushes at the natural artesian flow rate.

An interval of shelly limestone between 1,015 and 1,050 feet below land surface contained the flow zone. Data from an analysis of 18 spinner flowmeter logs indicated that the principal part of the flow zone extended from 1,024 to 1,036 feet below land surface and that minor amounts of flow occurred to a depth of about 1,047 feet. A neutron porosity log indicated the bulk porosity of both the flow zone and confining layers to be 35 percent. Chloride and dissolved-solids concentrations of water in the flow zone were 1,200 and 2,700 milligrams per liter, respectively.

A three-dimensional, finite-difference flow and solute-transport code was used to simulate pressure data measured during an aquifer test and observed salinity increases in recovered water during storage and recovery cycles. The aquifer test conducted in February 1975 was simulated by using a hydraulic conductivity estimate of 800 feet per day and a rock compressibility estimate of 0.0000400 (pound per square inch)$^{-1}$. The equivalent transmissivity and storage coefficients were 9,600 cubic feet per day per square foot times foot of aquifer thickness and 7.8×10^{-5}, respectively. Simulation of observed salinity increases during the three recoveries required dispersivities of 65 feet, a molecular diffusivity of 0.0002 foot squared per day, and a regional pore velocity of 260 feet per year. Central differencing in space and time was used for the solute-transport computations as well as an experimental method of computing vertical dispersion that used a scaling factor of 0.013.

Additional simulations of the aquifer-test data and recovery salinities were obtained based on assumptions that (1) the flow zone was 21 feet thick, (2) flow-zone effective porosity was 20 percent, and (3) flow-zone hydraulic conductivity was bipolar anisotropic by a ratio of 10:1. The four sets of simulation values were used in model runs in which 10 years of annual injection, storage, and recovery cycles were simulated. Computed recovery efficiencies increased from 40 percent in the first year to 68 percent in later cycles. The high regional pore velocity required for model calibration substantially limited the recovery efficiency achieved in later cycles.

INTRODUCTION

The subtropical climate of southern Florida has attracted a large and rapidly expanding population in recent decades, a trend likely to continue. As a result

of the population increase, the need for potable water has increased dramatically. Large quantities of potable water are available from the surficial Biscayne aquifer of Dade, Broward, and Palm Beach Counties, and smaller quantities are available from surficial or shallow artesian aquifers on the west coast, on the upper east coast (Martin and St. Lucie Counties), and in the interior of the southern peninsula (fig. 1).

The population growth of southern Florida has raised concerns about the adequacy of current sources of water supply to meet future demands. Since the early 1970's, water-management agencies have sponsored investigations into ways of augmenting these sources, particularly during the seasonal dry period (November–May) that is characteristic of the subtropical climate of southern Florida. Potable water normally is available in considerable surplus during the annual wet season (June–October), when the

regional canal system is used to lower the water table throughout much of the area.

In 1974 the U.S. Geological Survey (USGS), in cooperation with the Central and Southern Florida Flood Control District, now the South Florida Water Management District (SFWMD), and the Miami-Dade Water and Sewer Authority (MDWSA) Department, began a pilot study to test the feasibility of injecting surplus potable water into the Floridan aquifer system for later retrieval when the supply of potable water became deficient. This water conservation strategy is particularly suited for the region because of its seasonal cycle of surplus and deficit of water supply. Because permeable zones in the Ocala Limestone and the upper part of the Avon Park Limestone of the Floridan aquifer system were known to contain brackish water, they were the injection zones selected for study.

EXPLANATION

$X — X'$ GEOLOGIC SECTION—Through location of natural gamma logs shown in figure 17

● SITE OF AQUIFER STORAGE AND
2   RECOVERY TESTS
  1 - Hialeah-Miami Springs Well Field
  2 - Lee County Water Plant
  3 - South Florida Water Management District Site
  4 - Jupiter site, Florida Department of Natural Resources

● LOCATION OF NATURAL GAMMA LOGS
G   SHOWN IN FIGURE 17 OR CITED IN TEXT
  A - Grossman Well, Chekika State Recreation Area
  B - Florida Power and Light observation well D, north Key Largo
  C - City of Hallandale reverse-osmosis supply well
  D - Florida Keys Aqueduct Authority reverse-osmosis supply well, Marathon Water Plant
  E - U.S. Geological Survey test well in John C. Pennekamp State Park
  F - Florida Keys Aqueduct Authority reverse-osmosis supply wells, Key Largo Water Plant
  G - U.S. Geological Survey test well on Alligator Alley

Location of area

0   50 MILES

0   50 KILOMETERS

Figure 1. Location of Upper Floridan aquifer wells in southern Florida cited in this report.

The proposed study originally envisaged successive deepenings of an aquifer storage and recovery (ASR) well and two observation wells after performing ASR cycles in higher zones of interest. However, the funding provided limited activity to the testing of the uppermost permeable zone and the drilling of one observation well. The Hialeah-Miami Springs Well Field in Dade County, which at that time was the primary source of potable water for domestic consumption in the Miami area, was the site selected for the tests (fig. 1, site 1).

The injection and observation wells were constructed in October, November, and December 1974. Three ASR tests were performed, beginning in July 1975. The recovery phase of the third and last test continued until January 1980. During well construction and the subsequent ASR tests, a variety of data were collected, including pressure data, water-quality data, and volumetric measurements of quantities of inflow and outflow as a function of time. The present study interprets this data set to gain insight into the hydrogeologic processes occurring at the test site during the ASR cycles and to better define the potential feasibility of this technology in southern Florida.

In 1980–81, data from the tests at Hialeah were used by the USGS in an areal assessment of the feasibility of ASR as a water-conservation alternative for southern Florida which was conducted in cooperation with the U.S. Army Corps of Engineers. The ASR process and operational experience acquired by that time were summarized in the report presenting the results of the assessment (Merritt and others, 1983), and their relation to water-management needs in specific areas was considered. Data describing conditions at the Hialeah site were used to design a generalized aquifer prototype to be used for digital modeling to determine relations between hydrogeologic and operational conditions and the recoverability of injected water (Merritt, 1985). The modeling consisted of sensitivity analyses in which a simulation of injection, storage, and recovery in the aquifer prototype was repeated as various parameters were altered to represent changes in hydrogeologic conditions or operational management.

As useful as the results of the sensitivity analyses were, the more challenging problem remained of actually simulating the injection, storage, and recovery of water at Hialeah. The additional difficulty of simulation modeling compared to using a model of a hypothetical prototype to test relations and concepts arises from the need for realistic identification of parameters describing the processes of flow and transport in the aquifer, usually given inadequate data that require experience and intuition to interpret. In the present study, such a simulation model was constructed and used for predictive analyses to indicate the quantity of potable water that could be made available by an operational ASR program.

Opportunities for the application of computer simulation have increased as a result of recent advances in computer technology that make possible the more efficient use of three-dimensional solute-transport models and that facilitate their application to data sets such as that from Hialeah. The techniques for computer simulation of the transport of fresh water and brackish water during injection and recovery operations presented in this report can be used by water managers to estimate the amount of injected water that can be recovered at sites where data to support simulation are available and, also, to test various design and management alternatives.

Purpose and Scope

The complete data set acquired at the Hialeah ASR site is presented in this report to describe hydrogeologic conditions in the Upper Floridan aquifer, to describe hydrogeologic processes occurring during the injection and recovery tests, and to support the approach used for the simulation analysis. Selected data from other locations on the East Coast are included to augment the description of Upper Floridan aquifer conditions and for a tentative delineation of an areally extensive flow zone used for ASR at some locations and for reverse-osmosis plant supply at other locations. The remainder of the report describes the use of solute-transport modeling techniques to further interpret data from the field study by simulating the transport of fresh water and brackish water during the injection and recovery cycles, and describes the use of the calibrated simulation for predictions of recovery efficiency under hypothetical operational conditions.

Acknowledgments

benefited greatly from the help of Frederick W. Meyer (USGS, retired), who directed the subsurface storage and recovery tests at Hialeah over a period of many years and provided substantial guidance that helped the author to interpret data from the tests. Many of Fred Meyer's suggestions were incorporated into the analyses that follow in the remainder of this report.

SUMMARY DESCRIPTION OF INJECTION AND RECOVERY TESTS

The following pages present a brief description of the activities at the field site of the injection and recovery tests. This is followed by a summary of test results and a description of data collected at the site. Evidence indicating plugging of the wellbore during injection is also discussed.

Well Construction and Preliminary Data Collection

The sequence of stages in the construction and testing of the injection and observation wells is shown in figure 2. Drilling was principally by mud rotary. Casing extended to a depth of 955 feet (ft) in the completed injection well and to 953 ft in the observation well. The injection-well borehole was drilled to a depth of 1,105 ft, and the observation-well borehole was drilled to a depth of 1,064 ft. The deepest part of the injection well (below 960 ft) was drilled by reverse air, using a closed circulation system with discharge to a storm sewer. A supply well that tapped the Biscayne aquifer (Preston No. 7) provided a water supply for the injection tests. Drilled in June 1972, this well was 106 ft deep and was cased with 42-inch (in.) pipe to 65 ft. A suction line extended from the supply well to the injection wellhead.
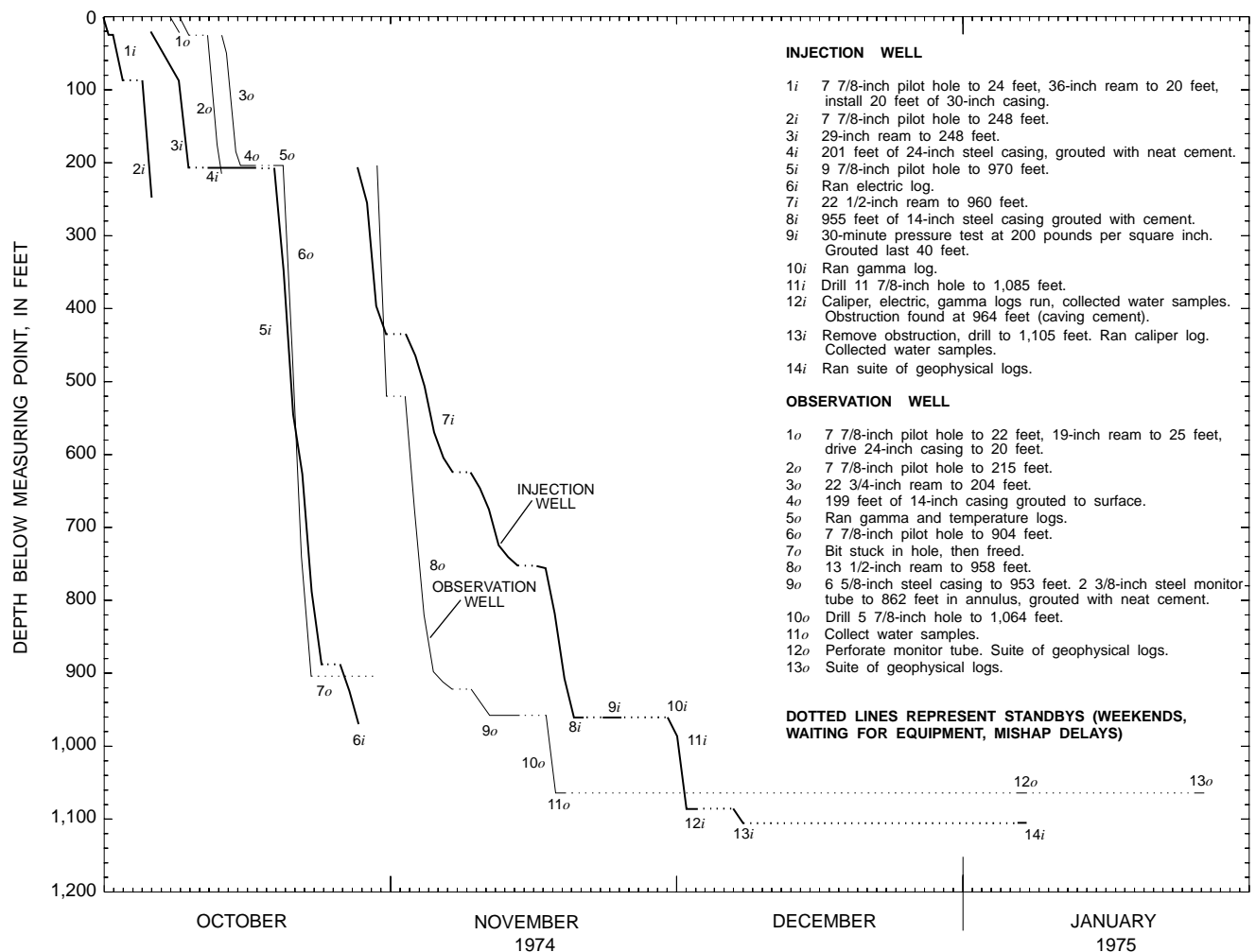
Figure 2. Details of the construction and testing of injection and observation wells at the Hialeah site.

During drilling, a 2-in. inside diameter (ID) steel tube was embedded in the cement annulus surrounding the 6 5/8-in. (OD) casing of the observation well to a depth of 862 ft. All casings in the injection and observation wells had a wall thickness of 3/8 in. except the 5 7/8-in. (ID) inner casing of the observation well, which had a wall thickness of 1/2 in. The 14-in. inner casing of the injection well was pressure tested at 200 pounds per square inch (lb/in^2) for 30 minutes (F.W. Meyer, USGS, written commun., 1974). USGS and Florida Geological Survey (FGS) identifiers for the wells, land-surface datums, and USGS datum measuring points at the injection and observation wells (selected as the tops of the concrete floors) are

Type of well	USGS local well number	FGS number	USGS site identifier	Datum, in feet above sea level	
				Land surface	Measuring point
Injection	G-3061	W-12997	254941080171701	8.39	9.44
Observation	G-3062	W-12998	254944080171801	5.43	5.93
Supply	S-3000	—	254943080172001	—	—

The injection and observation wells were located in Township 53 South, Range 41 East, Section 18, NW$^{1/4}$, SW$^{1/4}$ (near the junction of Okeechobee Road and West Third Avenue in Hialeah). The site was in the Hialeah-Preston Well Field near the north bank of the Miami Canal, on property adjacent to the Hialeah Water Treatment Plant. The observation well is about 289 ft north-northwest of the injection well. The wells and surrounding features present when construction was completed in 1974 are shown in figure 3. On June 4, 1980, the observation well was plugged with neat cement. The observation-well site now is covered by an MDWSA warehouse.

A comprehensive suite of data was obtained during and immediately after well construction. Geophysical logs made during this period are included in table 1, which is a complete and annotated summary of geophysical logging performed during the project. A driller's log of lithology recorded by the USGS at both the injection and observation wells is included as Appendix A. An analysis of cuttings from the two wells was made by the FGS, and descriptions of the lithology are included as Appendix B. The first two water samples collected for chemical and biological
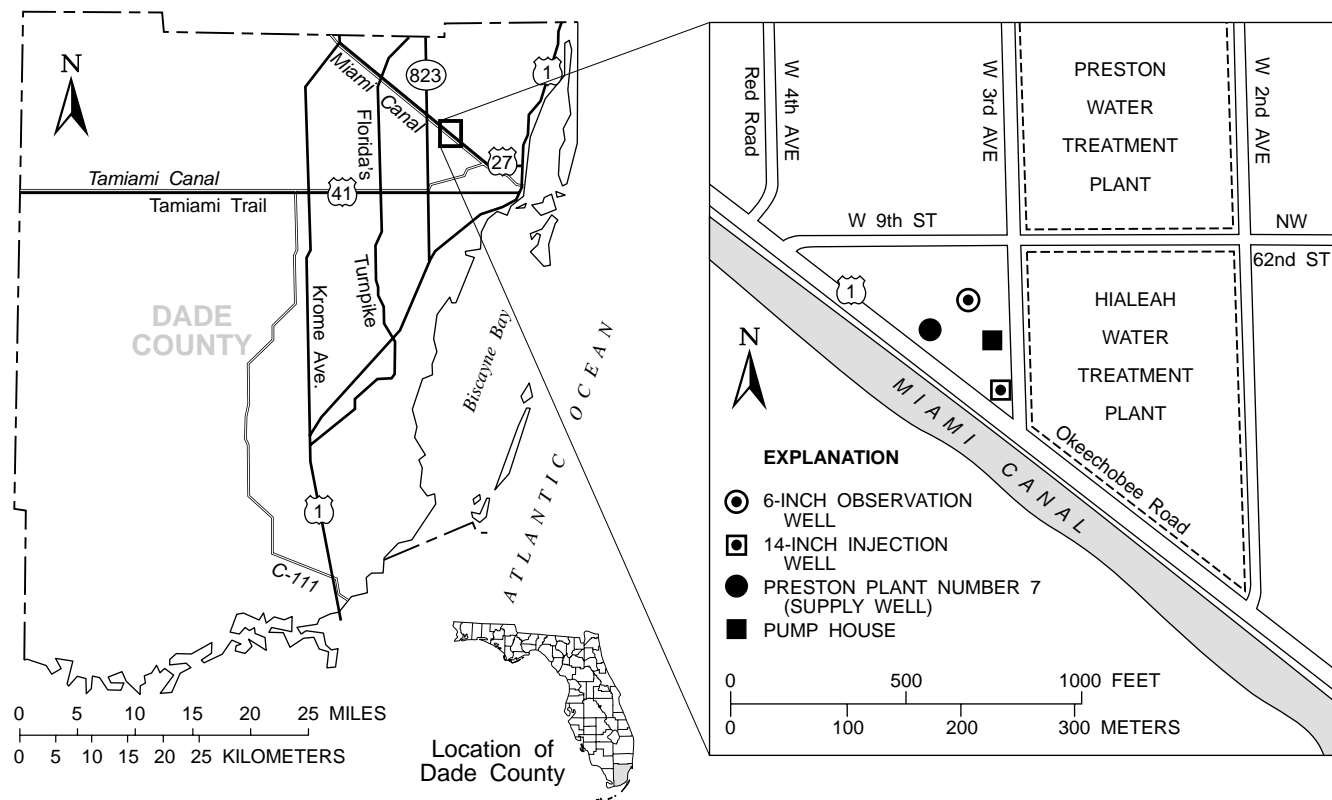
Figure 3. Location of wells and surrounding features at the Hialeah site at the time of well construction in 1974.

Table 1. Geophysical logging data obtained during construction and testing of the injection and observation wells and during subsequent storage and recovery tests at Hialeah, 1974–79

[All logs run by the U.S. Geological Survey, except where noted. OW, observation well; IW, injection well]

Date acquired	Type of log or data	Depth (feet)	Well	Remarks
		Construction		
10/21/74	Natural gamma	0–150	OW	Three days after cementing 14-inch casing.
	Temperature	0–125	OW	Same as above.
10/30/74	Electric	0–970	IW	Single-point resistivity and spontaneous potential. In a 9 7/8-in. pilot hole filled with aquagel. Shows correlation with layering of limestone and clay. Done in 14-in. casing with plug.
12/02/74	Natural gamma	0–970	IW	Poor log.
12/04/74	Electric	900–1,085	IW	Single-point resistivity and spontaneous potential. Three runs.
	Natural gamma	0–1,085	IW	Three runs. Poor reproducibility.
	Caliper	865–1,080	IW	Showed obstruction at 964 ft.
12/09/74	Caliper	869–1,105	IW	Open hole to total depth.
		Postconstruction Testing		
01/07/75	Cement bond and natural gamma	0–960	OW	Schlumberger log.
01/08/75	Oriented perforation	840–844	OW	A 2-inch monitor tube perforated at 840 feet. Schlumberger log.
	Caliper	0–1,061	OW	Open hole to total depth.
	Borehole compensated sonic	955–1,088	IW	Schlumberger log.
	Cement bond	0–964	IW	Poor bond, except in isolated intervals and bottom of well. Schlumberger log.
	Compensated neutron-formation density and natural gamma	0–1,096	IW	Used for porosity estimates. Schlumberger log.
	Induction-electrical log	950–1,088	IW	Correlated with hard layers, 975–985 ft. and 1,030–1,040 ft. Schlumberger log.
01/27/75	Caliper	918–1,053	OW	
	Temperature	7–1,057	OW	Well flowing about 288 gal/min (1.36 gal/min in 6-inch casing). Temperature decreases with depth.
	Natural gamma	3–1,056	OW	
	Temperature	940–1,085	OW	Inverse of previous temperature log. Well flowing. Three flowmeter stations—tool would not go below 984 ft.
	Neutron porosity	3–1,056	OW	
	Gamma-gamma density	4–1,056	OW	
	Standard electric	943–1,053	OW	Spontaneous potential, long and short normal formation resistivity.
	Fluid resistivity	800–1,056	OW	

Table 1. Geophysical logging data obtained during construction and testing of the injection and observation wells and during subsequent storage and recovery tests at Hialeah, 1974-79--Continued

Date acquired	Type of log or data	Depth (feet)	Well	Remarks
During First Recovery				
10/10/75	Caliper	930 - 1,093	IW	
	Temperature	0 - 1,104	IW	Shows warmer water below 1,047 feet. Temperature increases with depth.
	Natural gamma	0 - 1,100	IW	High counts 950 to 1,040 feet.
	Fluid resistivity	0 - 1,102	IW	Shows fresher water below 1,047 feet.
	Neutron porosity	0 - 1,099	IW	
	Gamma-gamma density	0 - 1,100	IW	
	Standard electric	953 - 1,103	IW	Spontaneous potential, long and short normal formation resistivity. Two runs.
	Spinner flowmeter	612 - 1,097	IW	Three runs.
Last Day of First Recovery				
10/20/75	Standard electric	0 - 1,105	IW	Spontaneous potential, long and short normal formation resistivity. Warmer water below 1,047 feet.
	Fluid resistivity	0 - 1,103	IW	No good.
	Spinner flowmeter	0 - 1,105	IW	Up and down runs. Flowing at 835 gallons per minute.
During Second Recovery				
05/25/76	Standard electric	946 - 1,098	IW	Spontaneous potential, long and short normal formation resistivity.
	Caliper, spinner flowmeter	930 - 1,100	IW	Up and down runs of flowmeter.
	Fluid resistivity	920 - 1,102	IW	Shows water freshening below 1,020 feet.
During Third Injection				
08/27/76	Spinner flowmeter	920 - 1,100	IW	Up and down runs before, during, and after backflush.
During Third Recovery				
04/20/78	Acoustic televiewer	950 - 1,096	IW	Only parts in U.S. Geological Survey files.
	Temperature	60 - 1,100	IW	Shows warmer water below 1,040 feet.
	Fluid resistivity	900 - 1,100	IW	Shows fresher water below 1,040 feet.
	Spinner flowmeter	800 - 1,087	IW	Up and down runs.
07/17/79	Acoustic televiewer	950 - 1,096	IW	Only some duplicates in U.S. Geological Survey files.
	Spinner flowmeter	930 - 1,092	IW	Two runs up, one run down.
	Fluid resistivity	40 - 1,098	IW	Water below 1,040 feet is slightly saltier.
	Temperature	20 - 1,100	IW	Decreases with depth to 1,040 feet. Warmer water below 1,040 feet. Cooler water below 1,060 feet.
	Caliper	800 - 1,098	IW	

analysis (from injection and observation wells) are measurements of the preinjection quality of native water in the injection zone immediately after well construction. A complete list of the results of chemical and biological analyses of water samples collected from the injection and observation wells during the testing program is presented in Appendix D. The chemical and biological analyses normally consisted of major inorganic ions, bacteria, chemical oxygen demand, biochemical oxygen demand, nutrients, total organic carbon, metals, field pH, alkalinity, and specific conductance.

Additional data were collected during the period between well completion and the beginning of freshwater injection in July 1975. The 2-in. monitor tube in the observation well was perforated at 840 ft on January 8, 1975, by Schlumberger, Inc., as they ran a suite of logs on the injection and observation wells, and water samples began to be collected from this depth. On January 27, 1975, the USGS obtained static and flowing geophysical logs at the observation well (table 1). On February 6, 1975, prior to the aquifer test of February 10, 1975, flow and shut-in artesian heads were measured in the observation well and the 2-in. monitor tube, and shut-in pressure was also measured in the injection well. The heads measured in the injection and observation wells should be regarded as the same within measurement error. Flow from the observation well was measured at a 5-in. discharge orifice at an elevation of about 8 ft above sea level. Flow from the monitor tube was measured at an elevation of 6.23 ft above sea level. A flow estimate from the injection well had previously been obtained on December 10, 1974, as the well was being completed to total depth. The elevation of the point of discharge is unknown. During drilling of the injection well, the first flow 10–20 gallons per minute (gal/min) was reported when the well reached 985 ft in depth. The measured head and flow values are given below:

Type of well or tube	Shut-in head (feet above sea level)	Flow (gallons per minute)
Injection well	42.24	600
Observation well	42.13	280
Two-inch monitor tube	20.33	.5

Test Parameters and Observed Recovery Efficiencies

Three test cycles of injection, storage, and recovery were conducted between July 1975 and January 1980. Specific details of the test schedules are indicated in the annotation column of Appendix C, which also lists periodic measurements of the volume of injection and recovery. Injection was by forced pumping, and recovery was by natural artesian flow. The cycles differed considerably in the total volume injected and length of storage period. The recovery phase of the third cycle continued for 2.5 years, until recovered water approached the quality of background aquifer water. Results of the three cycles have been previously cited by Merritt and others (1983) and Meyer (1989b) and are summarized below:

Test parameters	Cycle 1 (July 17–Oct. 20, 1975)	Cycle 2 (Jan. 5 –July 20, 1976)	Cycle 3 (July 23, 1976– Jan. 30, 1980)
Quantity injected (gallons $\times 10^6$)	41.9	85.0	208.0
Storage period (days)	2	54	181
Quantity of potable water recovered (gallons $\times 10^6$)	13.8	40.7	80.1
Recovery efficiency	32.9	47.8	38.5

Recovery efficiency, in the above table, refers to the customary measure of the productivity of an ASR cycle. Recovery efficiency is defined as the volume of potable water recovered, expressed as a percent of the volume of water injected. The first attempt to do the second injection was terminated prematurely by a pump failure after 8.8×10^6 gal had been injected. This volume is included in the quantity injected for cycle 2 in the above table. Injection resumed 19 days after the pump failure.

Types and Methods of Data Acquisition During the Tests

An intensive and comprehensive data-collection program was designed for the program of injection and recovery testing. Types of data acquired were pressure, volumetric, water-quality, and geophysical data. The methods of data collection are described in the following sections. Most of the data are shown in illustrations or are listed in appendixes at the end of this report.

Pressure Data

Pressure gages with readouts in feet of head were placed on the injection wellhead and at the sampling ports of two monitoring tubes used for water-sample collection in the observation well. The tubes, part of a system described later in more detail, were the red monitor extending to a depth of 957 ft, which is near the top of the open borehole and about 65 ft above the flow zone, and the white monitor, the 2-in. pipe cemented in the annulus and perforated at a depth of 840 ft. The perforations were separated from the flow zone by about 180 ft of clayey marl and dense limestone. The head data, converted to pressures and referenced to sea level, are plotted on plate 1.

Pressure data from the injection well and red monitor (pl. 1) clearly show the effects of injection, storage, and recovery and the effect of backflushing operations. The pressure increase during the aborted second injection in December 1975 is readily apparent. The decrease of pressure during backflushes was usually not measured or only partly measured, and dashed lines are used on plate 1 to suggest the extent of the decrease when not recorded. During the third injection cycle, pressures generally were not recorded between backflushes, and upward trends due to wellbore clogging are not shown as they are for the first and second injection cycles. Pressure data from the 840-ft white monitor show no clear trends during the three ASR cycles, illustrating the degree of confinement provided by the marl and limestone beds separating the monitored zone from the receiving zone.

Volumetric Data

Injection-well inflow and outflow were directed through a single flowmeter by a pipe-and-valve arrangement. Meter readings were recorded frequently during injection and recovery. The cumulative volume of injected and recovered water during the three ASR cycles is shown on plate 1. Incremental volumes of recovered water were given a negative arithmetic value in compiling the volumetric curve, so that total volume in the figure decreases during recovery. Because the volume recovered during the third ASR cycle was quite large, the illustrated cumulative volume decreases below zero after November 1978.

A computed first difference of volumes recorded during injection and recovery was used to approximate the current rate (pl. 1). Like the pressure data, volumetric data were not collected often enough during the third injection phase to show the rate decrease between backflushes caused by wellbore clogging as they did in the first two injection phases. A tabulation of the volumetric data, calculated rates, and corresponding chloride concentration in recovered water is included in Appendix C.

Water-Quality Data

A considerable number of water samples were collected for field and laboratory analysis during the three ASR cycles. Most of the analytic results are stored in the computer files in the USGS office in Miami, Fla.

Before the first injection, a multiport sampling apparatus was installed in the injection horizon of the observation well. The apparatus consisted of a system of monitor tubes extending to various depths within the 6-in. open-hole part of the well. The tubes were attached to a 1/2-in. polyvinyl chloride (PVC) center pipe with a rosette attachment at each coupling of the center pipe (every 21 ft). Around the perimeter of the rosettes were five holes through which lengths of the 5/8-in. flexible plastic monitor tubing (polypipe) were inserted. The five polypipe tubes were color coded at the wellhead and extended to 957 ft (red monitor), 978 ft (green monitor), 999 ft (gold monitor), 1,020 ft (silver monitor), and 1,041 ft (black monitor). Depths are referenced to a flange about 4 ft above land surface, and about 3.5 ft above the measuring point used for referencing the geophysical logs; hence, the tube depths are shown slightly higher in subsequent illustrations. The center pipe extending to 1,062 ft was included in the automatic sampling system (blue monitor).

In the first few days of the first injection, daily samples were obtained manually from the monitor tubes and analyzed for specific conductance and chloride. After 5 days, an automatic sampler/recorder system was made operational. The sampler was pumped continuously at a rate of 5 gal/min. Every 30 minutes, the temperature, specific conductance, dissolved oxygen, and pH of the water were measured and recorded, and the sampler rotated to a different source tube. In this manner, each depth was sampled once every 3 hours. Of the automatically recorded data, only the silver monitor data (1,020 ft) were entered into the computer files. The 2-in. pipe extending to 840 ft (white monitor) was sampled separately.

Periodically, the automatic system was turned off, and samples were pumped from each of the six monitored depths and from the 2-in. pipe for field and laboratory measurements of temperature, specific conductance, and chloride. These data are shown on plate

1 for the three cycles. Automatic sampler-recorder data for the period of the first injection breakthrough (arrival of injected water at the observation well) are shown later in the report. The sampler/recorder was not used after the first cycle.

During the first injection, water from the supply well was sampled frequently for measurements of temperature, specific conductance, and chloride. Supply-well chloride data for all three cycles are shown on plate 1, and temperature data are shown later in the report. Five days into the first injection, a supply-well sample was obtained for chemical and biological analyses (App. D). Eighteen days into the first injection, a water sample was collected from the silver monitor for chemical and biological analyses.

The first injection was terminated at 1200 hours on September 8, 1975, in order to prepare for a short recovery test. About 1 hour later, the automatic sampler/recorder detected a significant freshening in the sample from the observation-well silver monitor (at 1,020 ft). After a few hours, as the other monitor tubes were sampled by the automatic sampling system, freshening was detected at all other monitoring depths except for the white monitor (at 840 ft) located in the overlying confining unit. Specific conductance data from the six injection-zone monitors during the period when freshening occurred are shown later in the report.

The first recovery began 2 days after the end of injection. Automatic sampler data continued to be recorded for the first 8 days of recovery. White-monitor data continued to be collected manually. After 8 days, weekly manual sampling of the six injection-zone monitor tubes was initiated for temperature, specific conductance, and chloride.

Water recovered from the injection well was also sampled and analyzed. During the initial 8 days of the first recovery, hourly measurements were made in the recovered water for temperature, specific conductance, dissolved oxygen, and pH. After 8 days, the measurement frequency was reduced to once per day. Temperature, specific conductance, and chloride were measured, and a flowmeter reading was recorded. Water samples collected 6, 13, 20, and 35 days into recovery received chemical and biological analysis (App. D).

During the second and third injections, sampling of the supply-well water for measurement of temperature, specific conductance, and chloride continued as before, but on a weekly schedule. One sample was collected for chemical and biological analyses during each injection (App. D).

During the second and third ASR cycles, samples were obtained from the seven monitor tubes in the observation well and analyzed for specific conductance, chloride, and sometimes temperature. The sampling was conducted weekly until the end of the third injection, bimonthly during the third storage, weekly for the first 6 months of the third recovery, monthly for another 10 months, and quarterly until January 1980. Water samples were collected from the seven monitoring tubes for chemical and biological analysis near the end of the second recovery (after 77 days of recovery); near the end of the third injection (after 181 days of injection), when water recovered from the monitor tubes consisted primarily of injected water; and near the end of the third recovery (after 729 days of recovery), when water in the monitoring zones virtually had returned to background quality (pl. 1).

During the second and third recovery cycles, measurements of the specific conductance and chloride concentration of the water recovered at the injection well were made frequently and tabulated with corresponding flowmeter readings. At the beginning of the second recovery, the measurement frequency was from one to five times each week, but was reduced to weekly near the end of the recovery. The measurement frequency was weekly during the first 6 months of the third recovery phase, but then was reduced to monthly and then quarterly, as at the observation well. Samples for chemical and biological analysis were obtained just prior to the second recovery, after 22 days of recovery, and near the end of the second recovery (after 77 days). Additional samples for chemical and biological analysis were collected just prior to the third recovery and near the end of the third recovery (after 729 days). Results of all chemical and biological analyses are listed in Appendix D.

Other water samples collected during the study were analyzed by university and private laboratories and by research laboratories of the USGS. Water samples were periodically sent to a private laboratory, Applied Research Laboratories of Florida, Inc., in Hialeah, for analysis of nitrate-reducing, sulfate-reducing, and iron-reducing bacteria. Results currently

available in USGS files are listed in Appendix D. Water samples were sent to the USGS research laboratory in Reston, Va., for dissolved-gas analyses. Results (D.H. Fisher, USGS, written commun., 1975, 1977) are also summarized in Appendix D. Three water samples (August 4, 1975, injection-supply water; September 23 and 30, 1975, backflowing water) were sent to Florida State University for uranium-isotope analysis (Meyer, 1989a).

Geophysical Data

Geophysical logging was performed by the USGS in the injection well on six occasions during the three ASR cycles. Five of these occasions were during recovery. The remaining logging was done before, during, and after a backflushing operation during the third injection. These six logging operations are depicted graphically on plate 1, and the logs obtained are listed in table 1.

The geophysical logging emphasis during the ASR cycles was on spinner flowmeter, temperature, and fluid-resistivity logs, which reveal the relative hydraulic characteristics of various strata within the injection interval (955–1,105 ft). However, caliper logs were obtained on three occasions and electric logs on two occasions. On October 10, 1975, natural gamma, gamma-gamma density, and neutron porosity logs were run in the injection well. Acoustic televiewer images were obtained in the open hole of the injection well on April 20, 1978, and July 17, 1979.

Wellbore Clogging

During injection, the wellhead pressure rose as the rate of injection dropped as a result of clogging of the wellbore. This is illustrated by pressure and rate data shown on plate 1 for the first and second ASR cycles. In the third cycle, measurements were made weekly at the time of backflushes, and pressure and rate changes in the intervening days were not measured. The 1-hour backflushes that began in the second cycle were effective in restoring injectivity, as shown by the general uniformity in peak pressures and injection rates. In the third ASR cycle, backflushes were by artesian flow for 2 to 3 hours at a rate of 500 to 600 gal/min. The well was not acidized.

According to F.W. Meyer (oral commun., 1986), air entrainment was not a problem after some initial difficulties with the pump were resolved. Furthermore, an X-ray diffraction analysis of the backflushed sediment revealed that it consisted mainly of very fine particles of calcite and an iron compound (not scale) that had precipitated (F.W. Meyer, oral commun., 1990).

Spinner flowmeter logs run before, during, and following a backflushing operation on August 27, 1976, during the third injection, were analyzed to detect any changes in the vertical distribution of permeability that occurred as a result of plugging. The data do not indicate that any such change occurred.

HYDROGEOLOGIC CONDITIONS IN AQUIFER USED FOR STORAGE OF FRESHWATER

A characterization of subsurface formations and the spatial variation of their properties is essential for an understanding of the design of the freshwater injection, storage, and recovery tests and their results. This characterization begins with a regional description of stratigraphy and hydrostratigraphy, which is followed by a detailed description of stratigraphy and properties of important formation sequences at the Hialeah site.

Regional Stratigraphy and Hydrostratigraphy

A generalized stratigraphic column showing the major formations and hydrologic units in southeastern Florida is presented in figure 4. Some authors (Miller, 1986; Scott, 1988) include the Tampa Limestone as part of the overlying Hawthorn Formation, but Meyer (1989a) treats it separately. The ASR wells in Hialeah and St. Lucie County tap permeable strata near the base of the Suwannee Limestone, as do wells used to supply brackish water for reverse-osmosis plants in the Florida Keys. The ASR well in St. Lucie County also taps permeable strata at the base of the Ocala Limestone that underlies the Suwannee Limestone. The Ocala Limestone is thin or absent in most of Monroe, Dade, and Broward Counties, and in south-central Palm Beach County, either never having been deposited or having been mostly eroded away (F.W. Meyer, USGS, oral commun., 1983). Chen (1965), however, infers the existence of a thin (less than 100 ft) layer of Ocala Limestone throughout the area on the basis of a few incomplete samples. Vertically adjacent limestone units of the lower part of the Suwannee Limestone and of the Ocala Limestone and upper part of the Avon Park Formation are considered the upper part of the Floridan aquifer system, referred to as the Upper Floridan aquifer, and contain thin, discrete zones of high permeability.

SERIES	FORMATION	HYDROLOGIC UNIT	INFORMAL NAMES
Pleistocene	Miami Oolite / Fort Thompson Formation / Anastasia Formation	Surficial Aquifer System	"Biscayne Aquifer"
Pliocene	Tamiami Formation		
Miocene	Hawthorn Formation	Intermediate Confining Unit	
Miocene	Tampa Limestone (if present)		
Oligocene	Suwannee Limestone		
Eocene	Ocala Limestone (where present)	Floridan Aquifer System	Upper Floridan Aquifer
Eocene	Avon Park Formation		middle confining unit
Eocene	Oldsmar Formation		Lower Floridan Aquifer (or "boulder zone")
		Sub-Floridan Confining Unit	
Paleocene	Cedar Keys Formation		

Figure 4. Generalized stratigraphic column for southeastern Florida showing major formations and hydrogeologic units.

Water quality in the Upper Floridan aquifer grades from brackish to saline with depth; hence, the permeable strata of the Upper Floridan aquifer is considered the most likely source of water in southeastern Florida for reverse-osmosis plant supply, or the most likely receptacle for temporary storage of freshwater. Where the aquifer contains water with less than 10,000 mg/L of dissolved solids, it is protected from contamination by Florida State law to ensure its continued availability for these and other uses. Water in the Upper Floridan aquifer originates as surface recharge in central Florida. Figure 5 shows estimated Upper Floridan hydraulic-head gradients and general direction of flows in the southern part of the Florida peninsula. Also shown is the region where water in the aquifer moving away from points of recharge retains a sufficient degree of freshwater recharge quality to be suitable for public consumption.

Stratigraphic and hydrostratigraphic units underlying the Upper Floridan aquifer generally are not suitable for freshwater storage because of their lack of permeability or the high salinity of the water contained within them. The lower part of the Avon Park Formation was formerly referred to as the Lake City Limestone, distinguished from overlying rocks primarily by its faunal composition, but Miller (1986) included it as part of the Avon Park Formation. The Lake City Limestone is no longer recognized as a formation by the USGS. The middle confining unit of the Floridan aquifer system contains discrete zones with solution porosity that generally are highly dolomitized and made up of very hard rock. No known aquifers match the high transmissivity of the cavernous, dolomitic Lower Floridan aquifer, better known by the drillers' term, boulder zone. This aquifer contains anomalously cold water of seawater-like composition. Meyer (1989a) presents data to support the thesis of Kohout (1965) that boulder-zone water originates as westerly flow through karst features or faults underneath the Straits of Florida near Fort Lauderdale. The boulder zone presently is used for the disposal of liquid wastes.

Stratigraphy and General Lithology at the Hialeah Site

A generalized sequence of predominant rock types at the Hialeah ASR site, based on a consideration of drillers' logs and sample descriptions from the injection and observation wells (Apps. A and B), is presented in figure 6. The upper 120 ft of limestone and sandstone at the site corresponds to the Pleistocene deposits that make up the upper part of the surficial aquifer system (the Biscayne aquifer and its overlying layer of compacted sands). Sandy, shelly, clayey marls interbedded with dense limestone or clay were found between a depth of 120 and about 975 ft. These beds correspond to the Tamiami Formation of Pliocene age, the Hawthorn Formation and Tampa Limestone of Miocene age, and the upper part of the Suwannee Limestone of Oligocene age. F.W. Meyer (USGS, written commun., 1975–80) picked 950 ft as the top of the Suwannee Limestone.
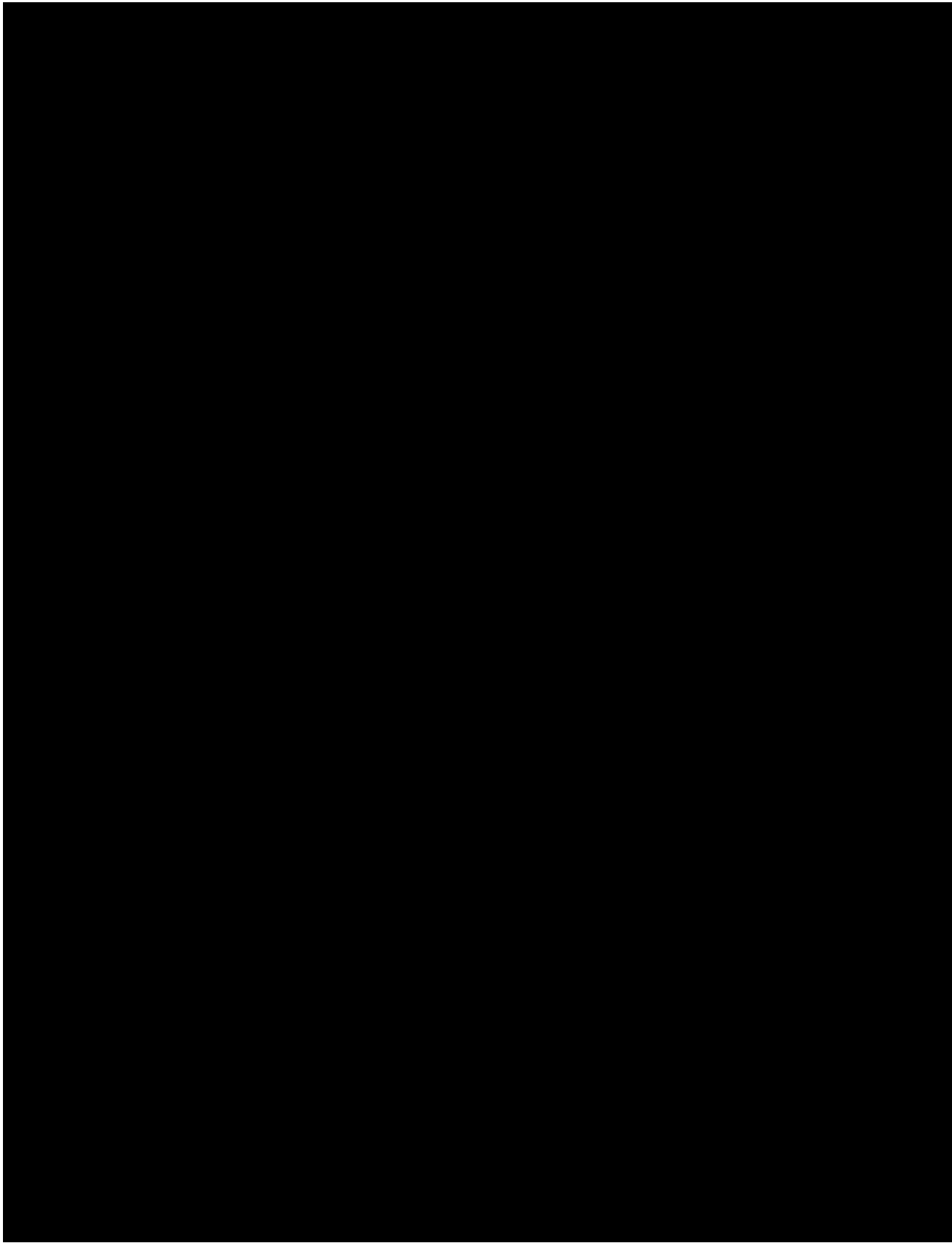
Figure 5. The potentiometric surface of the Upper Floridan aquifer in peninsular Florida in May 1980 and the area in which water in the aquifer is potable (from Meyer, 1989a).
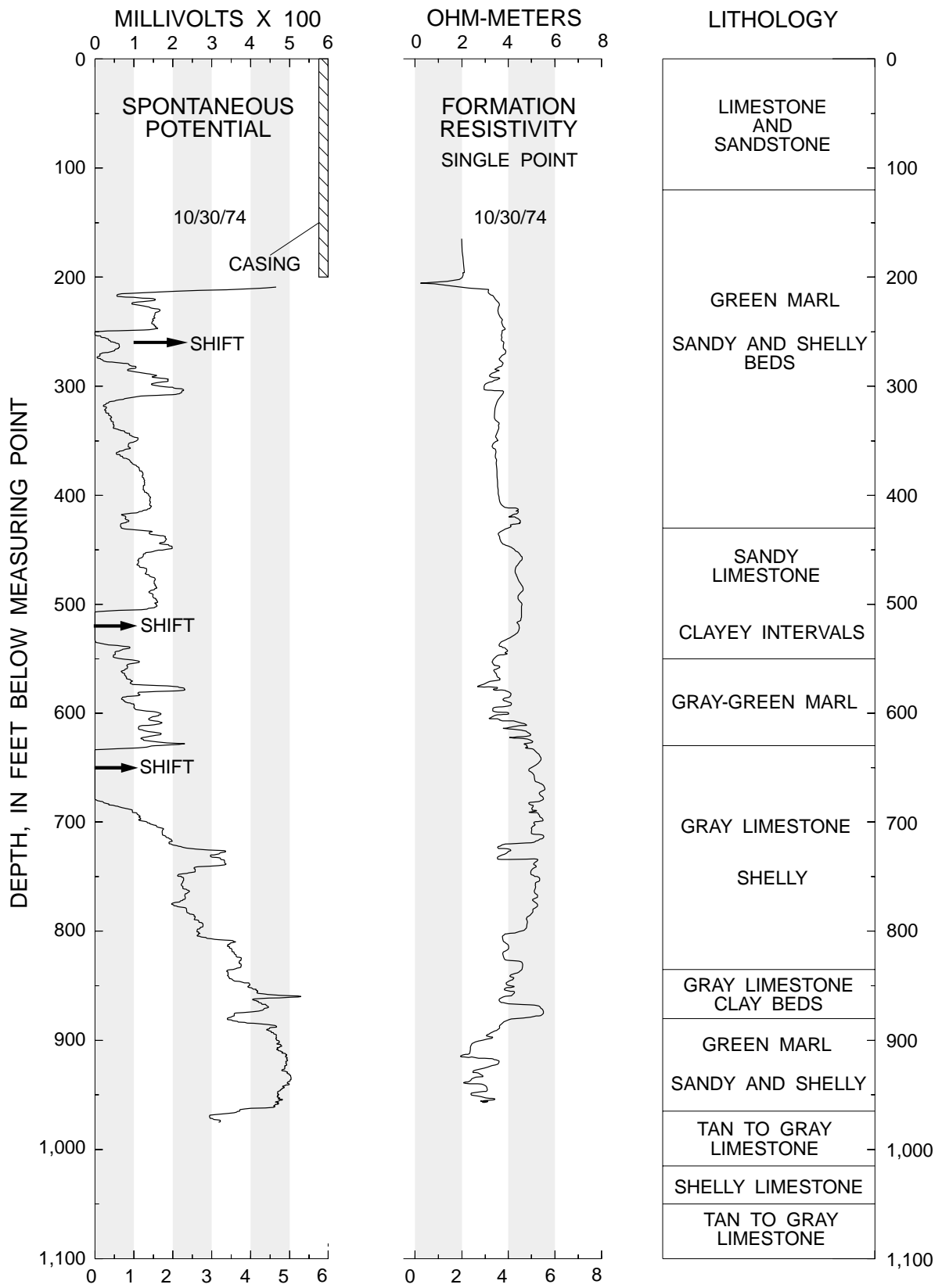
Figure 6. Electric logs of the Hialeah injection well (G-3061) and generalized lithology at the site.

Spontaneous-potential and single-point resistivity logs (fig. 6) were run to 975 ft in the nominal 10-in. injection-well pilot hole filled with aquagel on October 30, 1974. A correlation between the two log traces is evident. Increases in the spontaneous-potential readings that correlate with resistivity decreases indicate beds that predominantly are clay. The spontaneous-potential trace drifted, probably as a result of not grounding the borehole fluid, and was shifted three times to keep the pen on the left side of the chart. Inasmuch as the degree of the shifts is not indicated on the log, no attempt was made to compensate for them when the logs were digitized for report illustrations. The resistivity signal trace was highly oscillatory; thus, a trace of a line drawn through the center of the oscillating signal was digitized and provides the pertinent information. The single-point resistivity probe also commonly shows drift effects. The lower resistivity readings near the bottom of the hole probably indicate a more saline fluid.

The vertically contiguous, consolidated limestone beds of the Floridan aquifer system begin at a depth of about 975 ft and correspond to the lower part of the Suwannee Limestone of Oligocene age and the Avon Park Formation of Eocene age. The interval between depths of 1,015 and 1,050 ft is very shelly. Increases in flow were noted by the drillers as drilling progressed through this interval (App. A). The completed injection well was open to the depth interval between 955 and 1,105 ft, herein termed the injection zone. The receiving zone, or flow zone, is defined as the permeable interval between approximate depths of 1,024 and 1,036 ft that receives most of the inflowing freshwater.

Properties of the Injection Zone

Injection-zone properties needed to facilitate interpretation of the results of the injection and recovery tests are lithology, thickness of beds, hydraulic properties (hydraulic conductivity, porosity, and dispersivity), and the chemical quality of the water contained in the formation. These properties are described in the following sections.

Lithology

The generalized lithology of the depth interval 900–1,100 ft in the injection well (G-3061) is shown schematically in figure 7, which also depicts caliper, formation resistivity, natural gamma, and neutron porosity logs for correlation. The caliper log shows a decrease in diameter within the 14-in. casing below 940 ft from remains of the cement plug that was drilled through with a 12-in. bit. The log also shows part of the 22 1/2-in. reamed hole, just below the bottom of the casing, where cement washed out when drilling was resumed with a smaller bit. The caliper log does not show evidence of cavernous porosity or large solution features. In fact, the log gives no indication that any part of the injection zone has solution porosity. Thin hole enlargements at depths of 1,010, 1,050, 1,070, and 1,090 ft are probably the result of washouts occurring during successive stages of the drilling. Acoustic televiewer logs also failed to show evidence of solution porosity.

Other geophysical logs correlate with lithologic data. The large natural gamma counts from the bottom of the casing to 975 ft correlate with other wells regionally, as will be shown later in the report. The lithologic description for the injection well (App. B) notes phosphorite grains in the clay found in the depth interval from 900 to 975 ft. This mineral contains trace amounts of naturally radioactive material. The formation-resistivity logs (fig. 7) show high-resistivity zones centered at 986 and 1,032 ft, both apparently correlating with increases in natural gamma activity and a decrease of porosity on the neutron log. At the first depth, the drillers noted very hard streaks in the limestone. A hard dolomitic layer is found at the second depth, and the drillers log cites an increase in flow in this interval (App. A). Dolomite beds typically show higher resistivity because of their lower porosity and are sometimes found at the erosional surfaces of formations. The acoustic televiewer logs (not reproduced herein because of their generally poor quality) show what seem to be distinct bedding interfaces at 986 and 1,032 ft (F.W. Meyer, oral commun., 1975). A hypothesis consistent with these observations is that the hard beds mark upper and lower erosional surfaces of a thin section of the Ocala Formation. Verification of the existence of a thin bed of Ocala Formation rocks at this location, however, would require additional data acquisition and analysis.

A similar suite of geophysical logs (fig. 8) from the observation well (G-3062) helps to establish background conditions in the injection zone prior to the ASR cycles. The 16- and 64-in. normal-resistivity logs, the caliper log, and the natural gamma log have interpretations that are similar to those of logs from the injection well. The temperature and fluid-resistivity logs are discussed in the following sections. The schematic diagram (fig. 8) shows depths of the monitor tubes installed in the observation well.
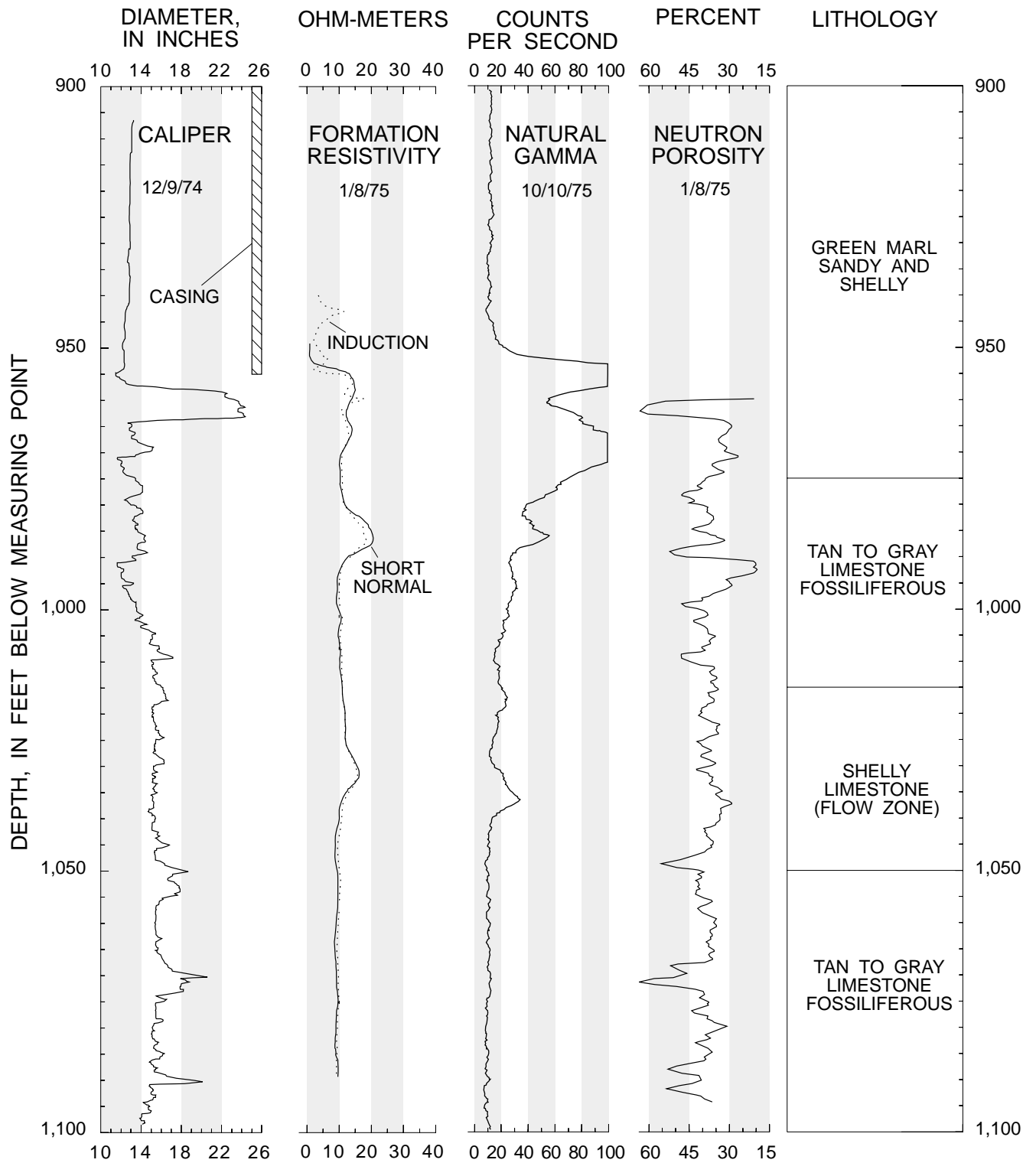
Figure 7. Geophysical logs of the Hialeah injection well (G-3061) and generalized lithology of the injection zone.
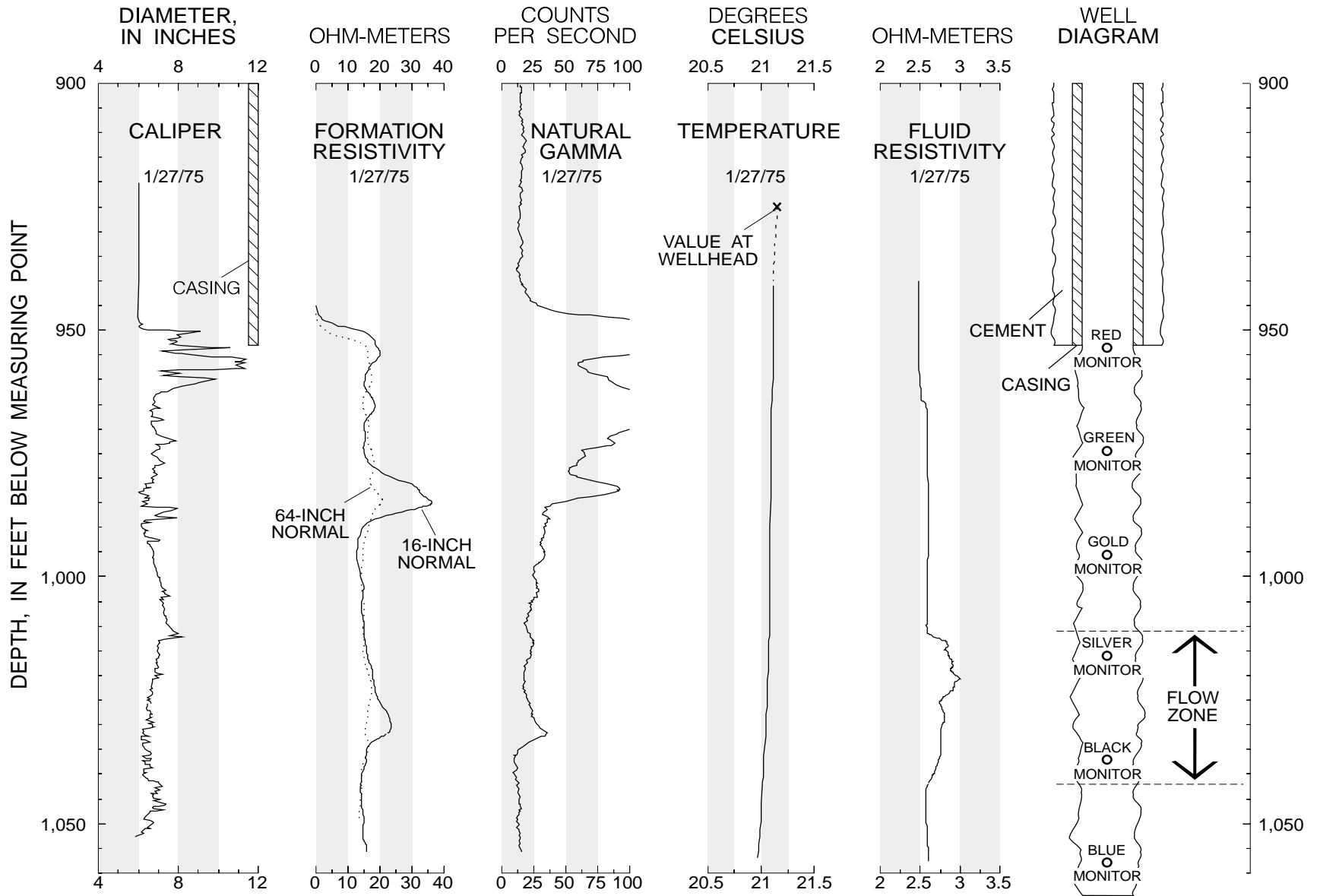
igure 8. Geophysical logs of the Hialeah observation well (G-3062) and depths of monitor tubes.

Transmissivity

Aquifer tests were conducted to measure the composite transmissive capability of the 150-ft injection zone, known to be made up of strata of strongly contrasting permeability. When this information is combined with a knowledge of the thickness, distribution, and relative contribution of permeable flow zones obtained by geophysical logging under flowing conditions, a better understanding of the disposition of the water injected during the ASR process can be gained, and the transmissivity of each flow zone can be estimated. Estimates of hydraulic conductivity in individual zones can then be derived by dividing flow-zone transmissivities by their approximate thicknesses. The generic computer code used in this study requires input of estimates of hydraulic conductivity and the thickness and distribution of flow zones and confining layers for simulation of freshwater injection, storage, and recovery.

The first aquifer test was conducted on February 10, 1975, by allowing the 6-in. observation well at Hialeah to discharge for 100 minutes at 250 gallons per minute (gal/min) as pressures were measured in the injection well and in the 2-in. monitor tube open at 840 ft in the observation well. Discharge was measured using an orifice plate on the observation well. Two pressure gages, their readouts in feet of head, were used in the injection well. These gages had a display range of 0–60 ft of head at 0.2-ft scale divisions. The maximum drawdown at the injection well was 1.8 ft. Pressure changes during recovery were observed for 15 minutes immediately following the closing of the orifice. The following day, a second aquifer test, a constant-head discharge test, was performed.

During the first aquifer test, values of head from the two injection-well gages differed by about 2 ft and showed slightly different trends. Both drawdown data sets were analyzed for estimates of transmissivity (T) and storage coefficient (S) using the method of Jacob and Lohman (1952). Data from one gage, considered to be the more representative, were also analyzed using the Theis type-curve method. On the basis of the various analyses, transmissivity was estimated to be about 11,000 [(ft^3/d)/ft^2]ft (Meyer, 1989b). The maximum drawdown in the 2-in. monitor tube was 0.2 ft (F.W. Meyer, written commun., February 1975), indicating that minor leakage occurred across the marly confining beds separating the injection zone from the perforations at 840 ft.

Flow-Zone Depth and Thickness

A delineation of the relative permeability of the various strata within the injection zone was partly based on a study of data collected during spinner flowmeter logging during injection and recovery. The quantitative analytic procedure developed for this study is described below. Also presented is a parallel description of the flow-zone depth and thickness based on an evaluation of fluid-resistivity and temperature logs.

Analysis of Data From Spinner Flowmeter Logs

Two sets of spinner flowmeter data were collected from the injection well on October 20, 1975, while the well backflowed under artesian pressure. These data are shown in figure 9, together with caliper log data, to illustrate a typical analysis for obtaining a vertical profile of the relative amount of flow in the wellbore. One set of data was recorded as the probe was lowered into the well, and the other as the tool was raised.

Spinner flowmeter probes contain a device that rotates in response to the relative speed of fluid movement past the probe. Measurements of the rotation speed are transmitted to the logger in counts per second. However, the probe does not indicate the direction of relative flow, only the rate of the spinner rotation. When the probe was lowered to the bottom of the well on October 20, 1975 (fig. 9), the direction of relative flow past the probe remained in the upward direction throughout the entire logged interval, including the stagnant zone between the flow zone and the bottom of the well. However, a different situation prevailed as the probe was raised from the bottom. The upward moving probe responded to apparent downward flow (relative to the changing position of the probe) in the stagnant zone. As the probe moved upward past the flow zone, relative flow through the probe reversed direction and was upward in the direction of discharge from the well. Therefore, as the relative flow direction changed, the spinner slowed, and a null reading was recorded, as shown at 1,028 ft in figure 9. Analysis of the recorded data to produce a vertical-flow profile requires reversing the arithmetic sign of the data at the depth where the null occurs.
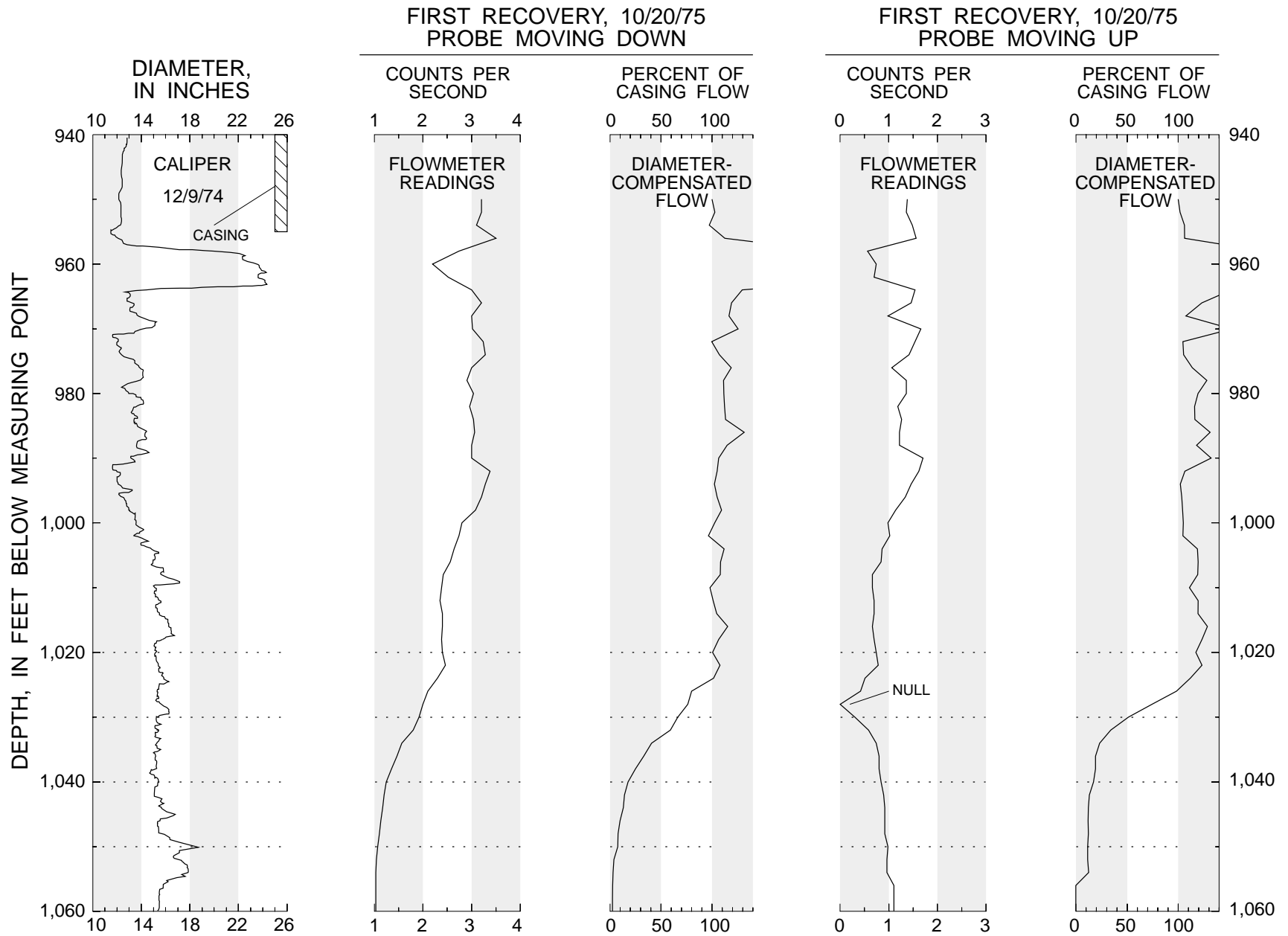
Figure 9. Conversion of a typical set of spinner flowmeter data to wellbore flow measurements.

Stationary spinner flowmeter measurements, in which the rotation speed is observed while the probe is hung at a fixed elevation, are more reliable than continuous readings that must be corrected for tool velocity, but often fail to clearly show the depths at which changes in flow occur. During the Hialeah tests, stationary flowmeter measurements were obtained during the logging sequences of May 25, 1976, and April 20, 1978 (fig. 10). On May 25, 1976, the stationary reading at 1,046 ft was only 7 percent of that measured in the casing, and a zero reading was obtained at 1,059 ft. On April 20, 1978, a zero reading was obtained at 1,040 ft. These measurements proved that flow in the bottom of the hole was negligible and aided in interpreting other geophysical logs.

Whether spinner flowmeter measurements are continuous or discrete, the measured velocity varies with the diameter of the borehole as well as with the quantity of flow produced. Therefore, in quantitative analyses, flowmeter data must be adjusted to compensate for borehole diameter. For example, the flowmeter data values recorded as the probe moved downward on October 20, 1975, show a decline below 992 ft. However, the borehole diameter increases, and the diameter-compensated flow values remain nearly uniform to a depth of 1,024 ft.

Quantitative analysis of flowmeter data consists of the diameter compensation and an adjustment for the velocity of the probe during descent or ascent. Flow at a given depth $Q(h)$ can be expressed as a percentage $\Delta Q(h)$ of flow within the lower part of the casing Q_0 where the radius r_0 is considered to be locally uniform. The computation can be written as

$$\Delta Q(h) = 100\frac{Q(h)}{Q_0} = 100\ \frac{\pi r(h)^2}{\pi r_0^2}\left(\frac{C(h)\beta - V_t(h)}{C_0\beta - V_0}\right) \quad (1)$$

where: $r(h)$ is the borehole radius at depth h,
$C(h)$ is the measured counts per second at depth h,
C_0 is the measured counts per second in the casing,
β is a conversion factor relating counts per second to velocity,
$V_t(h)$ is the velocity of the tool at depth h, and
V_0 is the velocity of the tool at the depth where C_0 is measured in the casing.

In flowmeter logging in long boreholes, the probe velocity can vary appreciably, and a record usually is made of the tool velocity at regular depth intervals. In the flowmeter logging conducted during the Hialeah ASR tests, however, the logged interval was short (generally 940–1,100 ft), and at best, a single value for probe velocity is noted on the logs. Therefore, the assumption was made in the analysis that the probe velocity was uniform throughout; that is,

$$V_t(h) = V_t = V_0 \quad (2)$$

Furthermore, because stagnant water is present in the bottom of the borehole, the probe velocity is related to counts recorded in the bottom of the hole C_b; that is

$$V_t = \beta C_b \quad (3)$$

Equation 1 now reduces to

$$\Delta Q = 100\frac{r(h)^2}{r_0^2}\frac{[C(h) - C_b]}{(C_0 - C_b)} = 100\frac{r(h)^2}{r_0^2}\frac{\Delta C(h)}{\Delta C_0} \quad (4)$$

In this formulation, counts at depth h, $C(h)$, are referenced to counts in the bottom of the hole (C_b) and adjusted by the ratio of the squares of the radii. This provides a simple formula for digital computation.

Many problems are associated with the quantitative analysis of spinner flowmeter logs. When the probe passes through thin zones of larger diameter, the moving fluid often apparently does not develop a uniform velocity throughout the enlarged borehole; thus, the diameter compensation can lead to error. When the probe moves in the direction of well discharge and the spinner reverses direction, the counts do not always read zero, or null, on the chart; thus, errors can occur in computing the degree of flow augmentation in this interval. Depth errors can occur as a result of cable stretch or errors in depth orientation. Such errors can be critical in making diameter compensations and in precise evaluation of the depths at which significant flow augmentation occurs. Errors can be introduced related to the physical operation of the spinner device; the device may be more sensitive to flow from one direction than the other, and a time lag can occur in the response of the device to changes in borehole flow, depending on the probe velocity.

Each of the 18 spinner flowmeter logs run during the ASR cycles was digitized at 2-ft depth increments and converted to relative volumes of flow using equation 4. Nulls were identified and assigned $C(h)$ values of zero, while data from lower depths were considered to be negative values and data from higher depths were considered to be positive values. Depth errors due to cable stretch or calibration error were identified by comparing low count intervals with the large-diameter interval centered at 960 ft in the injection well, and depth adjustments ranging from 0 to 6 ft were made to all recorded depths in the logged interval. Results of the analyses are shown in figure 10.

Examination of the computed flows indicates a depth of 1,024 ft to be the top of the flow zone. Evidence identifying the bottom of the flow zone is less clear, but the bottom is most likely at 1,036 ft, indicating a flow-zone thickness of only 12 ft. On the basis of some logs, the zone might extend to a depth of 1,040, 1,044, or 1,050 ft, indicating possible flow-zone thicknesses of 16, 20, or 26 ft.

A slight amount of flow between depths of 955 and 965 ft was noted during drilling (App. A), but the flowmeter log analyses show no evidence of it; thus, the amount of flow from this depth interval apparently is negligible compared with that from the principal flow zone (1,024–1,036 ft). No appreciable contribution to flow seemed to originate from the indicated bedding interface at 986 ft. Any slight contribution would have been masked by the effect of irregularities in the borehole diameter.

Spinner flowmeter logs in the observation well could have been used to verify that the narrow flow zone in the injection well was similar in character at the location of the observation well, and in supporting the hypothesis that the zone was similar throughout the region of injected freshwater flows. A flowmeter log was attempted in the observation well on January 27, 1975, but the probe would not pass below a depth of 983 ft. The installation of multidepth samplers in the observation well at the beginning of the ASR cycles rendered subsequent flowmeter logging of this well infeasible.

The flowmeter logs of August 27, 1976, as previously noted, are useful in assessing the degree to which the vertical permeability distribution may be affected by borehole plugging during injection. The spinner was raised and lowered during (1) injection before a backflush, when plugging had substantially reduced injectivity; (2) the backflush; and (3) injection

immediately following the backflush, after most of the natural injectivity had been restored. An examination of the converted logs (fig. 10) shows more apparent difference between the up and down logs of each set than between any sets of logs. All tend to confirm the previously accepted hypothesis that the flow zone lies between depths of 1,024 and 1,036 ft, and there is no indication that any change in the vertical distribution of injectivity has occurred.

The flowmeter logs shown in figure 10 cover a period of injection, storage, and recovery lasting nearly 4 years. The similarity of the results throughout this time period indicates that no long-term changes in the vertical distribution of injectivity have occurred.

Interpretation of Data From Temperature and Fluid-Resistivity Logs

Logs of temperature and fluid resistivity run before and during the ASR cycles are used as additional means to corroborate the delineation of the flow zone. These logs are also used to aid interpretation of interesting facets of the injection and recovery process and the effect of the process upon water quality.

Temperature and fluid-resistivity logs run in the observation well on January 27, 1975 (fig. 8) were for the purpose of establishing background conditions prior to ASR cycles. The fluid-resistivity log, probably run during artesian flow, shows inflows of increasing resistivity (fresher water) between 1,011 and 1,042 ft, an interval which corresponds to 1,015 and 1,046 ft in the injection well because of the different elevations of the measuring points. The interval also correlates with the interval of shelly limestone (fig. 7) that contains the flow zone.

One possible interpretation of a zone of fresher water surrounded above and below by more saline water is that the zone is sufficiently permeable to be partly flushed by flow from upgradient areas of freshwater recharge. The Floridan aquifer system crops out in central Florida, where it receives atmospheric recharge and contains potable water (fig. 5). The peak resistivity in the log of January 27, 1975, is at a depth of 1,020 ft (1,024 ft in the injection well, the probable top of the permeable flow zone). The temperature log, run as the well flowed under artesian pressure, shows temperature to be nearly uniform from land surface to about 1,010 ft, below which the temperature decreases about 0.2 °C in 50 ft, an indication that inflow occurs in this interval.
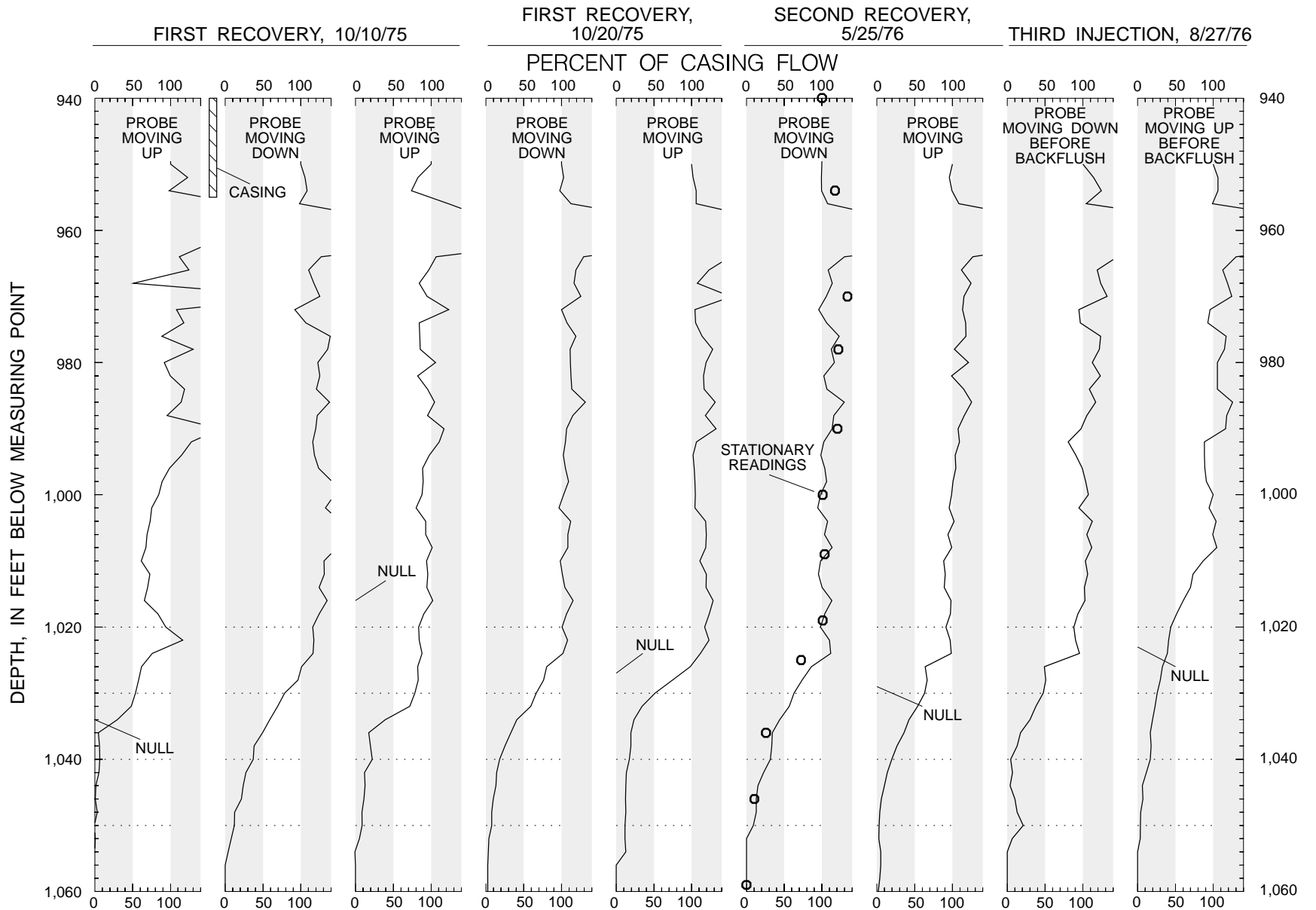
FIRST RECOVERY, 10/10/75

FIRST RECOVERY, 10/20/75

SECOND RECOVERY, 5/25/76

THIRD INJECTION, 8/27/76

PERCENT OF CASING FLOW

DEPTH, IN FEET BELOW MEASURING POINT

PROBE MOVING UP

CASING

PROBE MOVING DOWN

PROBE MOVING UP

NULL

NULL

PROBE MOVING DOWN

PROBE MOVING UP

NULL

PROBE MOVING DOWN

PROBE MOVING UP

NULL

PROBE MOVING DOWN

STATIONARY READINGS

PROBE MOVING UP

NULL

PROBE MOVING DOWN BEFORE BACKFLUSH

PROBE MOVING UP BEFORE BACKFLUSH

NULL

Figure 10. Wellbore flow measurements from conversion of spinner flowmeter logs of the injection well (G-3061) during three injection and recovery cycles (1975-79).
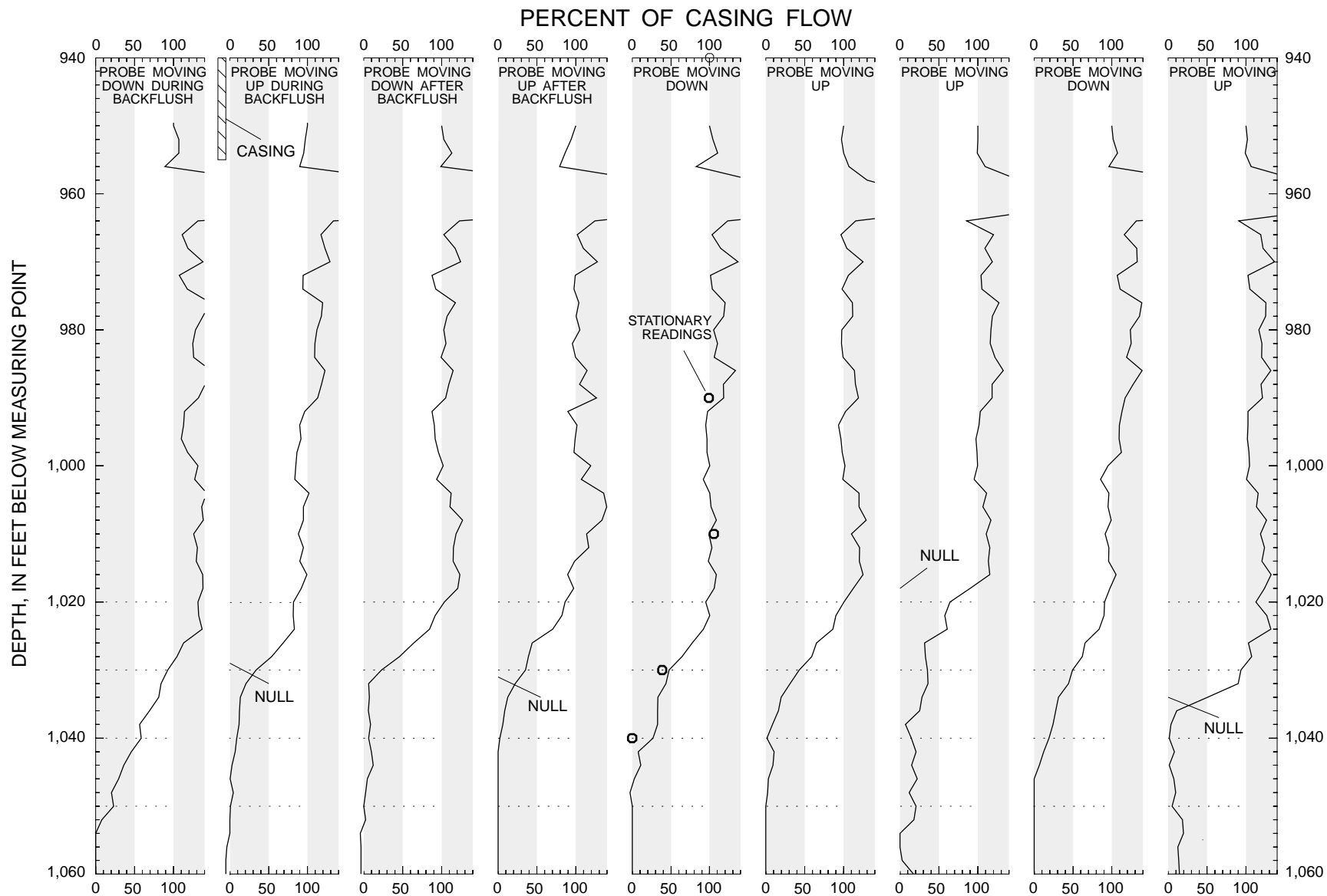
Figure 10. Wellbore flow measurements from conversion of spinner flowmeter logs of the injection well (G-3061) during three injection and recovery cycles (1975-79)--Continued.

Selected logs of temperature and fluid resistivity in the injection zone obtained as water backflowed during the three recovery phases are shown in figure 11. For comparison purposes, the temperature log run on October 10, 1975, 30 days into the first recovery, when the chloride concentration of recovered water had reached 300 milligrams per liter (mg/L), is shown together with the observation-well temperature log of January 27, 1975, which depicts preinjection conditions. Measurements of the temperature of water from the supply well during the three injection phases are shown in figure 12. The temperature of injected water in the first ASR cycle averaged 25.55 °C, in contrast with the preinjection temperature in the injection zone of about 21.2 °C. The temperature of recovered water on October 10, 1975, was about 24 °C, but the temperature increased rapidly to about 25 °C below 1,047 ft (fig. 11). Fluid resistivity on the same date also increased markedly below 1,047 ft. Below 1,047 ft, therefore, is a zone of warmer, fresher water that is likely stagnant injected water either forced into the zone of relatively low permeability underlying the flow zone during the previous injection or forced downhole by turbulent convection. At 300 mg/L of chloride concentration, recovered water contains about 22 percent native water. The temperature decrease from 25.5 °C to 24 °C probably is caused by mixing and thermal diffusion.

A break in the fluid-resistivity trace of October 10, 1975, and a slight break in the temperature trace of the same date, occurs just below 1,025 ft, indicating a concentration of flow at this depth. That the water becomes relatively more saline and slightly cooler above this elevation also suggests more rapid recovery of injected water from cavities at this elevation.

The fluid-resistivity log run on May 25, 1976, 22 days into the second recovery phase, when the chloride concentration of recovered water had reached 124 mg/L (about 6.5 percent native water), shows a more gradual resistivity increase with depth, beginning at about 1,018 ft and becoming more pronounced after about 1,047 ft (fig. 11). No temperature log was obtained. Again, there seems to be stagnant freshwater in the bottom of the hole, particularly below 1,047 ft.

The temperature and fluid-resistivity logs of April 20, 1978, 276 days into the third recovery, when the chloride concentration of recovered water had reached about 600 mg/L (about 48 percent native water), again show stagnant, warmer freshwater in the bottom of the hole below 1,043 ft. The average temperature of the injected water in the third ASR cycle

was 25.93 °C. On April 20, 1978, recovered water above 1,020 ft had a temperature of about 22.8 °C (fig. 11), close to the preinjection background of 21.2 °C, apparently a result of both mixing and at least 457 days of thermal diffusion (the storage period was 181 days). A slight break in the trace of the fluid-resistivity log at about 1,022 ft suggests a concentration of inflow, possibly correlating with similar indications at 1,025 ft during the first recovery and at 1,018 ft during the second recovery. The slight difference in elevations could easily be attributed to depth measurement error. The temperature log of July 17, 1979, 729 days into the third recovery, when the chloride concentration of recovered water was 1,060 mg/L (about 88 percent of that in the native water), shows the recovered water temperature to have dropped to about 22.0 °C, even closer to that of the native water before injection. The fluid-resistivity log of the same date shows slightly more saline water below 1,030 ft. Apparently, recovery has been of sufficient duration to have flushed the stagnant freshwater from the bottom of the hole and surrounding rocks, though some of the thermal energy remains.

All of the temperature logs show some cooling of the warmer water near the bottom of the hole. This could be due to the closer proximity of stagnant warm water in the bottom of the hole to the vast thermal sink below.

On the basis of temperature and fluid-resistivity logs and the preceding analysis of the spinner flowmeter logs, it seems that a depth of 1,024 ft approximately marks the top of the flow zone and may be a point source for much of the flow. The bottom of the flow zone now seems to be in the 1,043- to 1,047-ft range. However, the proportionate amount of flow that occurs below 1,036 ft may be insignificant.

Porosity

A review of data that leads to estimates of aquifer porosity is useful because the generic simulator used in this study implicitly represents aquifer storativity with input specifications of effective porosity, rock and water compressibility, and thicknesses of permeable flow zones. Effective porosity, which changes slightly as pressure varies and the aquifer pores expand or contract, is a direct measure of the amount of injected freshwater that can be accepted by a unit pore volume of the aquifer. Total porosity is a measure of the amount of water contained within a unit pore volume and may be greater than effective porosity if some of the water is contained in pores that are not connected to flow pathways.
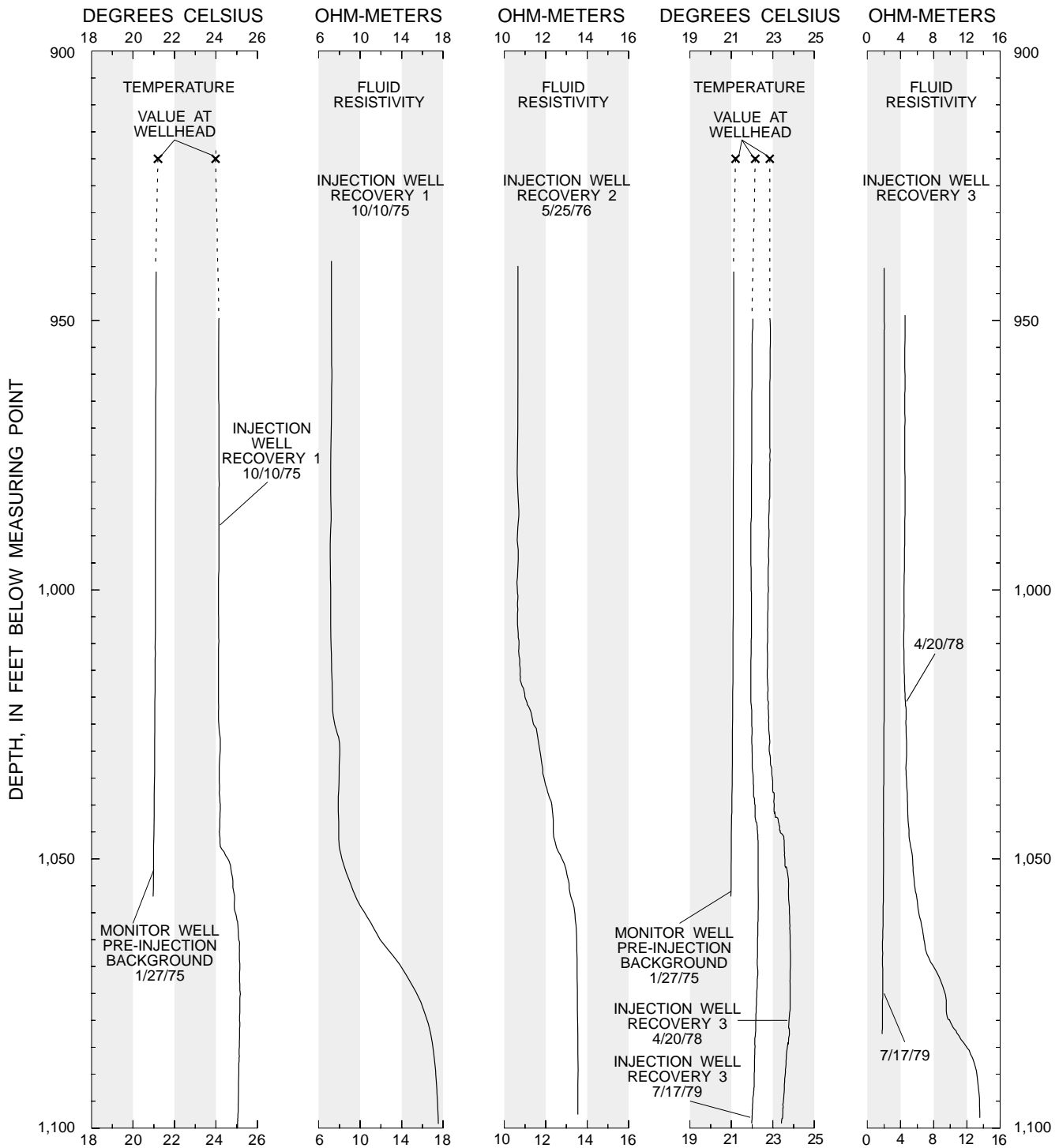
Figure 11. Temperature and fluid-resistivity logs of the injection well (G-3061) before and during aquifer storage and recovery cycles.

Direct measurements of injection-zone total porosity consist of the neutron porosity log run in the injection well by Schlumberger, Inc., on January 8, 1975, and neutron porosity logs run by the USGS in the injection and observation wells on October 10, 1975, and January 27, 1975, respectively. The Schlum- berger log data, illustrated in figure 7, were stated by the contractor to have been compensated for borehole effects. Porosity seems to average about 35 percent throughout the injection zone. Large variations between extreme values of 20 and 65 percent occur within discrete intervals. Although no reason exists to
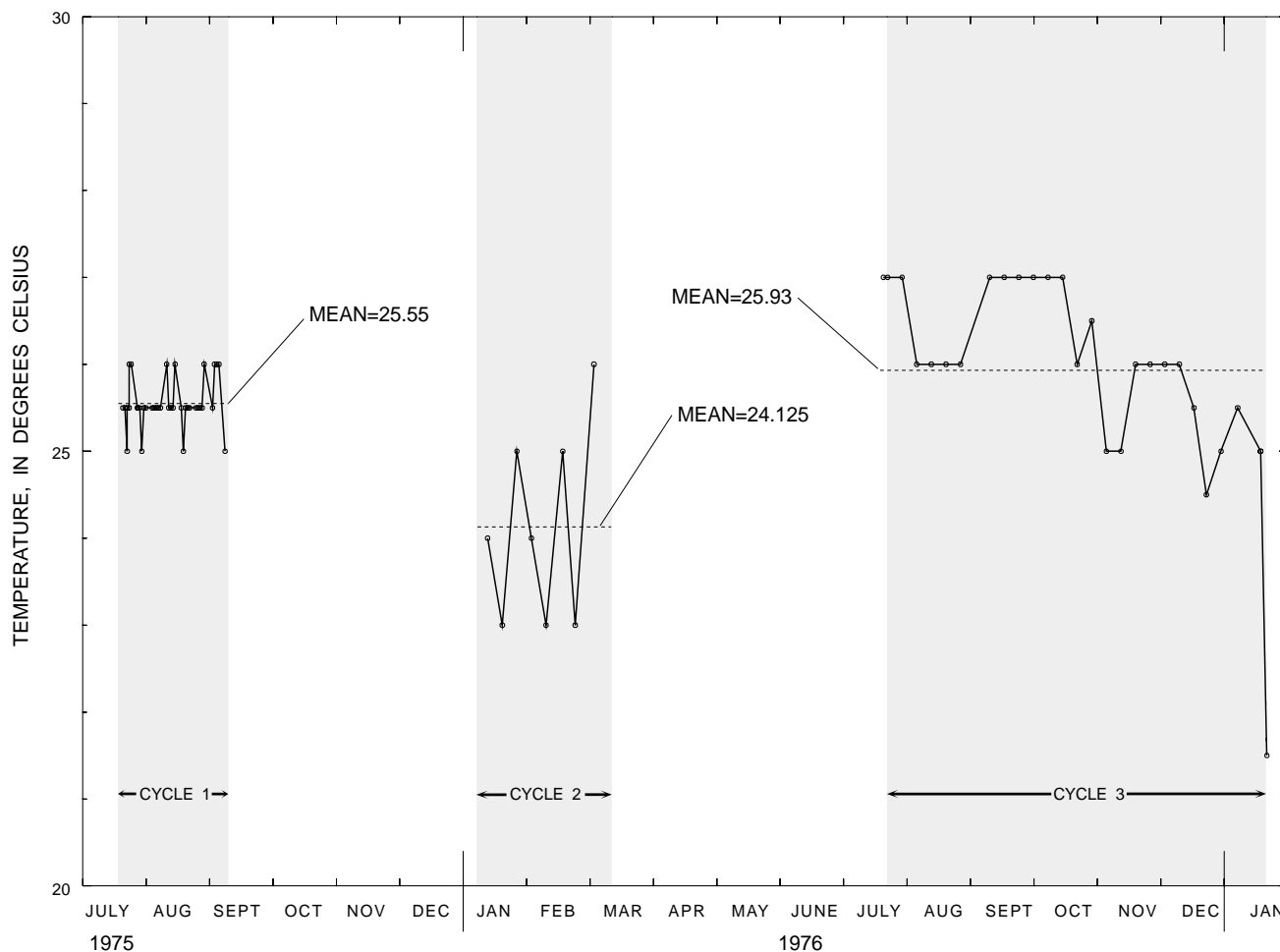
Figure 12. Temperature of water from the injection supply well during aquifer storage and recovery cycles.

question the validity of the lower values, the high-porosity spikes probably indicate where exceptional borehole irregularity has caused an overestimate of the amount of the compensation. The USGS logs were not compensated for borehole effects and were not used for porosity estimates.

Estimates of storage coefficient obtained from analyses of aquifer-test data can sometimes be used to check porosity data and corresponding estimates of rock compressibility and aquifer thickness. However, the disparity among the storage coefficients estimated from the Theis and Jacob-Lohman analyses of the February 10, 1975, aquifer test discouraged attempts to make such detailed comparisons.

The neutron porosity log measured the total water content of the formation, including that contained in either pores within the rock or in solution features. Of striking interest is the fact that the average value of 35 percent seems to be the water content not only of the solution-riddled flow zone, but also of

overlying and underlying layers of negligible solution porosity. However, a 35 percent value for total porosity does seem to be consistent with the result of laboratory analyses of cores from the relatively impermeable confining layers that overlie the Lower Floridan aquifer (boulder zone). A cursory review of many core analyses performed by private laboratories for engineering consultants managing the construction of municipal waste-disposal wells indicates that porosities of 25–40 percent typically are measured on cores that are predominantly limestone. Porosities of dolomite cores, on the other hand, generally fall into a lower range of 1–15 percent.

Water Quality

A characterization of the quality of the native water is needed for an understanding of factors that affect flow processes, recoverability, wellbore plugging, and the quality of recovered water. Inclusion in

Appendix D of measurements of the chemical and biological constituents of native, injected, and recovered water provides the data to readers for many possible uses. One of the most interesting potential uses is to determine changes in the quality of the injected water after a period of residence in the aquifer. However, the interpretive scope of this report is limited to a discussion of water-quality characteristics affecting ASR flow processes and recoverability and the simulation of the ASR process with computer models. Therefore, the chemical characteristic of principal interest is density.

The degree of buoyancy stratification that occurs depends on the density contrast between injected and native water. Recoverability of injected water is reduced by buoyancy stratification (Merritt, 1985). Recoverability also is determined by the degree of dispersive mixing with the native water, another reason for accurately describing the salinity of the native water. The higher the salinity of the native water, the less the amount of mixed injected and native water that will be potable. Buoyancy stratification and dispersive mixing are processes that must be accurately represented to achieve the simulation objectives of this study.

Direct measurements of density usually lack sufficient accuracy for many purposes (Meyer, 1989a), and water density is more accurately estimated as a function of known salinity and temperature. Salinity is based herein on measurements of dissolved solids, which correlate well with chloride concentrations in brackish waters of the Upper Floridan aquifer.

A characterization of the salinity of native water in the injection zone is based on preinjection water-quality samples from the injection and observation wells, on water-quality data obtained from the observation-well monitor tubes early in the first ASR cycle, and from the preinjection fluid-resistivity log run in the observation well on January 27, 1975. The monitor-tube data obtained later in the ASR cycles help to corroborate this interpretation and also facilitate an understanding of flow processes during ASR cycles.

Preinjection Sampling and Geophysical Logging

The water-quality samples (App. D), obtained on November 20, 1974, from the observation well and on December 4, 1974, from the injection well represent a composite of water quality from all elevations within the 150-ft open borehole, dominated by the quality of water from elevations at which the formation has high permeability (the flow zone). The chloride concentration measured in each well was 1,200 mg/L, and the dissolved-solids concentration was about 2,700 mg/L.

A partial description of water-quality variation within the injection zone is obtained from a study of the preinjection temperature and fluid-resistivity logs from the observation well on January 27, 1975 (fig. 8). Before the logging, the observation well was allowed to flow on November 20, 1974, sampled, and then shut in. The well was logged on January 8, 1975, by Schlumberger, Inc. (caliper and cement bond), and the 2-in. monitor tube was perforated. The sequence of the logs run on January 27, 1975, is not known. Annotation on the temperature log indicates that the log was run under flowing conditions. The data show a temperature increase up the hole that is more rapid below about 1,015 ft than above 1,015 ft. This tends to indicate that most contributions of flow occur below about 1,015 ft. A fluid-velocity log was also attempted, but the probe would not pass below 983 ft. No annotation was found on the log to indicate that the well was flowing while the fluid-resistivity log was run. However, F.W. Meyer (written commun., 1980) has interpreted it as a production (flowing) log. The data depict an unusual description of resistivity variations within the wellbore that presents some interpretive difficulties. To describe these difficulties and their resolution, the usual method of interpreting flowing fluid-resistivity logs is briefly considered.

Generally, fluid-resistivity logs run during production (flow from the well) tend to show resistivity changes at elevations where the volume of flow from the well is augmented by appreciable amounts of water of different salinity from that of water flowing from lower zones in the well. At those elevations, the fluid resistivity changes to represent the new composite salinity of water from the new zone and from the lower zones. Often, in the Upper Floridan aquifer, salinity decreases upward, and the resistivity trace shows increases at permeable-zone elevations as the probe moves upward. The fluid-resistivity logs in figure 11 show a reverse pattern. In these logging runs, the probe was raised from a pool of stagnant freshwater at the bottom of the well and passed through permeable zones where a brackish mixture of native and injected waters flowed from the formation into the borehole under artesian pressure. As the probe passed through these zones, the measured resistivity decreased.

Because the trace of the January 27, 1975, flowing-resistivity log (fig. 8) shows both positive and negative deflections, the apparent conclusion is that water of lower salinity contributes to the flow at lower elevations and is then augmented by water of higher salinity at higher elevations. In fact, the log indicates water above 1,011 ft to be about equal in salinity to that at the bottom of the well, below 1,043 ft. Because the existence of a permeable zone containing water of higher salinity is unlikely, the data suggest that the instrument could have drifted out of calibration. The principal significance of these data is to show that a zone of low salinity at 1,020 ft (1,024 ft in the injection well) is surrounded above and below by more saline water. Possibly, water in the flow zone grades from lower salinity in the center of the flow zone to higher salinity at the upper and lower boundaries. The resistivity variation indicated by the log is not large. Water at the bottom of the well is stagnant and probably does not represent background conditions in the aquifer. This water may contain residual drilling fluid or may represent downward turbulent dispersion from the flow zone.

The resistivity values above 1,012 ft generally represent the salinity of the composite flow from the flow zone, and the actual salinity of water in the relatively impermeable rocks at those elevations might be greater. For purposes of this study, the native water in the confining zones is assumed to be more saline than water from the higher 840-ft white monitor, where the chloride concentration of samples was between 1,700 and 2,300 mg/L and the dissolved solids concentration varied from 3,900 to 5,000 mg/L. This assumption is based on the general trend of increasing salinity with depth that occurs within the Upper Floridan aquifer except in discrete flow zones flushed by fresher water.

The physical conceptual model accepted as a hypothesis for computer simulation was that of a flow zone within the interval 1,012–1,043 ft (1,016–1,047 ft in the injection well). Water is freshest in the center of the zone but may be more saline in the upper and lower parts of the zone because of greater permeability in the center and ionic diffusion or seepage of more saline water from overlying and underlying relatively impermeable rocks as flow in the zone moves downgradient from distant areas of freshwater recharge in central Florida (fig. 5). The composite chloride and dissolved-solids concentrations are about 1,200 and 2,700 mg/L, as measured in preinjection

water samples. The contribution of flow from the lower part of the flow zone (above 1,043 ft) may be slight but would substantially change the salinity detected by the logger because water below is static. Therefore, this interpretation of the fluid-resistivity log generally is consistent with results of the flow-meter log analysis.

A preinjection fluid-resistivity log was run by the SFWMD at the St. Lucie County ASR site (Wedderburn and Knapp, 1983, p. 34). This log is strikingly similar to the Hialeah fluid-resistivity log of January 27, 1975 (fig. 8). A high-resistivity spike on the trace corresponds to the lower flow zone occurring at the contact between the Ocala Limestone and Avon Park Formation. Similar to the USGS log from Hialeah, no annotation is present on the log to indicate that the well was flowing; however, the log has been interpreted as a flowing log by Wedderburn and Knapp (1983, p. 32). Flowing water above the uppermost flow zone is lower in salinity (has higher resistivity) than stagnant water in the bottom of the well below the flow zones, as would be expected if the flow originates from a permeable zone containing fresher water. The fact that the lowest degree of salinity occurs near the center of the flow zone suggests a gradation of water quality within the flow zone, so that water flowing from the well will be more saline than the freshest water near the center of the flow zone.

Monitor-Tube Data From the Three Test Cycles

Interpretation of the fluid-resistivity log of January 27, 1975, is corroborated by water-quality data from the first ASR cycle taken from the monitor tubes in the observation well (pl. 1). The mean values of chloride concentration in water from tubes sampling the injection zone prior to detection of the injectant are listed in the following table:

Color code	Depth (feet)	Number of samples	Average chloride concentration (milligrams per liter)
Red	957	18	1,594
Green	978	19	1,574
Gold	999	18	1,500
Silver	1,020	18	1,211
Black	1,041	18	1,278
Blue	1,062	22	1,441

The 840-ft zone (white monitor) was sampled 41 times prior to injectant breakthrough at the observation well, and the average chloride concentration was 1,895 mg/L. This provides firm validation for the hypothesis that the flow zone is overlain by zones of more saline water.

The relation of the early chloride data from the monitor tubes to actual injection-zone water quality is better understood by considering data from the observation-well monitor tubes later in the ASR cycles. A very rapid change in water quality just after the end of the first injection on September 8, 1975, indicates the possibility that unmixed injected water has reached the observation-well borehole (pl. 1 and fig. 13). These changes are first apparent within the flow zone (fig. 8, silver and black monitors) but are detected hours later in the remaining monitors near sections of the borehole that are assumed to be relatively impermeable on the basis of the temperature and fluid-resistivity logs and the injection-well flow analysis. This indicates that the monitoring zones were not completely isolated by the rosettes holding the

monitor tubes and that samples from each monitor are composites of water at that elevation and from other elevations within the borehole. Thus, water samples from the red, green, gold, and blue monitors acquired before arrival of the injected water at the observation well probably do not accurately represent the quality of water in the surrounding rocks, but partly contain lower-salinity water from the presumed flow zone. This supports the hypothesis that water in the relatively impermeable rocks overlying and underlying the flow zone is appreciably more saline than indicated by samples from the monitor tubes.

A sampling following the hiatus between the first recovery and second injection shows water in the red, green, gold, and blue monitors to have increased to concentrations of about 1,400 mg/L of chloride, unlike water from the silver and black flow-zone monitors. The increases may have been caused by ionic diffusion and are further evidence that relatively impermeable parts of the injection zone contain water of greater salinity than the flow zone.
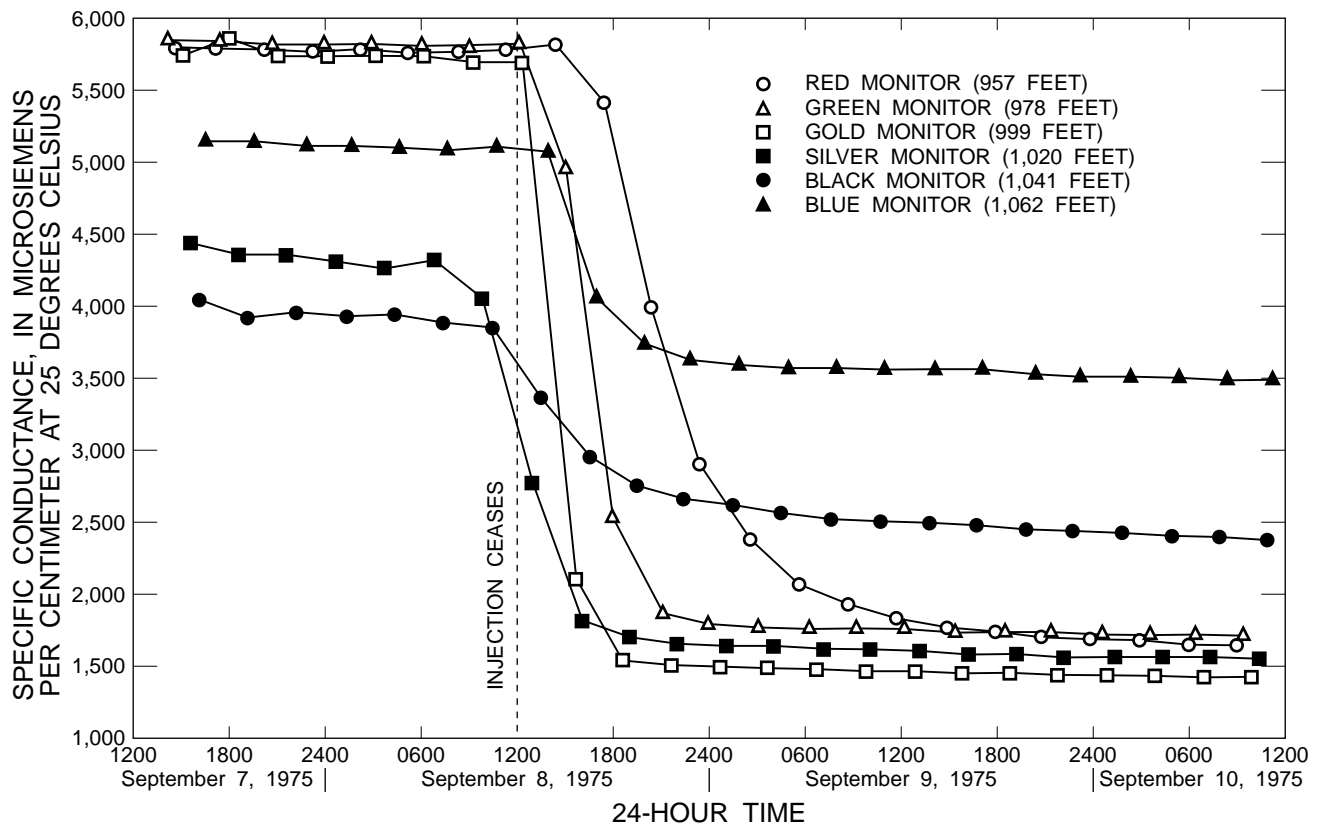
Figure 13. Automatic sampler-recorder data indicating freshening of water from monitor tubes after the first injection.

Later in the ASR cycles, the least saline water tended to be pumped from the silver and black monitors, which are the ones closest to the flow zone (pl. 1). Blue-monitor samples often were as fresh as samples from higher monitor tubes, apparently as the inflow of injected water and pumping of the monitor tube caused freshwater to move downhole. However, during storage and recovery periods, blue-monitor samples often became more saline, possibly as more saline water seeped into the well from surrounding rocks at the bottom of the well, displacing freshwater rising upward by buoyancy. This phenomenon was repeatedly reversed, possibly as a result of variation in the amount of pumping for water samples, and ceased to occur to any significant degree late in the third recovery, when water in the flow zone approached native-water salinity and the salinity contrast was reduced.

That water from all monitors late in the third recovery approached the flow-zone chloride concentration of 1,200 mg/L is further validation that water in the flow zone was appreciably less saline than that sampled from the 840-ft monitor tube. Although the salinity of water from the 840-ft zone (pl. 1) showed some irregularities that do not seem related to the ASR cycles, the salinity of water from this monitor zone remained consistently higher than that of water from all lower monitoring zones.

Dispersive Properties of Aquifer Material

The degree to which injected water mixes with the native brackish water is a key factor determining how much usable water can be recovered after sub-surface storage. The mixing process is referred to as dispersion or dispersive mixing. Concepts related to dispersive mixing in radial flow from wells are developed by Hoopes and Harleman (1967). Dispersion concepts are discussed by Merritt (1985) in relation to modeling ASR cycles in the Upper Floridan aquifer.

Hydrodynamic dispersion is a term that represents the combined effects of molecular diffusion and mechanical dispersion. The concept of mechanical dispersion was formulated in the context of porous media and postulates that, because the myriad pathways through connected pores differ in size and tortuosity, radially oriented fluid movement in some will be retarded or accelerated in comparison with others. Therefore, in radial flow from an injection well, water particles will not have uniform outward speed, and in the vicinity of the interface separating injected and native water, some connected pore channels will have been flushed with the injectant, but others will still contain native water. Therefore, on a spatially averaged basis, there is a spreading, or dispersion, of the interface. Reeder and others (1976) use a simplified version of the formula derived by Hoopes and Harleman (1967) to represent the relative proportions of injected and native waters within the dispersed interface, written as

$$C/C_0 = 1/2 erfc\left[\frac{r-R}{(4/3\alpha_l R)^{1/2}}\right] \quad (5)$$

where: erfc is the complementary error function,
  α_l is longitudinal dispersivity (L),
  C/C_0 is a unitless fraction having values ranging from 0 to 1 representing the relative concentration at radius r of some tracer present only in the injected water, and
  R is defined by $V = \pi\theta hR^2$ (θ is aquifer porosity and h is the thickness of the injection zone).

R would be the precise radius of the injected water body if there were no dispersion. This approximation (eq. 5) is valid at large radii R and where $r \simeq R$ (in a relatively small interval surrounding the midpoint R) and assumes that molecular diffusivity is negligible in a vertically uniform aquifer. The width of the transition zone depends on the value of longitudinal dispersivity (α_l). Thus, fitting the formula to observed breakthrough data (concentration values showing the passage of a dispersed interface past an observation well) can be a method of deriving a dispersivity value from field measurements (Ehrlich and others, 1979).

Data from the very rapid apparent breakthrough at the observation-well silver monitor on September 8, 1975 (fig. 13), hours after the first injection ceased, were fitted to equation 5 for an estimate of α_l. Assuming isotropic flow in a 12-ft flow zone, an injection rate of about 80,000 cubic feet per day (ft³/d) on September 8, 1975, and porosity of 35 percent, the rate of radial flow from the injection well would be 10.48 feet per day (ft/d) at a 289-ft radius, the distance to the observation well. The concentration of injected water within the silver-monitor sample was estimated to be 11 percent at 0955 hours and 50 percent at 1242 hours, during which time the front would have moved 1.22 ft. Setting

$$0.11 = 1/2(1 - erf)\left(\frac{1.22ft}{(4/3\alpha_l 289ft)^{1/2}}\right) \quad (6)$$

α_l resolves to be 0.0072 ft. This value is about 3 or 4 orders of magnitude less than customary estimates of longitudinal dispersivity in large-scale tracer movement in aquifers and is, therefore, subject to considerable skepticism. In fact, it is highly unlikely for the breakthrough to have coincidentally occurred within hours after an arbitrary decision to halt injection had been implemented. Whether or not such a breakthrough could occur after injection stopped, given assumed hydrogeologic conditions, is another question subsequently considered as part of the modeling analysis.

Interpretation of Observation-Well Salinity Changes During the Three Test Cycles

Another curious aspect of the breakthrough data was the inconsistency of the apparent arrival time in the first cycle with the description of the flow zone based on evidence provided by the geophysical logs. Assuming planar isotropy, the hypothetical radius of the injected water body after 53 days of injection at an average rate of 105,661 ft^3/d (549 gal/min) can be estimated from the relation

$$V = \pi r^2 \theta h = Qt \qquad (7)$$

where: V is the volume injected (L^3);
  r is the radius (L) of the injected water body at time t, ignoring dispersion;
  θ is aquifer porosity (unitless);
  h is aquifer thickness (L);
  Q is the average injection rate (L^3/T); and
  t is the time (53 days).

Assuming that q was 35 percent and aquifer thickness h was 12 ft, the radius of the injected water mass at 53 days should have been 651.5 ft. A 53-day radius of 289 ft could be achieved only by assuming a flow-zone thickness of 61 ft (35 percent porosity) or 32.8 ft (65 percent porosity). Both scenarios are very unlikely, given the evidence of the geophysical data. Assuming planar isotropy and nominal parameters of h = 12 ft and q = 35 percent, the theoretical volume injected when the freshwater radius reached 289 ft was 1,102,033 ft^3. As shown in the list of Appendix C, this volume was injected by day 8 of the first injection.

To better understand this anomaly and better visualize salinity changes in the observation well during the first and second injections, the manually collected samples shown in plate 1 are enlarged in figure 14 for the injection period and the period immediately following. Water samples collected from the silver and black monitors during the first injection show three periods of rapidly decreasing chloride concentrations before the end of the first injection. This raises the possibility that water in the observation well might have contained some injected water long before the end of the cycle. In fact, the first of the three periods of decreasing chloride concentrations falls between 6 and 12 days, close to the hypothetical arrival time of 8 days.

The salinity contrast showing breakthrough during the second and third injections was reduced because of the presence at the observation well of a residual amount of freshwater from the previous ASR cycle. Large salinity fluctuations in monitor-tube samples occurred during the second injection, as in the first. Immediately following the end of the second injection, there was a substantial lowering of chloride concentration in all monitor tubes (to 100 mg/L at the silver monitor) similar to that following the end of the first injection. However, assuming horizontal isotropy, the theoretical arrival time at the observation well (when 1,102,033 ft^3 has been injected) would have been January 12, 1976, after 7 days. Because the first observation-well sampling was on January 12, no data describing water quality in the observation well in the first 7 days of the second injection are available. Samples from the silver monitor tube showed a slight salinity decrease from 700 to 500 mg/L in chloride concentration almost immediately after the beginning of the third injection, between the second and ninth days, when samples were collected. The theoretical arrival time again should have been about 7 days, and the observed decrease may have indicated arrival of the injected water.

If the weak evidence of 7- or 8-day breakthrough times in the first and third cycles is rejected, at least two hypotheses can be postulated to explain inconsistencies between observed arrival times and the conceptual model formulated on the basis of geophysical logging. The first hypothesis is that the aquifer is horizontally anisotropic. The estimated direction of flow in the Upper Floridan aquifer at Hialeah is almost due east (fig. 5). The observation well is north-northwest of the injection well nearly at a right angle to the estimated regional flow direction. If solution porosity features have developed that favor aquifer flow in the direction of the regional gradient, horizontal anisotropy would exist, and the observation well would lie
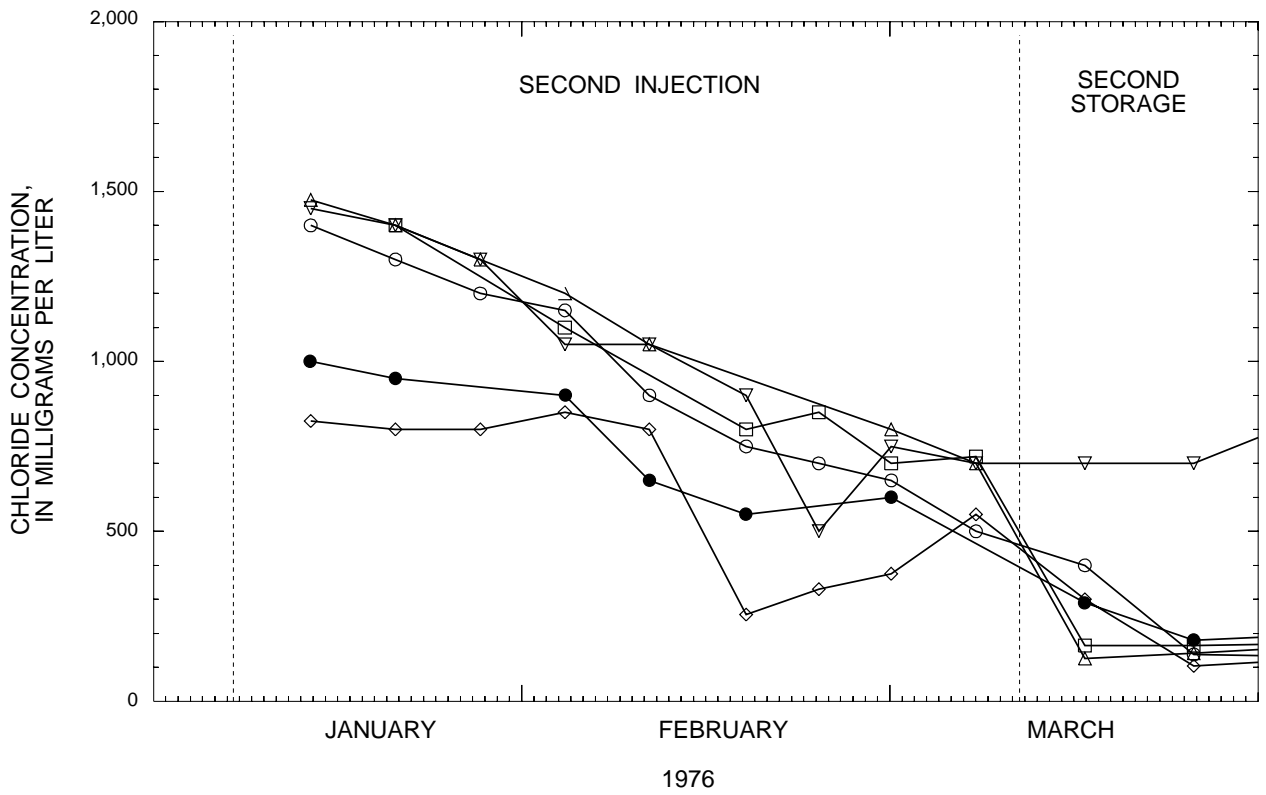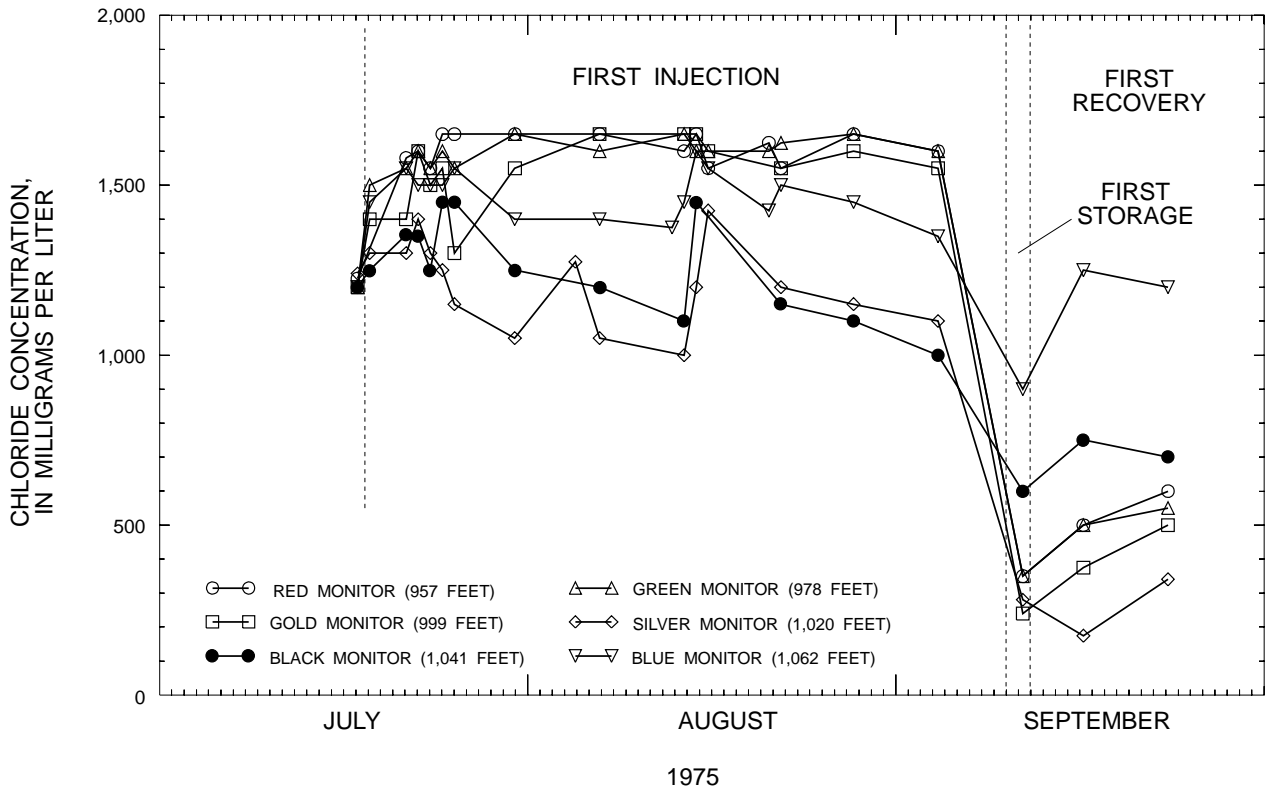
Figure 14. Chloride concentrations from observation-well monitor tubes during and after the first and second injections.

in a direction from the injection well in which the aquifer had less permeability than in the direction of the regional gradient. The flow of injected freshwater in the direction of the observation well would be slower than predicted by the isotropic conceptual model. The observed pressure at the observation well would be less than that at an equal distance in the preferred flow direction, leading to an erroneous interpretation of the aquifer-test data unless anisotropy was assumed in the analysis.

Another hypothesis is that the breakthrough data are misleading because of complex and poorly understood hydraulic properties of the aquifer in the vicinity of the observation well. The principal flow conduits might bypass the well, and complex solution features might permit the full interception of injected-water flow only after the injection pressure gradient ceases or after an extended period of time.

The latter hypothesis illustrates limitations that apply to the application of porous-media concepts of transmissivity and mechanical dispersion to secondary-porosity carbonate aquifers. The chloride concentration increases during the three recoveries were gradual, suggesting a dispersivity of many tens of feet. However, dispersivities of this magnitude may represent a more complex set of processes than considered in the development of the mechanical dispersion concept for porous media. Flow of injected water may be partly confined to an interconnected series of major and minor conduits, and mixing may occur, in part, as seepage of native water from the rock surrounding the conduits. The dispersion represented in the simulations of salinity increases during recovery, therefore, may be a representation of aquifer flow and mixing processes on a larger scale than implied by the uniform porous-media concept of solute transport. Hydraulic conductivity and dispersivity estimates may be inadequate to describe fluid movement and mixing at an isolated point, such as the location of the observation well at the Hialeah site.

Regional Flow at the Hialeah Site

An understanding of the velocity (speed and direction) of flow in the Upper Floridan aquifer in the vicinity of the Hialeah ASR site is helpful because background (regional or manmade) hydraulic gradients can substantially affect the recoverability of freshwater stored underground (Merritt, 1985). The regional gradient and the flow-zone hydraulic conduc-

tivity, thickness, and porosity determine the rate at which injected freshwater drifts downgradient, generally to the east. Thus, the influence of background gradients must be considered in the computer simulation of recovery salinity changes.

Figure 5 shows the estimated potentiometric surface and corresponding flow directions in the Upper Floridan aquifer in May 1980. The potentiometric surface in the southern part of the peninsula in the 1974–80 time period of the ASR cycles would be similar because the native water is not potable, and the only known manmade influences at that time were flowing wells located at some distance from the ASR site. Because these wells had been flowing for many years, a hydraulic equilibrium probably would have been established.

The potentiometric contours shown in southern Florida (fig. 5) are largely inferred on the basis of widely scattered data from wells containing waters of varying density. Subject to this qualification, it seems that flow in the Upper Floridan aquifer in the vicinity of Hialeah, a northwestern suburb of Miami, is maintained by an eastward hydraulic gradient of about 10 ft in 25 miles (mi), or about 0.4 ft/mi. Earlier estimates ranged from 0.1 to 0.22 ft/mi but were revised on the basis of new data and reinterpretation of data from wells in central Florida (Meyer, 1989a).

Hydrogeologic Conditions at Other Sites of Aquifer Storage and Recovery Tests

Some corroboration for the analysis of hydrogeologic conditions at the Hialeah ASR site can be obtained from a survey of data from other ASR sites where similar technical objectives dictated collection of similar types of data. The following sections present a partial evaluation of data from the town of Jupiter site and the St. Lucie County site.

Town of Jupiter Site

Tests of the subsurface storage and recovery of freshwater were performed from September 1973 to October 1976 for the Florida Department of Natural Resources at Jupiter in Palm Beach County (fig. 1, site 4). The data set collected at the Jupiter ASR site has been largely lost except for an unpublished executive summary report prepared for the Florida Department of Natural Resources by J.J. Plappert in February 1977, and suites of geophysical logs run at various times by the FGS and the USGS. The

geophysical data have not been previously published, and it was considered worthwhile to reproduce several logs for inclusion in this report.

The flow zone used for ASR cycles at the Jupiter site was found within the Avon Park Formation at about 1,220 ft. This conclusion was based on an analysis of caliper (January 30, 1975) and spinner flowmeter (July 25, 1974) logs run in the injection well by the FGS (fig. 15). Quantitative analysis of the flowmeter data was as previously described for the flowmeter data from the Hialeah site, but the diameter compensation was complicated in this case by the high rugosity of the borehole. The borehole flow, expressed as a percentage of that in the casing, is seen in figure 15 to have been generally uniform at 100 percent to a depth of 1,220 ft, below which it quickly diminishes to zero within another 10 ft.

Caliper and spinner flowmeter logs (fig. 16) were run in the observation well by the USGS on December 2, 1975. The borehole was smaller in diameter and less rugose. Results of the analysis suggest that borehole flow diminishes with depth between 1,207 and 1,228 ft, the most marked decrease occurring below a depth of 1,222 ft. Rock samples from the observation well examined by the Florida Bureau of Geology (written commun., 1975) indicate calcareous sandstone from 910 to 990 ft in depth and limestone (calcarenite) from 1,000 to about 1,250 ft in depth, except that the 1,140- to 1,200-ft depth interval is described as a foram-hash limestone. The interval from 1,200 to 1,240 ft is described as more porous than the other intervals.

The flow zone at Jupiter is, therefore, similar to the one at Hialeah in that it is also a thin, discrete zone of permeable limestone. The native water was also brackish in quality, having a chloride concentration of about 2,000 mg/L.

St. Lucie County Site

In 1981–83 the SFWMD conducted a single, low-volume ASR test in St. Lucie County (fig. 1, site 3). Results are documented by Wedderburn and Knapp (1983). Data gathered were static and flowing geophysical logs, pump tests of various depth intervals, pressure data at observation wells during ASR tests, and analysis of water-quality field parameters during recovery. The volume of injection was insufficient for the injected water to reach the observation well. Plans for further testing were canceled when analysis of results of the first test indicated that costs

for recovered water were not competitive with current costs for domestic and irrigation water, and that available water for injection was of relatively poor quality because of its high dissolved-solids concentration.

Analysis of rock samples and spinner flowmeter data (Wedderburn and Knapp, 1983, p. 22) indicates appreciable quantities of flow originating from thin, discrete zones at formation contacts at depths of 650 ft (Suwannee-Ocala contact) and 740 ft (the Ocala-Avon Park contact), and small contributions of flow from four other discrete zones extending to a depth of 1,000 ft. The rock type generally was limestone (calcilutite) in elevations near the principal flow zones. However, the major flow zone at a depth of 750 ft approximately corresponded in elevation to a thin bed of dolomite. Coarse phosphate was present (about 15 percent) in an interval of high gamma counts above a depth of 650 ft. Below 800 ft are alternating beds of calcilutite, dolomite, and calcarenite. Water from the flow zones was brackish, with chloride concentrations ranging from 800 to 1,000 mg/L. The St. Lucie County data support the general conclusion that zones of significant permeability within the Upper Floridan aquifer, and potential zones for ASR, occur as discrete permeable zones often not much more than 10 ft thick.

Regional Extent of a Potential Aquifer Storage and Recovery Zone

In the present section, data from other ASR test sites and selected non-ASR site locations are considered for the more specific purpose of providing evidence for the existence of one areally extensive, brackish flow zone of moderate permeability. Besides its potential for ASR use, such a zone could also have potential for withdrawal of water to supply reverse-osmosis plants or to be used for blending with fresher water.

Some indication of the areal occurrence of a permeable zone containing brackish water in southeastern Florida can be gained by examination of natural gamma logs and related flow information from six locations (fig. 17) in southeastern Florida (section X-X' in fig. 1). These logs and others, shown later in the report, were digitized using a point cursor. At a certain depth, each log shows an interval of low natural gamma activity overlain by an interval of intense natural gamma activity.
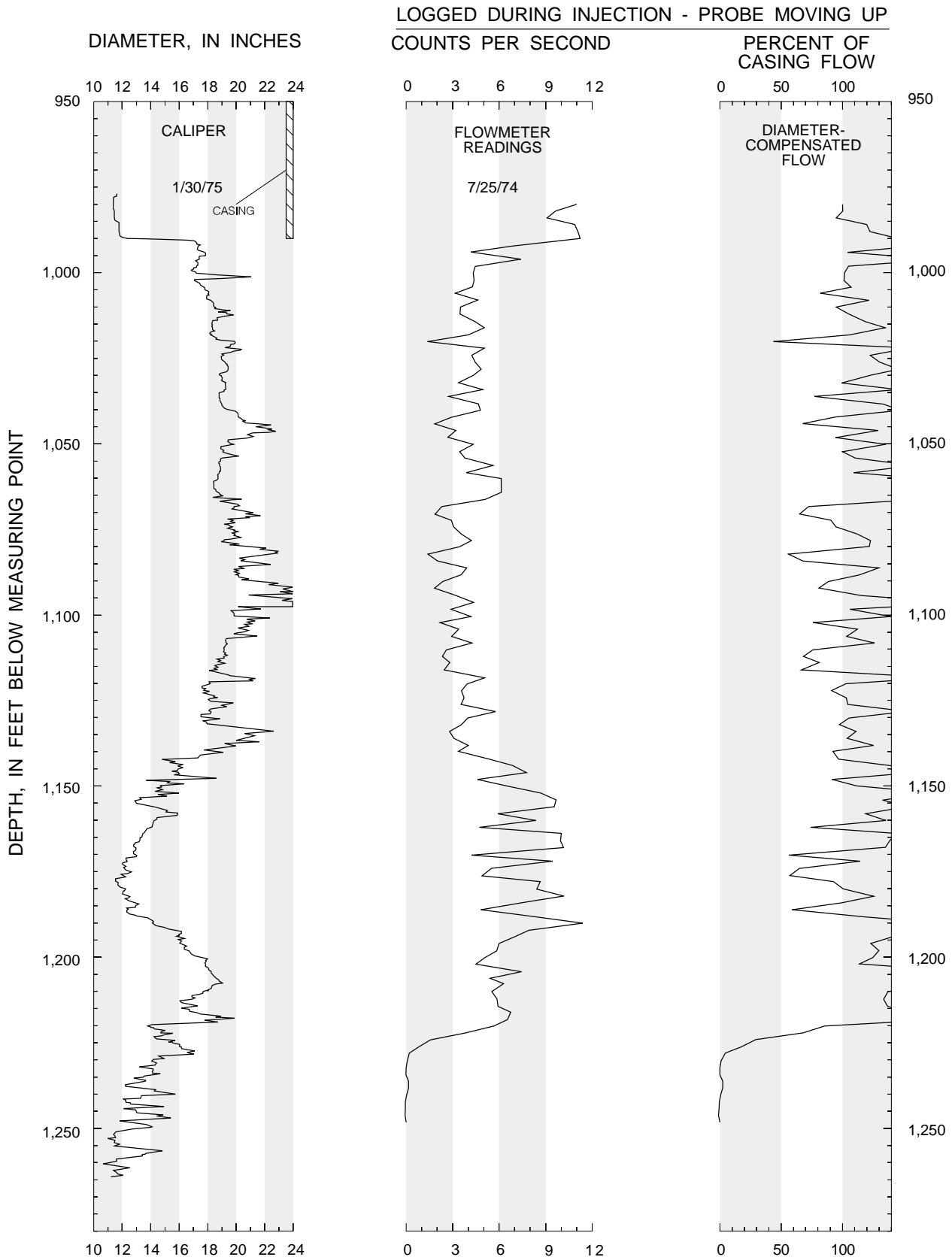
Figure 15. Results of analysis of data from spinner flowmeter logging of the injection well (PB-747) at the Town of Jupiter site.
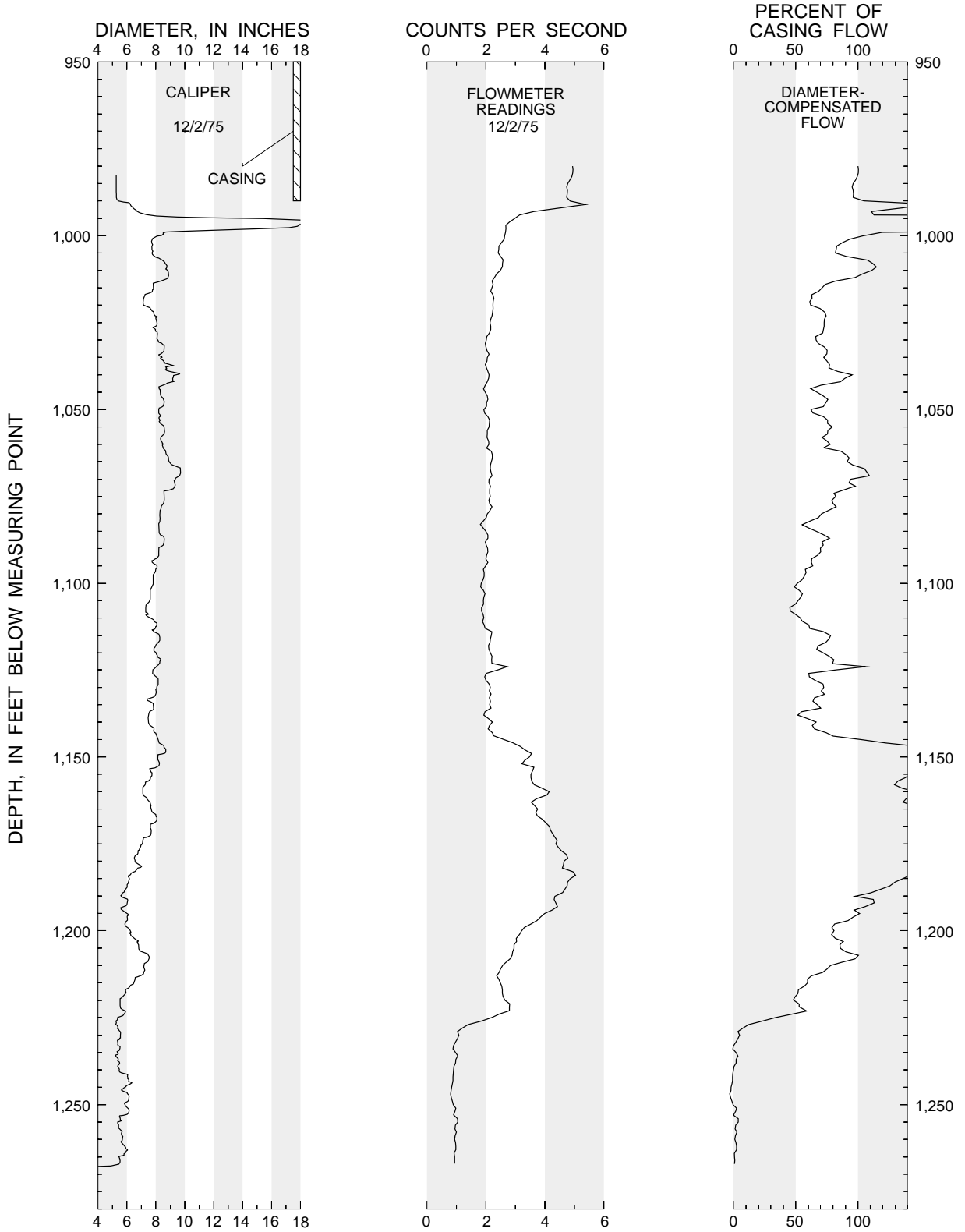
Figure 16. Results of analysis of data from spinner flowmeter logging of the observation well (PB-1145) at the Town of Jupiter site.

Figure 17. Natural gamma logs from selected Upper Floridan aquifer wells in southeastern Florida and elevations of known flow zones.

The high natural gamma activity usually is considered to be caused by the presence of phosphatic material containing traces of uranium. The underlying interval of low natural gamma activity is considered by some investigators to coincide with the top strata of Eocene age (the Ocala Limestone where present or the Avon Park Formation where the Ocala Limestone is absent). A clear example of this natural gamma contrast is presented by Meyer (1989a, p. 13), who correlates it with his determination of the Oligocene-Eocene contact in the Alligator Alley test well (Meyer, 1989a) near the Broward-Collier County line (fig. 1, site G).

At the site of the Florida Power and Light observation well D in undeveloped north Key Largo, Monroe County (fig. 1, site B), the interval of high natural gamma activity shown by the USGS log of October 19, 1975, is centered at a depth of 1,100 ft, and gamma activity decreases substantially with greater depth. A similar high-low activity contrast is found at a depth of 1,260 ft in the Florida Keys Aqueduct Authority reverse-osmosis supply well in Marathon (fig. 1, site D), as shown by the USGS natural gamma log of October 16, 1977. No flow information is available from well D, in which the casing extends to a depth of 1,425 ft. However, data from two reverse-osmosis plant supply wells a few miles to the southwest (fig. 1, site F) at the Florida Keys Aqueduct Authority Water Plant in the town of Key Largo (USGS natural gamma and flowmeter logs of October 16, 1975, and flowmeter log of June 14, 1978) and at a USGS test well in John C. Pennekamp State Park, just to the north of the town of Key Largo (USGS natural gamma log of October 16, 1975, and drillers log), show producing zones associated with intervals of high gamma activity centered at depths of 1,190 and 1,200 ft, respectively, that seem to correlate with the 1,100-ft depth interval in well D. However, the Florida Keys Aqueduct Authority and USGS wells were not sufficiently deep for the natural gamma logs to show an underlying interval of low gamma activity. A sample description (CH$_2$M HILL, Inc., written commun., 1974) picks a depth of 1,150 ft as the top of the Eocene in well D. Harbans Puri (FGS, written commun., 1965) picks a depth of 1,034 ft as the top of the Eocene in the USGS test well, which is at variance with the other finding. Water-quality data from the three wells indicate chloride concentrations ranging from 2,200 to 3,300 mg/L.

The recently plugged Grossman well was located in the Chekika State Recreation Area in central Dade County (fig. 1, site A). A sample description by L. Jordan (Sun Oil Company, written commun., November 1944) picks the top of the Eocene at a depth of about 1,150 ft; however, Jordan admits some uncertainty about the pick. Three series of readings from the stationary spinner flowmeter logs run by the FGS on June 11 and August 15, 1969, indicate a depth interval of 1,180–1,200 ft to be the sole flow-producing zone. The natural gamma log by the SFWMD shows the high-low gamma contrast at a depth of 1,170 ft.

At Hialeah the major receiving zone for injected freshwater was shown to be approximately between 1,024 and 1,036 ft in depth, and a depth of 1,045 ft was considered the approximate top of the Eocene. Thus, the flow zone at the three locations so far considered is approximately coincidental with the erosional surface of the Ocala Limestone or the Avon Park Formation as identified by several investigators. Both the Grossman well and the Hialeah ASR well produced water with a chloride concentration of about 1,200 mg/L.

A test well was recently drilled for the city of Hallandale in Broward County (fig. 1, site C) to determine whether a source of brackish water could be found for use by a reverse-osmosis plant. The plant is needed to augment supply from the municipal well field, which will soon be abandoned because of saltwater intrusion from the ocean. As in the other wells, a major flow zone was found just below the high-low gamma contrast at a depth of about 930 ft. Lithologic data are not presently available to verify that this elevation is coincidental with the top of the rocks of Eocene age. Other data indicate that most of the flow occurs at a depth of 935 ft, and an abrupt shift on a temperature log run during flow indicates that inflow at that elevation is anomalously warm compared with that from below. The chloride and dissolved-solids concentrations of water flowing from the well were 2,100 and 4,500 mg/L, respectively. These values are higher than those from the Grossman and Hialeah wells, possibly because the site is so close to the formation subcrop at the continental shelf about 3–4 mi east of the Atlantic coast.

At Jupiter, geologic sample descriptions provided by the FGS (written commun., 1974) pick the top of the Ocala Limestone at a depth of 1,060 ft in the injection well (no samples below 1,100 ft) and at a depth of 1,120 ft in the nearby observation well. A

pick of 970 ft in depth would correlate better with the top of the part of the natural gamma log run by the FGS on January 30, 1975 where low gamma activity occurred. However, the principal flow zone was found below a depth of 1,200 ft. Because the casing was set at a depth of 990 ft, if a flow zone existed near the elevation of the interval of contrasting gamma activity, it could have been cased off and remained undetected.

The top of the Ocala Limestone in the St. Lucie County ASR well was identified to be at a depth of 660 ft, and the top of the Avon Park Formation to be at a depth of 760 ft. The two depths correspond closely with the two principal flow zones identified with spinner flowmeter logging (Wedderburn and Knapp, 1983, p. 22), and the upper depth corresponds with a sharp reduction in gamma activity (fig. 17; Wedderburn and Knapp, 1983, p. 15). The well extended to a depth of 1,000 ft, but only minor amounts of flow occurred below 770 ft in depth. Water from the principal flow zone at a depth of 760 ft had a chloride concentration of about 900 mg/L.

On the basis of limited but relatively consistent evidence, it seems that formation contacts at the surface of rocks of Eocene age (the Ocala Limestone where present, or the Avon Park Formation) are the most probable depth intervals for the occurrence of permeable zones containing brackish water suitable for temporary storage of freshwater. A significant correlation exists between the elevation of the surface of rocks of Eocene age and the position of a sharp contrast in natural gamma activity (high above, low below) found in natural gamma logs at widely scattered locations along the southeast coast.

DIGITAL SIMULATION OF RECOVERED WATER QUALITY

The following sections begin with a description of the selection of a simulator and the selection of some parametric coefficients to represent aquifer characteristics based on data acquired at the Hialeah test site. A hydraulic calibration of the simulator is accomplished by a replication of data acquired during the aquifer test at the site. This is followed by a solute-transport simulation in which chloride increases during recovery are replicated by further calibration. Then various problems are considered that are related to the lack of accuracy with which aquifer characteristics are determined on the basis of field data and to the related problem of nonuniqueness of the calibration.

Estimates of multiple-cycle recovery efficiency are then made. The report concludes with a comparison of model-computed solute concentrations with data collected from the observation well.

Simulation Code

The Subsurface Waste Injection Program (SWIP) code, the principal tool of investigation in this study, was developed by INTERCOMP Resource Development and Engineering, Inc. (1976), under sponsorship of the USGS. SWIP was later revised for the USGS by the same firm, renamed INTERA Environmental Consultants, Inc. (1979). Despite its intended use as a special package for waste injection problems, the SWIP code received wider use within the USGS as a general-purpose, three-dimensional simulator of solute and thermal-energy transport in ground water. The application of SWIP in USGS activities has been limited to a few users. A newer code developed by agency personnel, HST3D (Kipp, 1987), incorporated some parts of the SWIP code with adaptation. Outside the agency, the SWIP code has been adapted for special purposes by various public and private organizations.

Absolute pressure is the independent variable of the flow equation, and the model accounts for fluid density and viscosity dependence on temporal changes of pressure, temperature, and solute concentration. Solution of equations for flow and both solute and thermal transport is by standard finite-difference techniques, in which backward and central differencing in time and space are available as user options for solution of the solute- and thermal-transport equations. A Gaussian elimination technique is used to reduce the solution matrix size that results from coupling of the three equations. The aquifer simulated may be fully confined or have a free surface, and the equations may be solved in either Cartesian or cylindrical coordinates.

Fractional values (C) describe the relative concentrations of two miscible fluids ($C = 0$ and $C = 1$) in the aquifer. Any fluids present within the aquifer or entering it in simulation exercises are considered to be mixtures of these two fluids by the appropriate specification of C values. This approach works well for the problem of simulating the mixing of waters of different salinities that was a purpose of this study. $C = 0$ was used to represent pure freshwater, and $C = 1$ represented the most saline water residing within the aquifer or entering it as an influx. Injected water, the salinity of

water in some parts of the aquifer, and water in mixtures of injected and native waters were assigned or were computed to have C values that described their salinity relative to the two extreme salinities. Values of density are associated by SWIP with the extreme values of solute fraction ($C = 0$ and $C = 1$) and are used in calculations of flows driven by density gradients and in adjusting hydraulic parameters.

A more comprehensive description of the SWIP code, with reference to its application in ASR cycle modeling, has been provided by Merritt (1985). In 15 years of using the SWIP code, the author has made a number of modifications to adapt it to various applications. Most modifications have been nonmathematical in nature, and those that are revisions or extensions of the mathematical procedures of the 1979 version of SWIP have been coded as options to preserve the original solution methodology for use when needed. This study required the use of modifications affecting the computation of advective and dispersive fluxes of solute. A description of the original and experimental algorithms and their effect on computations is documented separately (Merritt, 1993), and a summary is presented later in this report.

Design of Hialeah Aquifer Storage and Recovery Simulator

The selection of parameter values and computational methods, the design of the grid, and the assignment of boundary conditions of pressure and solute fraction are described in the following sections. The rationale for design and value selections is explained, as is their basis in available data. The result of this process of selection is completion of the design of a simulator in which the process of injection, storage, and recovery of freshwater is represented, which can be used for a simulation of the salinity of the water recovered during the withdrawal stage. The substantial database acquired at the data site is used both in designing the simulator and in providing comparison data for the simulation of changes in the salinity of the recovered water.

Fluid Density and Viscosity Representation

The fluid densities assigned to injected and native waters were based on the measured or estimated concentration of dissolved solids in each fluid. Direct measurements of density were not considered to have adequate accuracy. The simulator required a density value to be associated with a solute fraction of $C = 0$,

which was selected to represent pure water (zero dissolved solids). The assigned density of 62.3046 pounds per cubic foot (lb/ft^3) at 21 °C and atmospheric pressure were obtained from a standard handbook. Isothermal conditions at 70 °F (21.1°C) were assumed to prevail in all simulations on the basis of the preinjection temperature log in the observation well (fig. 8). Injected-water temperatures (fig. 12) ranged between 21.5 °C and 27 °C, but any effects of injecting somewhat warmer water were ignored. Values of density at 15 °C corresponding to various salinities were obtained from standard tables and were converted to 21 °C values by the factor 0.998892, the ratio of the densities of pure water at 15 °C and 21 °C. Measured injected-water dissolved-solids concentrations were about 400 mg/L, and the measured dissolved-solids concentrations of preinjection water samples from the injection zone were about 2,700 mg/L. As previously shown, water in the center of the flow zone may have been less saline, and water above and below more saline, than this composite value, but the composite value was assigned uniformly to the entire flow zone.

A solute-fraction value of $C = 1$ was associated with the most saline water in the aquifer, that in the relatively impermeable parts of the injection zone. The dissolved-solids concentration was estimated to be about 6,000 mg/L (about 20 percent greater than the average dissolved-solids concentration of samples from the 840-ft monitor tube). The corresponding density was 62.5414 lb/ft^3. Solute-fraction values of 0.0667 and 0.4500 were then assigned to the injected water and flow-zone water based on the ratio of dissolved solids to the estimated dissolved solids of the confining-zone water. The average chloride concentration of the injected water was 65 mg/L, and that of the flow-zone water was 1,200 mg/L. Computing the proportion of injected water in a mix of 250-mg/L chloride concentration to be 0.8370, the dissolved-solids concentration is estimated to be about 775 mg/L, using the injected- and native-water dissolved-solids values given in the previous paragraph. The corresponding solute fraction is 0.1292, and this was the maximum value of potability used in simulations in which recovery efficiency was computed. In similar fashion, chloride concentrations of recovered water were related to equivalent dissolved-solids concentrations and solute fraction for comparison with solute fraction of recovered water computed by the model.

The viscosity of injected and native waters is assumed by SWIP to vary with temperature and solute fraction. Because isothermal conditions at 21 °C were assumed to prevail, because the density contrast was low, and because viscosities of freshwater and seawater differ by only 0.06 centipoise, viscosity was assumed invariant in simulations. The assigned value of viscosity was 0.98 centipoise, the viscosity of pure water at 21 °C. The temperature of injected water ranged as high as 27 °C, at which the viscosity of injected water would have been 0.86 centipoise. Values of hydraulic conductivity in the freshwater bubble, inversely proportional to viscosity (INTERCOMP Resource Development and Engineering, Inc., 1976), would increase by as much as 14 percent. However, the simulated transport of injected freshwater was not affected by small variations in hydraulic conductivity, and simulation of viscosity variations would have been cumbersome and would have had little effect on the results.

Grid Design and Boundary Conditions

Because vertical flows caused by buoyancy stratification within the flow zone during storage might prove to have some influence on recovery efficiency, despite the low density contrast, the flow zone was discretized into six 2-ft-thick layers for calibration. Overlying and underlying relatively impermeable parts of the injection zone (the confining zones) were each represented as three layers. The layers immediately adjacent to the injection zone were thin (0.5 ft) in order to minimize the effect of the large ratio of flow-zone to confining-zone hydraulic conductivities on vertical advective flow approximations. The vertical grid discretization is shown in figure 18.

A selection of Cartesian or cylindrical coordinate systems needed to be made for the horizontal discretization in the horizontal plane. Cylindrical coordinates are well suited to problems of radial flow from wells, and solution of the equations is computationally more efficient than when using Cartesian coordinates. However, downgradient advection caused by a regional flow gradient was considered to be a likely factor explaining the quality of recovered water observed in the ASR cycles, and downgradient advection could not be represented in cylindrical coordinates. In addition, the possibility that aquifer flow was anisotropic in the horizontal plane was a hypothesis considered as an explanation of breakthrough data at the observation well and also could only be simulated in a Cartesian system. The Cartesian grid in the horizontal plane used for calibration is shown in figures 18 and 19.

The fine detail of the grid immediately surrounding the injection well cannot be shown clearly in the small-scale illustration of the 40,050-ft square horizontal grid mesh (fig. 18) but is shown in the middle-scale (7,050×5,050 ft) and large-scale (1,550-ft square) depictions of the inner mesh (fig. 19). The horizontal grid dimension of 43×31 is greater in the x-coordinate direction because regional flow is represented as occurring in this direction, taking advantage of special SWIP coding designed to represent regional flow. This coding provides for automatic modification of both initial pressures and specified pressure boundary conditions. Simulations of anisotropy assume the preferred flow direction to be along the x-coordinate axis; therefore, finer x-coordinate grid definition farther from the well is also needed for anisotropic simulations.

Placing the model boundaries at some distance from the region of freshwater movement confines solute movement to the center of the grid and enables constant-pressure boundary conditions to be used as an adequate approximation to actual conditions, in which a slight pressure change would occur at the boundaries during injection and withdrawal. A Theis equation calculation for an injection rate of 150,000 ft^3/d, a transmissivity of 9,600 $[(ft^3/d)/ft^2]ft$, and a storage coefficient of 2.75×10^{-4} indicates a hydraulic-head increase of 3.9 ft at the boundary after 100 days of injection. However, the known injection and withdrawal rates and estimated aquifer storage properties were the controlling factors on injected-freshwater movement, rather than transmissivity or boundary specifications.

Grid-cell dimensions in the region of freshwater movement ranged from 50 to 100 ft near the well to 250 ft farther from the well. The greatest distance in the positive x-coordinate direction reached by a 50 percent mix of injected and native waters in isotropic analyses was column 34 (x-dimension 250 ft). The injection- and observation-well nodes are both in column 22 and are five grid nodes apart (fig. 19, rows 12 and 17), providing sufficient discretization between the wells to accurately represent the hydraulic response at the injection well in simulations of the aquifer test of February 10, 1975. In some later analyses, where heads and solute fractions at the observation well were unimportant, the interwell grid definition was reduced so that the horizontal grid dimension of the model was 43×29. In special analyses designed to test various numerical approximation algorithms and value selections, the vertical discretization was enhanced, and the horizontal discretization (described in detail below) was in cylindrical coordinates.

VERTICAL DISCRETIZATION
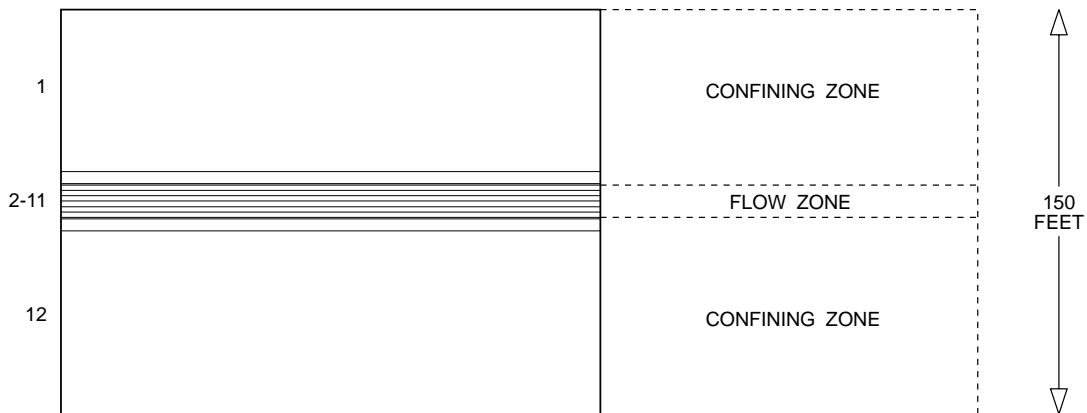
HORIZONTAL DISCRETIZATION
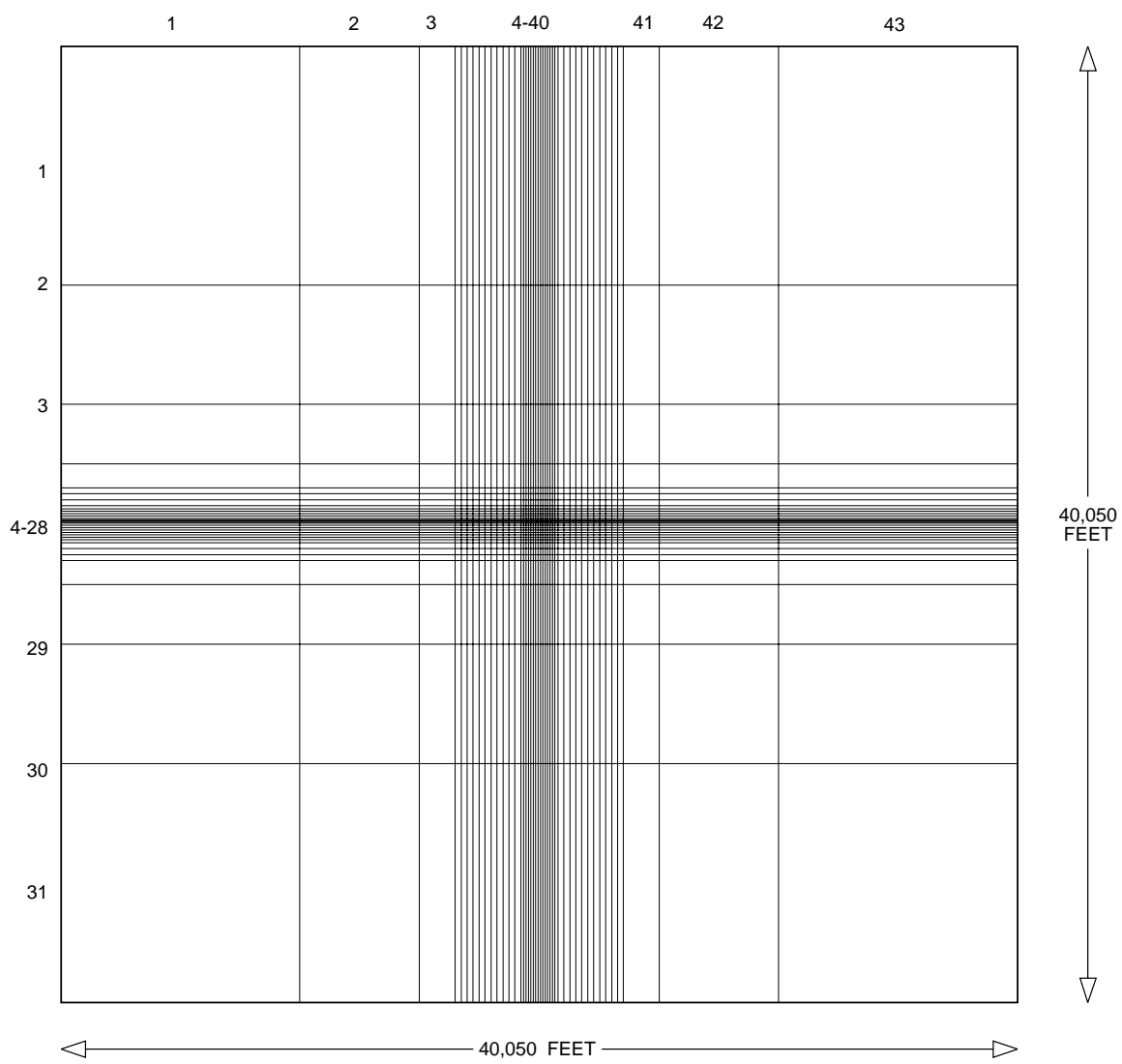
Figure 18. Vertical and horizontal discretization of the model grid used for the simulation of injection, storage, and recovery of freshwater at the Hialeah site.
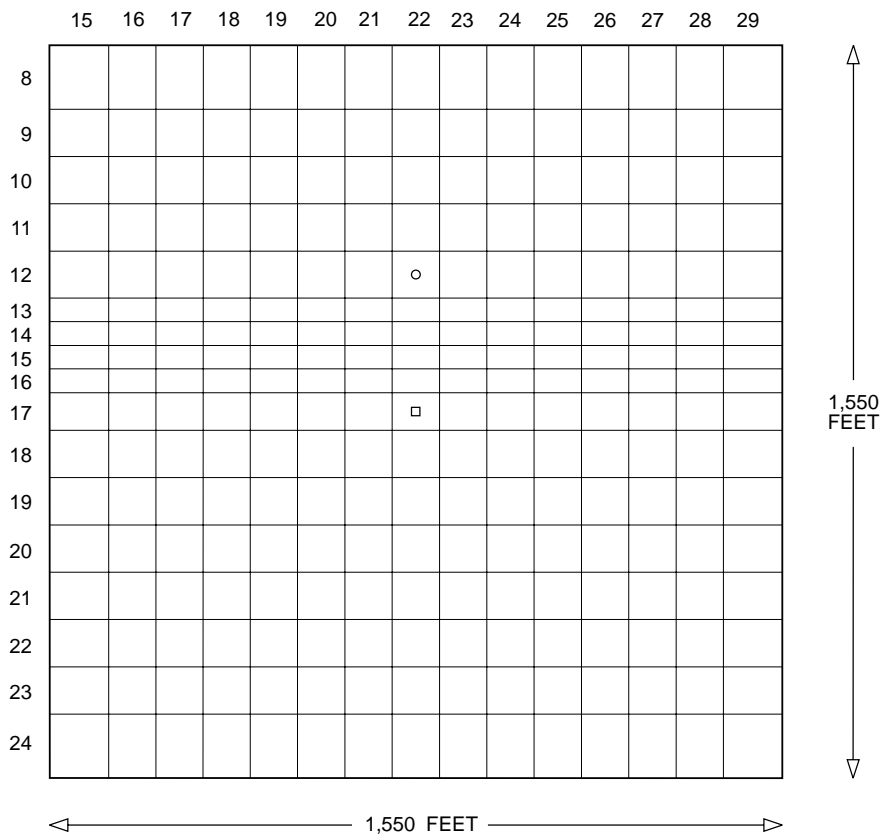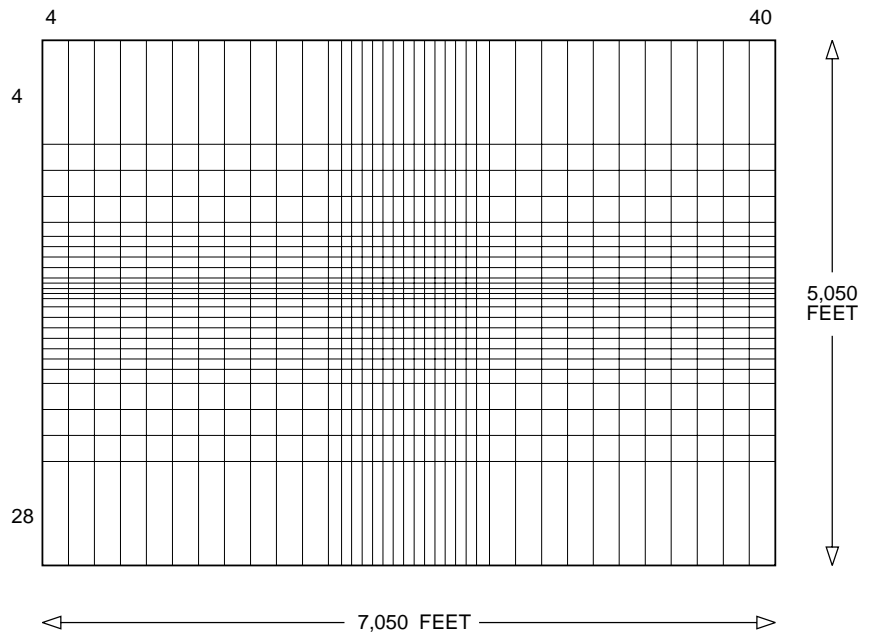
Figure 19. Horizontal discretization of larger and smaller areas surrounding the injection and observation wells within the model grid used for the simulation of injection, storage, and recovery of freshwater at the Hialeah site.

Selection of Numerical Computational Methods

Mechanical dispersion in the three coordinate directions at nodal locations is computed by the SWIP code as a function of the solute-concentration gradient, the total local fluid velocity (u), the angle of the velocity vector with respect to the coordinate directions, and longitudinal and transverse dispersivities (α_l and α_t, [L]) that specify the degree of dispersion both in the direction of flow (α_l) and perpendicular to the direction of flow (α_t). Molecular diffusion, computed as a function of the molecular diffusivity and the solute-concentration gradient, contributes additional dispersion, which in the direction of flow in large-scale grids is usually negligible in comparison with mechanical dispersion. The effect of both mechanical and molecular diffusion is termed hydrodynamic dispersion.

The numerical approximations used to represent the dispersion of solute and its relation to advective processes can, if improperly used, cause unrealistic solute-concentration values to be computed and can cause a misinterpretation of the hydrogeologic processes that are occurring. The selection of the best approximation method depends on the nature of the physical representation problem. For this reason, users of solute-transport models should consider the proposed selection of numerical algorithm methods and parameter values to determine whether the methods and values will lead to a representation that is physically realistic. Solute-transport simulation efforts often do not provide the resources for such an evaluation to be done, which is unfortunate in view of the critical nature of this aspect of the simulation problem.

The selection of the numerical approximation technique for evaluating the advective terms in the solute transport equation can be made from several optional selections, so these were tested in comparison with one another. Modifications made by the author to the model code include experimental algorithms for the computation of vertical advective and dispersive flux of solute. These new methods were tested in comparison with the original algorithms previously encoded in the 1979 version of the SWIP code.

A full description of the methods and results of the testing were documented by Merritt (1993). The following sections briefly summarize the results of this evaluation, which showed the interrelated effects of vertical mechanical dispersion and molecular diffusion from vertically adjacent confining layers to have a significant effect on the computation of recovery efficiency. This leads to a sophisticated calibration technique that accounts for molecular diffusion into the thin flow zone from overlying and underlying confining layers containing saline water.

Numerical Dispersion and Oscillatory Behavior

The SWIP code requires a user to select between backward and central methods of differencing the finite-difference approximations of the temporal and spatial derivatives in the transport equations. When backward spatial differencing is selected, a degree of first-order error is introduced into the solution that has the appearance of hydrodynamic dispersion. In one-dimensional computations the degree of numerical dispersion introduced into the solution has been shown (Lantz, 1971) to be $u\Delta x/2$, where α is the fluid velocity and Δx is the grid-cell dimension. The apparent dispersivity for the transport computation would be ($\alpha+\Delta x/2$), where α is the dispersivity specified to represent the degree of physical dispersion that occurs. Lantz also shows in the one-dimensional case that backward differencing of the time derivative led to additional numerical dispersion of degree $u^2\Delta t/2\theta$, where Δt is the incremental time step and θ is the effective porosity. Thus, the actual degree of dispersion in the solute-transport solution would seem to be that which would be represented by a dispersivity of ($\alpha + u\Delta t/2\theta$). In higher dimensions the numerical dispersion terms are more complex but continue to influence the apparent degree of dispersion in the solution.

When central differencing in time or space is the selected method, the corresponding finite-difference approximation is correct to the first order, and the first-order numerical dispersion terms are eliminated. Most of the degree of apparent dispersion in the transport solution depends on the dispersivities specified by the user, and is not determined by the local grid-cell size (given sufficiently fine discretization) or by a changing incremental time-step size. The different results obtained by use of the various techniques are illustrated with specific numerical examples in the aforementioned paper (Merritt, 1993). Central differencing techniques were selected for use in this study because it was desired to prevent the occurrence of numerical dispersion that would have been caused by the spatial discretization and time-step sequencing used in the simulations of injection and recovery if backward differencing techniques had been used.

The formulation of the dispersion terms in the SWIP code suggests an interpretation of the dispersion process as an interchange of equal amounts of fluid between adjacent grid nodes, with the fluid received by each having the solute concentration (or fluid mix) of the nodal center of the other cell. Intuitively, this representation may be understood to work best when a region of changing concentration is finely subdivided into many grid cells in the direction of fluid movement. Alternatively, the representation may work best in regions where the spatial variation of concentration is gradual relative to the grid spacing. Similar advisement on finely discretizing the zone of concentration change is offered by Kipp (1987, p. 116–117).

The dispersion representation does not function as effectively when concentration changes are abrupt relative to the grid spacing in the direction of flow. In this case, specification of a large longitudinal dispersivity can cause the computed concentration variation to be distributed over a larger spatial volume than is realistic. Specification of a small longitudinal dispersivity may allow spatial oscillations (caused by the tendency for the solution to overestimate the advective flux of solute between grid cells) to grow in the absence of the smoothing effect of dispersion (the overshoot and undershoot described by INTERCOMP Resource Development and Engineering, Inc.). Spatial oscillations, when using central differences, indicate an incompatibility between the selection of longitudinal dispersivity and the grid dimensions. In some models the range of values that can be assigned to longitudinal dispersivity may be restricted by a coarser than desired grid spacing mandated by the need for computational efficiency. Numerical oscillations at a grid node in sequential time steps indicate an incompatibility between the speed of solute movement and the computational time increment sequence used to simulate it.

Numerical criteria for avoiding oscillatory behavior were developed by Price and others (1966) and are cited in the SWIP code documentation (INTERCOMP Resource Development and Engineering, Inc., 1976) and in the HST3D code documentation (Kipp, 1987, p. 114). The ability to select grid-cell dimensions and dispersivities to realistically portray a zone of concentration change depends upon physical measurements or having some physical concept of the zone of dispersion based on real data, and on having adequate computational resources. In this study, data that explicitly describe the zone of dispersion are scanty, given the ambiguity of the freshwater breakthrough data at the observation well, and the spatial extent of the zone of dispersion can only be inferred on a spatially averaged basis from consideration of the chloride increases observed during recovery.

Experimental Algorithms for Dispersion and Advective Weighting

Transverse dispersivity describes the degree of dispersion in a plane perpendicular to the direction of flow without distinguishing between transverse dispersion within the plane of flow (the bedding plane) or perpendicular to it (dispersion in the crossbed or vertical direction), even though macroscopic hydraulic properties may be different or have different degrees of spatial continuity along the different directional components of fluid flow paths. In media with solution porosity, transverse dispersion may be partly related to the nonlongitudinal orientation of solution features along the flow path, but the extent to which this occurs may not be the same in the vertical direction as within the plane of flow.

When vertically adjacent layers are of different hydraulic conductivity, the more permeable layer may be partially flushed by water having a quality different from that of the other layer. This can occur as a result of flow in the more permeable layer from a recharge area or from an injection well that has not flushed the less permeable zone to a similar extent. Usually the flow direction is nearly parallel to the interface between layers. Because of common data limitations, the vertical transition of hydraulic properties and water quality usually is represented as a step function between adjacent layers of grid cells. In this case, use of central differencing for vertical advective flux of solute across the interface between layers would imply that water flowing across the interface would have a solute composition that is an average of that of the two waters. However, a more realistic conceptual model of seepage flux across the interface is as water having the quality of that in the originating layer. An upstream (backward) advective weighting scheme would seem to be more appropriate.

When vertically adjacent layers contain waters of different quality, the vertical component of dispersion implied by the dispersion algorithm may be inappropriate because the transition of water quality does not occur gradationally across the thicknesses of several grid cells and is nearly perpendicular to the direction of flow. Providing a finer vertical

discretization may not be computationally efficient, and there might not be any available data describing gradational hydraulic and water-quality variations.

Other problems can occur when there is a large difference in scale between the horizontal and vertical dimensions of grid cells. When transport processes occur over distances of several miles in aquifers a few tens of feet thick, computational economy may mandate that the ratio of average horizontal and vertical grid dimensions be as great as 1,000:1. A large longitudinal dispersivity may be required to match the coarse horizontal discretization. However, if small but still appreciable vertical flows occur, a large longitudinal dispersivity may lead to the simulation of a degree of vertical dispersion sufficient to obscure actual vertical variations in solute concentration.

Therefore, to provide the means for more physically realistic simulation of transport processes in the situation described, experimental algorithms for representing vertical advective and dispersive fluxes of solute were encoded as options in the SWIP simulator. The experimental algorithms implement the concepts described in the following statements:

- Mechanical dispersion in the vertical direction is identically zero between adjacent layers of different permeability [$K_x(k) \neq K_x(k-1)$, where K_x is the hydraulic conductivity in the x coordinate direction]. Molecular diffusion between layers occurs as before. Between layers of similar permeability [$K_x(k) = K_x(k-1)$], mechanical dispersion in the vertical direction is scaled by a user-specified factor S ($0 \leq S$).

- Vertical advective flux of solute receives upstream weighting (backward differencing) across the boundary between layers of different permeability [$K_x(k) \neq K_x(k-1)$], regardless of which weighting is used in the rest of the spatial domain of the model.

The experimental algorithms implement the conceptual view that solute flux across the boundaries between layers of different permeability occurs as molecular diffusion or as hydraulically driven seepage in which the water flux has the solute concentration of the source layer. The scaling factor is a user-specified parameter for use in application problems where bedding effects or the discretization may cause incompatibility in the description of horizontal and vertical dispersive processes within a hydraulically uniform layer.

A method of allowing longitudinal dispersivity to have a dependence on the flow direction is documented in the description of the two-dimensional

SUTRA model by Voss (1984). Voss used a relatively fine vertical discretization to provide a cross-sectional depiction of a sharp freshwater-saltwater transition zone parallel to flow lines in a description of the simulation of saltwater intrusion on the island of Oahu, Hawaii (Voss and Souza, 1987). This has some generic similarities to the treatment of the problem described herein, in which the sharp transition in density occurs across flow lines parallel to a confining-zone interface. The use of the approach involving flow-dependent longitudinal dispersivity in a hypothetical cross-sectional model of saltwater intrusion is described in a paper by Reilly (1990).

Results of Testing Algorithms and Parameter Values

The tests of the original and experimental algorithms and parameter value selections consisted of a series of computer runs simulating the first injection of 53 days. A cylindrical coordinate system was used in which horizontal grid dimensions (grid annuli widths) in the region of injected-freshwater movement were less than 80 ft. The vertical discretization depicted in figure 18 was enhanced to illustrate the theoretical variation in the solute-concentration field near the boundary between the flow zone and confining layers. The assigned values of flow-zone hydraulic conductivity were 800 ft/d in the horizontal direction and 80 ft/d in the vertical direction. Confining layers were assigned values of 0.1 ft/d for horizontal and vertical hydraulic conductivity. Porosity was uniformly 35 percent. A longitudinal dispersivity (α_l) of 20 ft was assigned arbitrarily and was considered to be compatible with the horizontal discretization. Variables of the tests were (1) original versus experimental methods; (2) transverse dispersivities (α_t) of 20 ft and 0.1 ft; (3) scaling factors of 1 (no scaling), 0.1, 0.01, 0.001, 0.0001, and 0 (no vertical mechanical dispersion); and (4) molecular diffusivity (D_m) values of 0.001, 0.0001, and 0.00001 ft^2/d. In addition to a detailed description of the transition zone between fresh water and saline water at the end of injection, the effect on recovery of freshwater was assessed by simulations of withdrawal at a rate of 62,047 ft^3/d, the average rate of the first recovery at Hialeah. Results of the tests are described in detail by the author in a previous paper (Merritt, 1993).

The tests showed that when the experimental algorithm is used to eliminate vertical dispersion across flow-zone boundaries, the primary influence upon recovery efficiency and the salinization of water

at the boundaries of the freshwater mass is the degree of molecular diffusion from the more saline surrounding rocks. The magnitude of this influence depends on the degree of vertical dispersion occurring within the flow zone, and this is controlled by the transverse dispersivity (α_t) and by the size of the scaling factor specified by the user to compensate for bedding effects or for the incompatibility of horizontal and vertical discretization scales in the application problem. When the original algorithm is used and vertical dispersion across flow-zone boundaries is allowed to occur and a relatively low value of longitudinal dispersivity (α_l) is specified, the degree to which recovery efficiency is reduced depends on the size of the transverse dispersivity (α_t) specified by the user. Changing to upstream weighting for vertical advective flux had little effect in any of these tests because the amount of seepage across flow-zone boundaries was negligible in comparison with the amount of flux from molecular diffusion.

The tests of recovery efficiency revealed much about the effect of mechanical dispersion and molecular diffusion on computed recovery efficiencies without, however, leading directly to parameter estimates for the simulation model. Because a large degree of computed dispersion across flow-zone boundaries does not seem to represent any known physical process, it is probable that algorithms and parameter selections that minimize the degree of computed dispersion would lead to the most realistic simulation. Either the experimental algorithm and a scaling factor or the original method with a small transverse dispersivity should probably be used. The representation of molecular diffusion of solute from vertically adjacent confining layers into the body of injected freshwater within the flow zone is a more realistic simulation procedure than one that entirely disregards the transfer of solute between the injection zone and confining layers by treating the latter as impermeable no-flow boundaries.

Dispersion Tests in a Horizontal Plane

Additional insights into the dependence of model behavior upon dispersivity selections are gained by performing model tests with different sets of dispersivities in three-dimensional Cartesian coordinates. The 53-day first injection at the average rate of 105,661 ft^3/d was simulated in the Cartesian grid system illustrated in figures 18 and 19. The regional hydraulic gradient was set equal to zero. The experi-

mental algorithms for computing vertical dispersion were used, and the longitudinal dispersivity (α_l) was set equal to 20 ft. The variables of the tests were the transverse dispersivity (α_t) and the vertical scaling factor (S). The aquifer was considered horizontally isotropic.

Two of the sets of values that were tested ($\alpha_l=\alpha_t$ =20 ft, S=0.01 versus α_l=20 ft, α_t=0.1 ft, and S=1.0) illustrated a significant facet of model behavior. Because the mechanical dispersion term in the vertical direction resulting from the larger value of α_t was scaled by 0.01, vertical mechanical dispersion in the flow zone varied only by an approximate factor of 2 in the two cases, and the radial extent of freshwater flow was not affected by large simulated dispersive fluxes across upper and lower boundaries because the experimental algorithms were used. However, α_t also determined the degree of transverse dispersion in the horizontal plane, and between the two cases, the horizontal transverse dispersivity differed by a factor of 200. The comparison was, therefore, between relatively large and small degrees of transverse dispersion in the x-y plane.

The results of the tests are shown in figure 20 as planar views of freshwater distribution about the well (lines of 750 mg/L dissolved solids) in layer 6 (layer 3 of the flow zone). When α_t=20 ft and S=0.01, the line is virtually a perfect circle, as would be expected in radial flow from a well unaffected by a background hydraulic gradient. The line depicting the case in which α_t=0.1 ft and S=1.0, however, shows bulges of fresher water along the positive and negative x- and y-axes that have no physical meaning and are evidence of the inaccuracy of the mathematical solution for radial flow in Cartesian coordinates when horizontal transverse dispersion is small. Even when horizontal boundaries of the model grid were extended from 20,000 to more than 270,000 ft from the well to mitigate the possible effect of the nonuniform distance to the location of specified boundary pressures, there was no apparent effect upon the nonradial spatial distribution of freshwater. Requiring that at least two iterations of the solution to the solute-transport equation be performed and the use of subroutine CRSS for an alternate computation of nonaxial transport (INTERA Environmental Consultants, Inc., 1979) only resulted in a slight increase of solute movement in the positive x, positive y and negative x, negative y directions (fig. 20) without appreciably improving the depiction of radial flow.
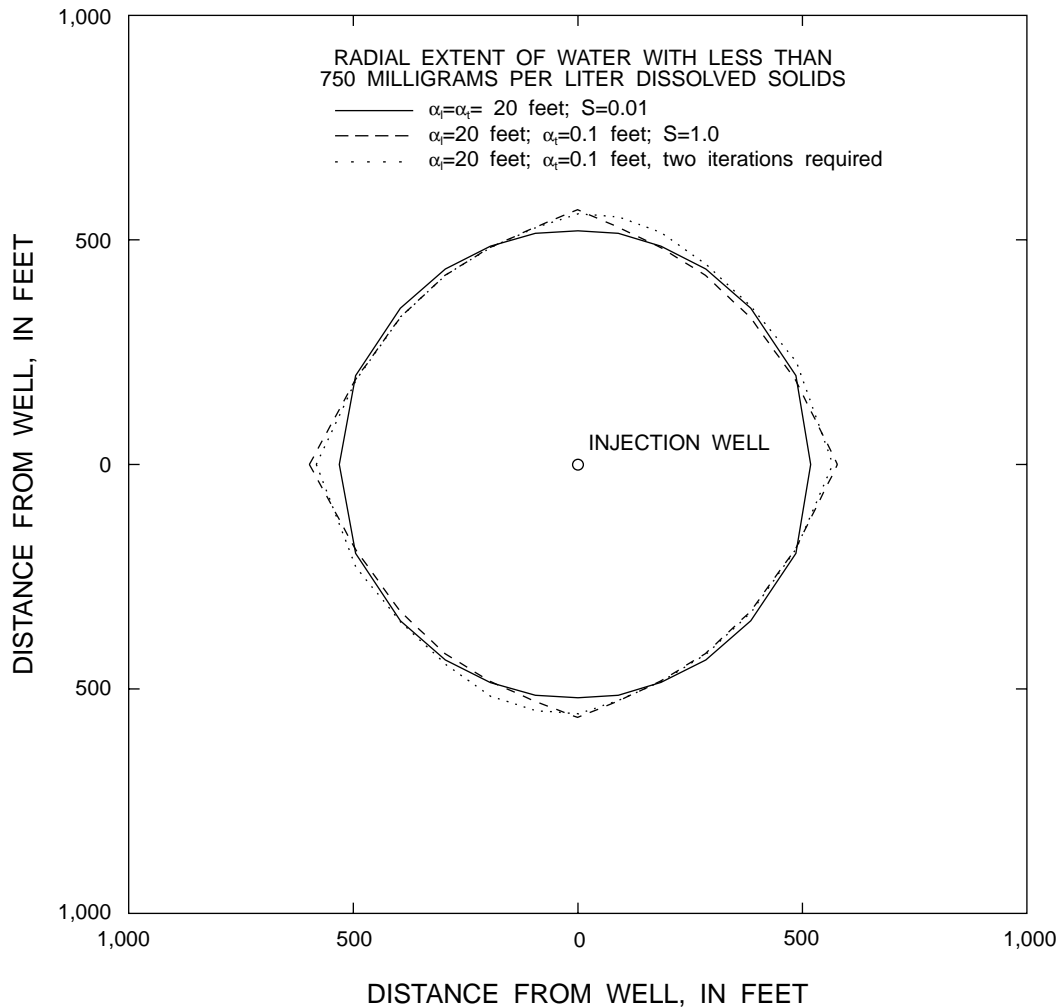
Figure 20. Plan view of the distribution of injected freshwater using two values of transverse dispersivity (α_t).

Simulations using the two sets of values were each followed by a simulation of recovery and computation of recovery efficiency. In case 1 (α_t=20 ft, S=0.01), recovery efficiency was 52.8 percent. In case 2 (α_t=0.1 ft, S=1.0), recovery efficiency was 53.1 percent. Thus, despite the apparent difference between computed freshwater distributions, the effect on computed recovery efficiency was slight. When case 2 with extended boundaries was followed by recovery, the computed recovery efficiency was 54.0 percent.

The result of these comparisons provides a basis for selecting the algorithms to be used for computing dispersion. Setting α_l=α_t, which produces the most realistic depiction of radial flow in Cartesian coordinates, is the preferred approach to the selection of values. This approach requires that some means be

found to reduce the degree of vertical dispersion across flow-zone boundaries; therefore, the experimental dispersion algorithm was used for the simulations. A scaling factor of about 0.01 was used for vertical transverse dispersion within the flow zone. This selection was arbitrary but was partly based on the 100:1 ratio of horizontal to vertical grid-cell dimensions within the region of freshwater invasion of the flow zone. The value of molecular diffusivity was determined as part of the calibration process.

Hydraulic Parameter Estimation Methods

Hydraulic parameter estimates were based on data from the aquifer test of February 10, 1975. The estimates are subject to the usual reservations applying to aquifer testing in carbonate terranes, where local nonuniformities in hydraulic properties at the with-

drawal or observation points can yield estimates atypical of the average hydraulic properties of the aquifer. The results of Theis and Jacob-Lohman analyses (Lohman, 1979) were previously cited. In this section, a description of SWIP code simulations of the aquifer test is presented. The simulations were for the purposes of (1) deriving final estimates of hydraulic parameters for simulation, (2) sensitivity testing, and (3) testing alternative conceptual models of aquifer physical and hydraulic properties.

Simulation of Aquifer-Test Data and Sensitivity Analyses

The calibration of the aquifer test was based on the assumption that the flow zone was 12 ft thick and that the entire injection zone had a porosity of 35 percent. The confining-layer hydraulic conductivities were set equal to a small value (0.01 ft/d). This value was arbitrary, as no data were available upon which to base the estimate. The three-dimensional Cartesian grid design used for the calibration is shown in figures 18 and 19. Injection and observation wells were five grid nodes apart. Withdrawal from the observation well at the controlled rate of 250 gal/min was specified for a simulated period of 100 minutes. Nonvarying specified-pressure boundary conditions at a minimum of 20,000 ft from the wells were used and corresponded to uniform initial conditions within the aquifer. A Theis formula computation showed that the drawdown at 20,000 ft from 100 minutes of pumping at the cited rate was negligible.

A good match of observed and simulated drawdowns is shown as curve C in the various graphs of figure 21. Each pair of graphs shows the comparison and results of a sensitivity analysis for the entire 100-minute test period and for an early time period (first 3 minutes). The apparent stepping pattern of early time observations merely represents the limited resolution of the scale of the measuring instrument. Values of 800 ft/d for hydraulic conductivity in the horizontal (x-coordinate and y-coordinate) directions provided the best match for later time data, but the computed early time response was not highly sensitive to 25 percent changes (lines K1 and K2, fig. 21A) in horizontal hydraulic conductivity. The 25 percent variations caused unrepresentative later time drawdowns to be computed, the divergence increasing with time. Vertical hydraulic conductivity, for which data were not available to provide a basis for estimates, was arbitrarily considered to be 10 percent of the horizontal hydraulic conductivity in each sensitivity analysis.

The estimated values of horizontal hydraulic conductivity, integrated over the 12-ft thickness of the flow zone, give a transmissivity value of 9,600 $[(ft^3/d)/ft^2]ft$. The integration should include the confining-zone thicknesses, but because of their low estimated hydraulic conductivity, the transmissivity value would merely increase by 1.33 $[(ft^3/d)/ft^2]ft$.

Early time observations were matched by varying rock compressibility, specified in (pounds per square inch)$^{-1}$. This procedure is similar to varying the storage coefficient in a two-dimensional areal hydraulic model because the storage coefficient (S) is considered (Lohman, 1979) to be a linear function of rock compressibility (C_r) according to the following formulation:

$$S = \theta \rho b(C_w + C_r) \qquad (8)$$

where: θ is porosity (unitless),
  b is layer thickness (L),
  ρ is fluid density ($P\,L^{-3}$), and
  C_w is water compressibility ($P^{-1}\,L^2$).

Of the terms in the equation, all have been assigned values except for C_r. The value of C_w, 0.000003 $(lb/in^2)^{-1}$, is readily obtained from various handbooks. A C_r value of 0.0000400 $(lb/in^2)^{-1}$ was used to simulate the observed early-time drawdowns. Substantial disagreement occurred in the early time range when this value was increased and decreased by 25 percent (lines C1 and C2 in fig. 21B). The calibrated C_r value, together with the hydraulic conductivity value of 800 ft/d, also provided a good simulation of later drawdown data.

The compressibility and porosity estimates can be related to a storage coefficient value. Applying relation 10 to the flow zone (b=12 ft), an equivalent storage coefficient of 7.8×10^{-5} is obtained. Lohman (1979) states that equation 10 was derived (Jacob, 1940) by neglecting any release of water from confining beds. Because there is an assumed ratio of 80,000:1 for the horizontal permeability of the flow zone and that of the overlying 65 ft and underlying 68 ft of relatively impermeable strata, this approximation seems to be a good one. The hydraulic-head change at the observation well was 1.8 ft at the end of the 100-minute test. An inspection of the SWIP simulation shows a head change of 1.6 ft at an elevation 2.75 ft above the flow zone and a head change of 0.06 ft at an elevation 35 ft above the flow zone. Only a small part of the upper low-permeability layer has released an appreciable amount of water to the flow zone.
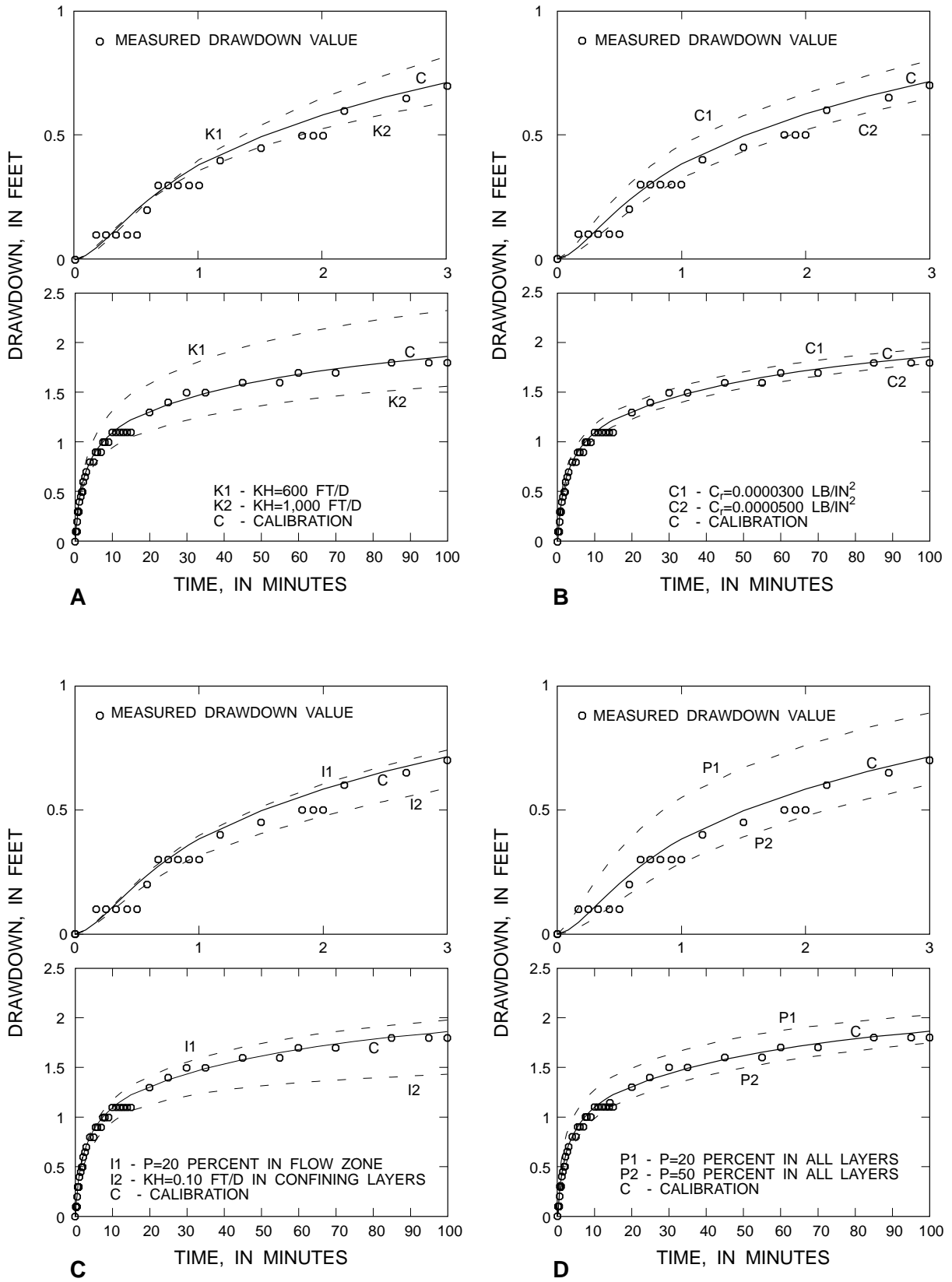
Figure 21. Simulation of the February 10, 1975, aquifer test data and sensitivity analyses. Results of sensitivity analyses are shown as dashed lines. KH, horizontal hydraulic conductivity, in feet per day (ft/d); P, porosity, in percent; CR, value of rock compressibility, in inverse pounds per square inch (lb/in^2).

As previously noted, the hydraulic-conductivity estimates for the confining layers were arbitrary, though permeability was known to be low. To gain an understanding of how much error could result by underestimating the value of this parameter, the model was run using a value of K_x=0.1 ft/d, 10 times greater than the value assigned for calibration of the aquifer test. The computed drawdowns are shown as curve I2 in figure 21C. Results of the test are relatively dramatic, showing a substantial underestimate of observed drawdowns at both early and late times. Thus, increasing by a factor of 10 the amount of injected water that can be accepted by 133 ft of relatively impermeable strata substantially lowers the hydraulic response of the flow zone. Other tests (not illustrated) indicated that the aquifer-test data could be simulated with flow-zone hydraulic-conductivity values of 750 ft/d and a rock compressibility value of 0.0000450 (lb/in^2)$^{-1}$ when the confining-layer hydraulic conductivity was considered to be 0.1 ft/d.

The solution dependence upon the specified porosity value of 35 percent for the entire injection zone was examined with sensitivity analyses that assumed that porosity in all zones was uniformly 20 and 50 percent. Results (curves P1 and P2 in fig. 21D) show significant discrepancies with observed data at early times. At later times, observed and computed data are offset to a degree that seems to change only slightly with increasing time.

Total porosity similarities between formations of dissimilar permeability, as indicated by the neutron porosity log of January 8, 1975, raise the issue of how total porosity relates to effective porosity, the pore or channel volume that is flushed by water moving in the aquifer. The SWIP code assumes that the specified pore volume of each layer receives flow from natural or user-specified sources, such as wells; thus, the specified SWIP porosity is considered to be effective porosity. Effective porosity is herein assumed to be equivalent to total porosity (35 percent) in the confining layers because the apparent lack of solution features implies that seepage through these rocks could occur at an equal rate in all pore spaces. The resistance to flow within the confining layers is accounted for by the specification of a low value for hydraulic conductivity rather than by considering porosity to be low. Specification of low values of effective porosity in the confining layers can lead to simulation error because inflow from the well is allocated to these layers on the basis of their low hydraulic

conductivity, and the model would assume that even minor inflows into the confining beds were quickly distributed throughout an unrealistically large volume.

In the flow zone, a dual-porosity scenario might be more appropriate if water were contained partly within connected solution channels and partly within pores in rock surrounding the solution channels. Movement of water within pores isolated from solution channels would be insignificant relative to movement within the solution channels, and hydraulic conductivity and effective porosity would refer to the flow properties and relative volume of the latter. Effective porosity, therefore, might be less than the estimated 35 percent in the flow zone.

To test this possibility, an additional sensitivity analysis assumed that the flow-zone effective porosity was 20 percent. The result is shown in figure 21C as curve I1, which indicates that observed drawdowns are overestimated at late times. The later time result is similar to that when the entire injection-zone porosity is assumed to be 20 percent. The fact that some pores or solution channels admit flow and permit related solute-concentration change at a slower or faster rate than others, in either the confining layers or the flow zone, is accounted for by the mechanical dispersion concept.

Alternative Calibrations of Aquifer Test

Alternative calibrations of the aquifer test were performed to obtain separate sets of aquifer hydraulic parameters representing hypotheses that (1) the flow-zone thickness was 21 ft, (2) the effective porosity of the flow zone was 20 percent, and (3) the flow-zone permeability was horizontally anisotropic. In the third case, a 10:1 bipolar model of anisotropic hydraulic conductivity ($K_x>K_y$) was specified, where K_x and K_y are values of hydraulic conductivity in the two horizontal coordinate directions. These three test cases are the conceptual models of the aquifer that seem to represent the most likely errors in the accepted conceptual model or to have the greatest generic significance for model calibration. These alternative conceptual models are later used for separate calibrations of the recovery data. The accepted and alternative calibrations of the aquifer-test data are shown in figure 22 for 100- and 3-minute time periods as line C (calibration based on the accepted conceptual model of the aquifer), line C1 (21-ft flow-zone thickness), line C2 (20 percent effective porosity), and line C3 (anisotropic permeability).
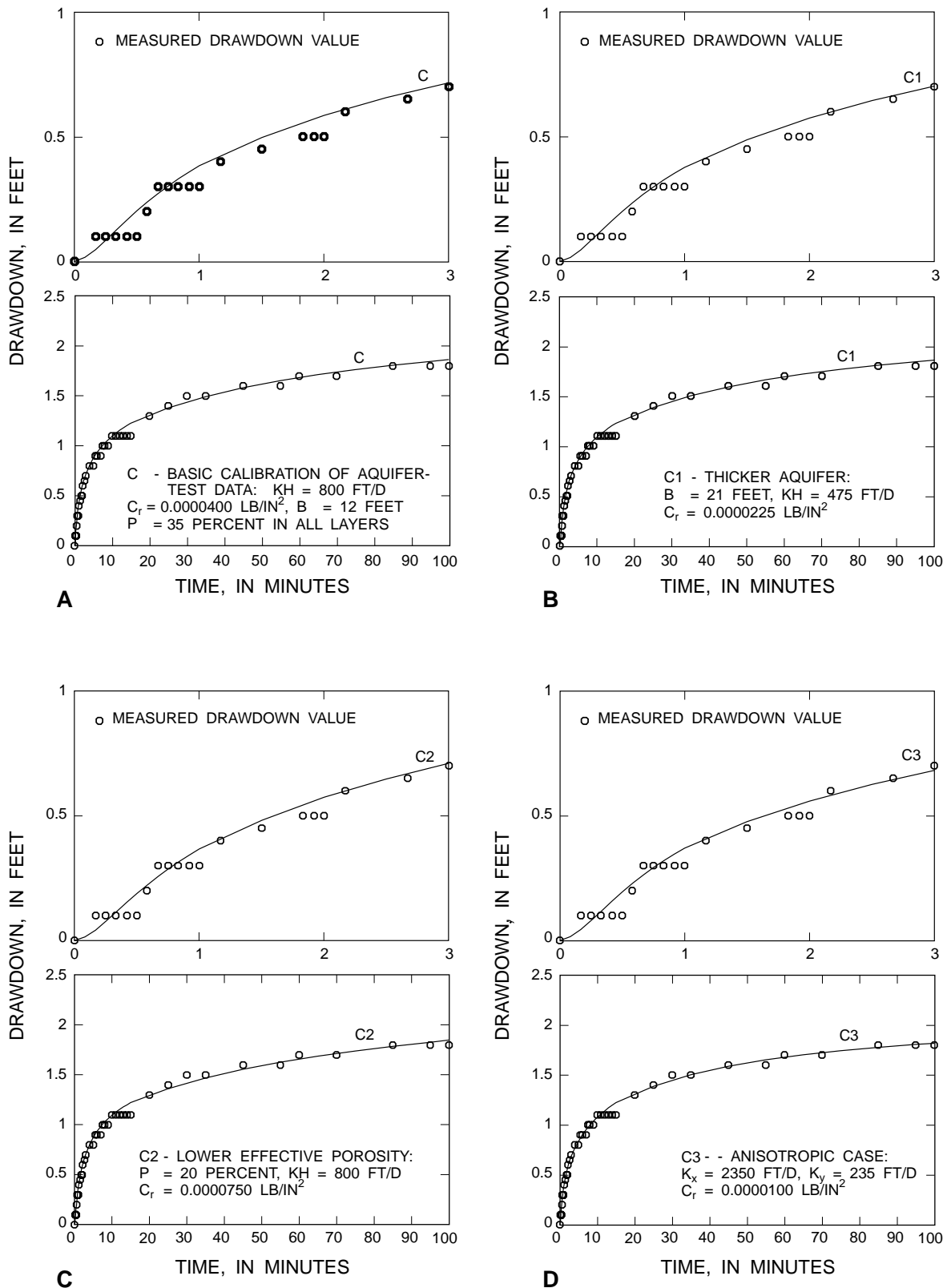
Figure 22. Alternative simulations of the February 10, 1975, aquifer-test data. KH, horizontal hydraulic conductivity, in feet per day (ft/d); K_X and K_Y, hydraulic conductivities in X and Y direction, in feet per day (ft/d); P, porosity, in percent; C_R, value of rock compressibility, in inverse pounds per square inch (lb/in^2); B, thickness of flow zone, in feet (ft).

The alternative calibrations match observed data as well as the calibration based on the accepted conceptual model. Estimating flow-zone effective porosity to be 20 percent (C2) requires that rock compressibility be increased to 0.0000750 $(\text{lb/in}^2)^{-1}$. Assuming that the flow-zone thickness is 21 ft (C1) requires that hydraulic conductivity be reduced to 475 ft/d and rock compressibility reduced to 0.0000225 $(\text{lb/in}^2)^{-1}$. Equivalent transmissivities (T) and storage coefficients (S) in the two cases are: (C2) T=9,600 $[(\text{ft}^3/\text{d})/\text{ft}^2]$ft and S=7.8×10^{-5}, the same as for the primary calibration; and (C1) T=9,975 $[(\text{ft}^3/\text{d})/\text{ft}^2]$ft and S = 7.2×10^{-5}.

When the flow zone was assumed to have a 10:1 bipolar anisotropy in the horizontal coordinate directions, and the observation well was assumed to be located in the direction of least permeability, calibration was achieved by setting K_x=2,350 ft/d and K_y=235 ft/d. The rock compressibility value (C_r) was 0.0000100 $(\text{lb/in}^2)^{-1}$. If expressed in bipolar components like hydraulic conductivity, then T_x=28,200 $[(\text{ft}^3/\text{d})/\text{ft}^2]$ft and T_y=2,820 $[(\text{ft}^3/\text{d})/\text{ft}^2]$ft. The storage coefficient would be 1.8×10^{-5}.

Simulation of Recovery Salinity Data

Simulation of the increasing salinity (chloride or dissolved-solids concentrations) of recovered water implied a replication of the volume of withdrawal when withdrawn water reached the limiting chloride concentration used to calculate recovery efficiency and was, therefore, also a simulation of observed recovery efficiencies. The simulation required selection of values to represent aquifer hydraulic, chemical, and dispersive properties, representation of injection and recovery rates and volumes, and a method of relating simulated recovered volume to observed chloride data for matching purposes.

Parameter Value Selection and Comparison Techniques

For the initial calibration effort, parameter values were selected on the basis of an evaluation of data collected at the site, the simulation of the aquifer test, and a consideration of insights derived from the tests of dispersion models. On the basis of site data, the flow zone was assumed to be 12 ft thick, have an effective porosity of 35 percent, and contain water of 2,700 mg/L dissolved-solids con-

centration. The confining layers were assumed to have effective porosity of 35 percent and contain water of 6,000 mg/L dissolved-solids concentration. The hydraulic conductivity of the confining layers was set at an arbitrary low value, 0.01 ft/d. On the basis of the aquifer-test simulation, the flow-zone hydraulic conductivity was assigned a value of 800 ft/d, and rock compressibility was assigned a value of 0.0000400 $(\text{lb/in}^2)^{-1}$. On the basis of dispersion model tests, the experimental algorithm of vertical dispersion computation was selected to eliminate vertical dispersion across the boundaries between the flow zone and confining layers. Longitudinal and transverse dispersivities were assigned the same value to realistically represent radial flow from the well in the Cartesian grid shown in figures 18 and 19, and a scaling factor of 0.013 (ratio of average horizontal and vertical grid-cell dimensions) was used to reduce the degree of vertical dispersion occurring within the flow zone.

The values of longitudinal and transverse dispersivity and the molecular diffusivity could not be directly estimated on the basis of available data, but were found to be of primary importance in simulating the observed recovery salinity data. Therefore, they were determined by a process of trial-and-error adjustment and curve matching. The regional flow gradient was initially estimated to be 0.4 ft/mi on the basis of the regional potentiometric-surface map drawn by Meyer (1989a). This parameter also proved to be of major importance in matching observed data and needed considerable adjustment. Model calibration, therefore, consisted primarily of adjusting dispersivities, the molecular diffusivity, and the regional seepage velocity that depended on the regional hydraulic gradient and aquifer hydraulic parameters.

The time history of injection, storage, and recovery periods and hiatuses between cycles was represented approximately as listed in Appendix C. The time periods and corresponding rates of flow were encoded in the simulation as given in the table below, in which time 0 corresponds to the start of the first injection on July 17, 1975.

Stage	Time period (days)	Rate of flow (cubic feet per day)
Injection 1	0–53	105,661
Recovery 1	54–93	62,047
Hiatus	94–165	0
Injection 2	166–235	162,026
Storage 2	236–289	0
Recovery 2	290–367	95,333
Injection 3	368–554	147,442
Storage 3	555–729	0
Recovery 3	730–1,655	59,084

The 2-day storage period between the first injection and recovery was ignored, and the volume of the aborted second injection (App. C; pl. 1) was included in that of the subsequent successful second injection. Injection and recovery rates were represented as averages over each injection and recovery stage. Recovery efficiency and the distribution of injected water in the receiving zone were shown not to be related to injection or withdrawal rate in simulations with the SWIP code (Merritt, 1985), so use of average rates did not affect simulation of recovery salinity data. The estimated volumes of backflushes were subtracted from injection volumes (because only one flowmeter was used) before computing average rates.

Because average recovery rates were used, it was necessary to find a way to relate computed solute-fraction values of recovered water at given simulation times to the measured chloride concentrations of recovered water samples, which were recorded at various times as the actual recovery rate varied (App. C; pl. 1). This problem was resolved by using recovery volume rather than time as the common factor. The observed chloride concentrations were assigned artificial times equal to the actual recovered volume divided by the average rate. Thus, observed data times shown in subsequent illustrations differ slightly from the actual measurement times.

Chloride concentrations measured during recoveries were related to dissolved-solids concentrations by interpolation on the basis of chloride and dissolved-solids concentrations of injected-water samples and preinjection flow-zone water samples, as previously described. Based on the estimated dissolved-solids concentrations, recovered water samples were assigned values of solute fraction for comparison with the computed solute fraction of recovered water. (Solute-fraction values were 1.0 for 6,000 mg/L dissolved-solids concentration, 0.45 for native flow-

zone water, and 0.0667 for injected water.) The SWIP code computes the solute fraction of withdrawn water as the weighted average of water withdrawn from each layer of the model. The weighting is a set of allocation factors that in these simulations was based on the relative thicknesses and hydraulic conductivities of the layers. Each of the six flow-zone layers had the same allocation factor, and allocation factors for the confining zone layers were so small as to make negligible their contribution to recovered volumes.

Basic Simulation

The process of calibrating the model to match observed recovery chloride data is illustrated in figure 23. An early simulation attempt (fig. 23A) was based on the supposition that the regional pore velocity had no influence on observed recovery data. The regional hydraulic gradient was set equal to zero. The dispersivity values were $\alpha_l = \alpha_t = 65$ ft, and molecular diffusivity was $D_m = 0.0002$ ft^2/d. A good match of the observed salinity increases was obtained in the first recovery and at the end of the third recovery, when recovered water salinity had returned nearly to the background level (the salinity of native flow-zone water). However, observed salinity exceeded computed values in the second recovery and during most of the third recovery, and the discrepancy was substantial.

To obtain a better match of observed and simulated data in the second and third cycles, the dispersivity values were increased to 100 ft (fig. 23B). The salinity increase is slightly faster in the third recovery, although computed values still are greatly exceeded by the observed data. However, computed salinity increases now substantially exceed observed increases in the first and second recoveries. It was evident that this simulation strategy could not be productive.

At this point, nonzero values of regional pore velocity were introduced, and the dispersivity values were reduced to the value of 65 ft that produced a good match in the first recovery. When pore velocity was set equal to 260 ft/yr, a good match was obtained in all three recoveries (fig. 23C). The computed salinity of recovered water in the brief first ASR cycle was unchanged by the use of a nonzero pore velocity. However, because recovery followed 54- and 181-day storage periods in the second and third ASR cycles and because the third recovery continued for 2.5 years, sufficient time elapsed for the simulation of a substantial downgradient shift of the injected freshwater mass. During the later part of the simulated second and third

recoveries, water entering the well from the upgradient direction was more saline than water coming from the downgradient direction. Thus, the computed recovery salinities increased relative to the earlier run with no regional flow and matched measured data.

This calibration (fig. 23C) will be referred to as the basic simulation to distinguish it from later simulations in which some of the parameter values not used as calibration adjustments were revised (alternative simulations). The downgradient shifts of injected freshwater caused by simulated regional flow are shown in figure 24, which shows planar views of lines of equal solute fraction in layer 6 (layer 3 of the flow zone) at selected times during the three ASR cycles. Other lines of equal computed solute fraction within the transition zone are also shown. The illustration helps to visualize the simulated distribution and movement of injected water within the flow zone during the ASR process, and also indicates the simulated degree of dispersion around the mass of potable water. Figure 24 was generated by selecting the locations of the solute value within each row of the model grid by linear interpolation between columns and then connecting the points successively. Small bulges along the y-axis are a consequence of using Cartesian coordinates to simulate radial flow from a well, as previously discussed, even when a large horizontal transverse dispersivity is specified. That this does not occur along the x-axis is due to the influence of regional flow.

Figure 24 shows the nearly circular injected water mass after the brief first injection and the injected water at the end of the second injection, when some downgradient drift is evident. The drift becomes progressively more pronounced after the second storage period of 54 days, at the end of the third injection, and at the end of the third storage period of 180 days. The transition zone is wider (more diffuse) downgradient of the injected well. After the end of the extended third recovery, water with a lower solute fraction than that of the native water (0.45) remains in the aquifer. This fresher water is a mixture of injected freshwater and native saline water. That small amounts of the fresh injected water remain in the aquifer at this time as a result of downgradient advection is especially remarkable because the volume of the third recovery was nearly twice that of the third injection and exceeded the volume of all three injections by 22 percent.

Using a pore velocity of 260 ft/yr for calibration requires a regional gradient of 1.6 ft/mi, given the

hydraulic conductivity estimate of 800 ft/d and porosity estimate of 35 percent. However, this value is 4 times that estimated on the basis of published potentiometric-surface data (Meyer, 1989a). Errors of this magnitude in the published estimates are unlikely, raising questions about the accuracy of the hydraulic conductivity estimates determined from simulating the aquifer-test data. In fact, results of individual aquifer tests in carbonate terraces are known to be unreliable because local heterogeneities are common. Thus, average flow-zone hydraulic conductivity possibly could be larger than estimated, perhaps even 4 times larger, or could be anisotropic. The unusual trends previously cited in observation-well water-quality data during the three injections, which suggest a partial early breakthrough of injected water, also suggest the possibility of local heterogeneities in flow-zone solution features that might affect results of an aquifer test.

Near the end of the third recovery, computed recovery salinities were nearly the same as when the hydraulic gradient was specified to be zero, as would be expected if computed values are approaching the natural flow-zone salinity (1,200 and 2,700 mg/L concentrations of chloride and dissolved solids, respectively). The last chloride concentration measurement of recovered water, on January 28, 1980, was 1,120 mg/L. However, the magnitude of computed solute-fraction values near the end of the third recovery was highly sensitive to the molecular diffusivity value (D_m), which determined the rate at which solute ions from the more saline confining layers diffused into the injected water occupying the flow zone in the vicinity of the well. Figures 23D–E illustrate the dependence of the simulation result upon the value of D_m, as determined by additional simulation runs in which the dispersivities and regional pore velocities were the same as in the calibration (fig. 23C). D_m was increased to 0.001 ft^2/d (fig. 23D) and decreased to zero (fig. 23E). When $D_m=0$, no appreciable change in computed recovery salinities is observed in the first recovery, but computed salinities in the longer second and third recoveries are too small, and the salinities seem to converge to a value that is too low near the end of the third recovery. This illustrates results of the previously described algorithm tests showing that the observed recovery salinity data are highly influenced by the degree of molecular diffusion from overlying and underlying rocks
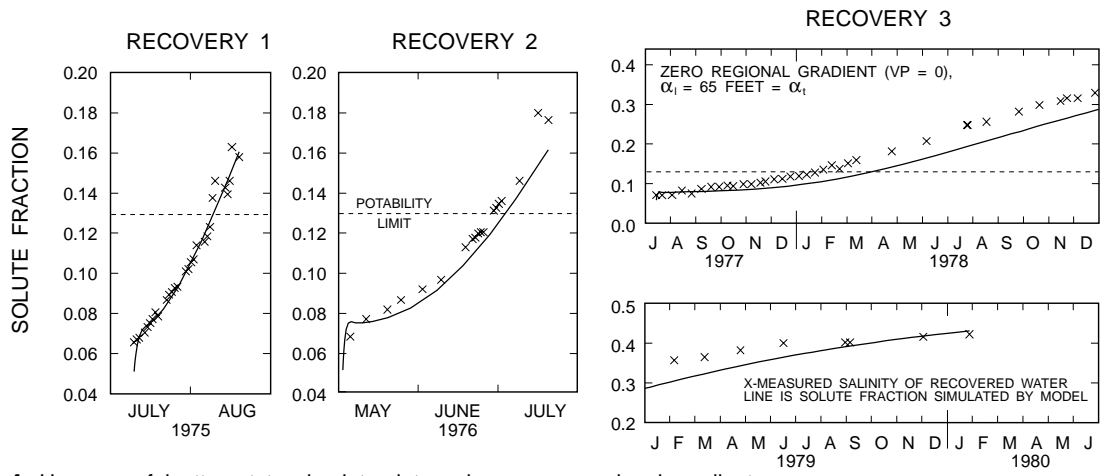
A. Unsuccessful attempt to simulate data using a zero regional gradient.
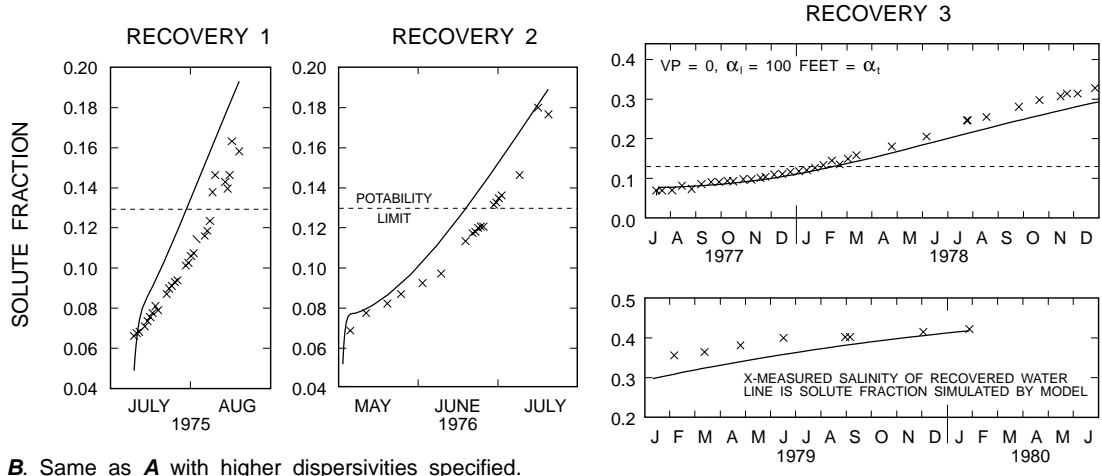
B. Same as **A** with higher dispersivities specified.
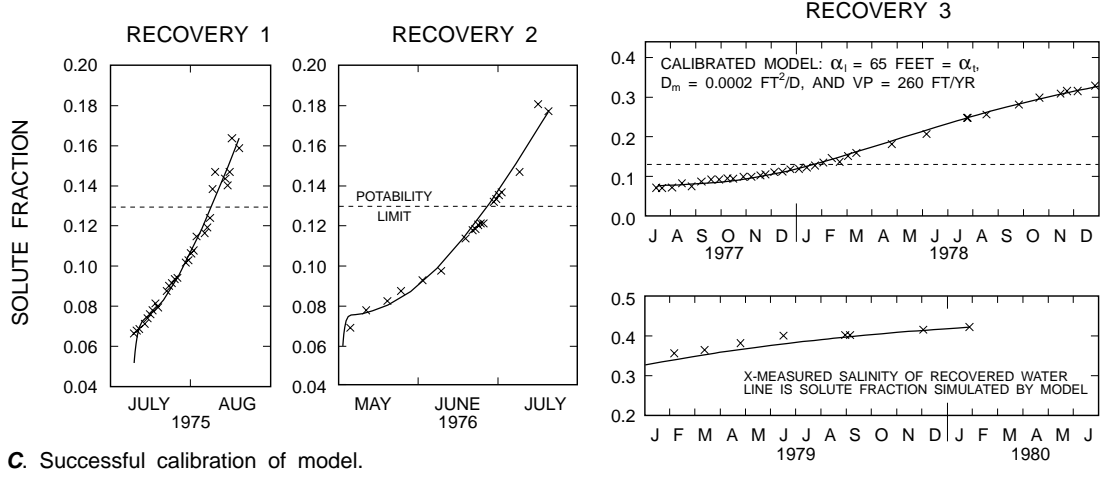
C. Successful calibration of model.

Figure 23. Results of the simulation of the salinity of recovered water and selected sensitivity analyses showing the calibration techniques. VP, aquifer pore velocity, in feet per year (ft/yr); α_l, α_t, longitudinal and transverse dispersivity, in feet; D_m, molecular diffusivity, in feet squared per day (ft^2/d).
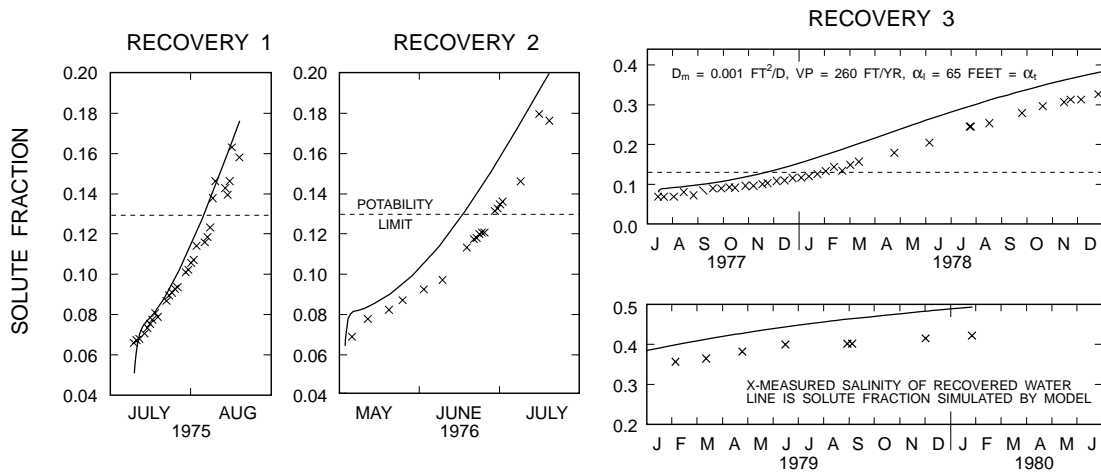
D. Sensitivity analysis: a higher value of molecular diffusivity is specified.
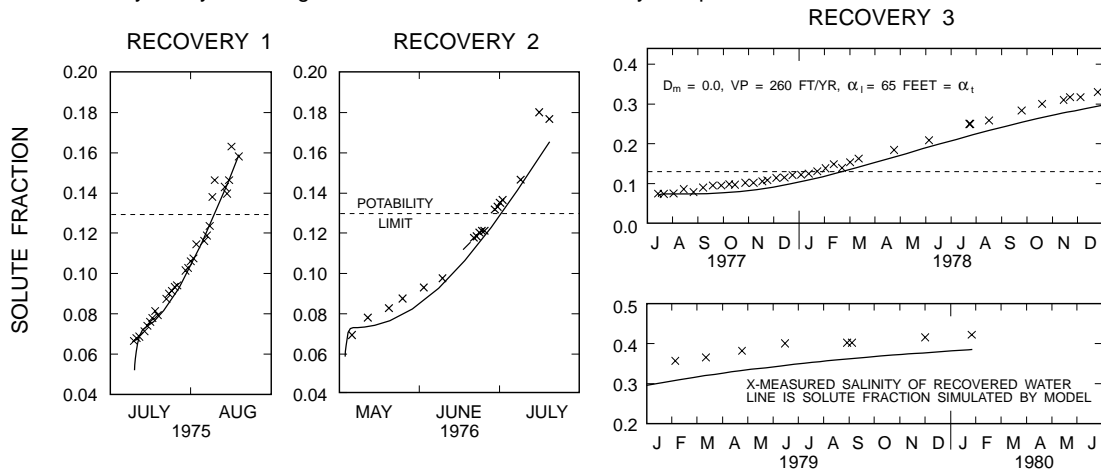
E. Sensitivity analysis: the value of molecular diffusivity is specified to be zero.

Figure 23. Results of the simulation of the salinity of recovered water and selected sensitivity analyses showing the calibration techniques--Continued.

containing more saline water. When D_m=0.001 ft^2/d, computed salinities are too large in all three recoveries and converge to a value that is too high near the end of the third recovery, indicating that the degree of molecular diffusion from adjacent layers has been overestimated.

On the basis of these observations, a convenient calibration strategy has evolved. The first recovery simulation is sensitive to the selection of dispersivities but insensitive to the selections of molecular diffusivity or regional pore velocity. The second and third recovery simulations are highly sensitive to regional pore velocity, and the computed salinity value near the end of the third recovery is especially sensitive to the specified value of molecular diffusivity, even when other calibration parameters are correct. Thus, these three parameters can be determined independently from comparison with separate parts of the observed data set. This set of conditions arises from the dissimilarity of the three

ASR cycles and, particularly, from the fact that the third recovery was continued long enough to clearly show the effect of downgradient advection and the effect of molecular diffusion as the salinity of recovered water approached background levels.

Alternative Simulations

The simulation technique described in the preceding section was applied in additional calibration exercises in which flow-zone properties of the basic simulation were changed to investigate the implications of possible error in the interpretation of the field data. The same variations of the conceptual model of the flow zone that were the basis of alternative calibrations of the aquifer test, and one additional variation, were also used for alternative simulations of recovery salinity data. The objective was to determine if the
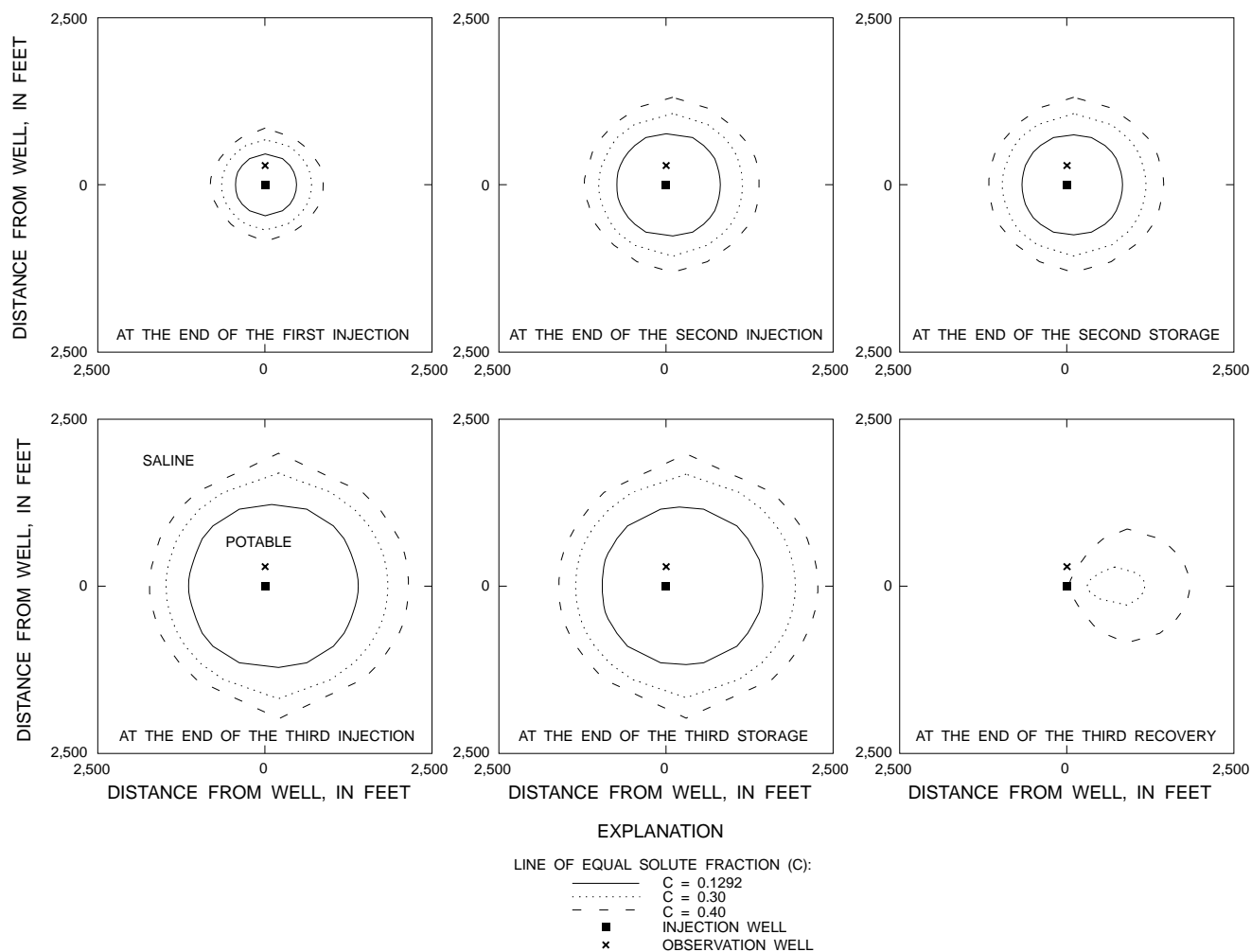
Figure 24. Horizontal distribution of injected freshwater at various stages of the aquifer storage and recovery cycles when permeability is horizontally isotropic. A solute fraction of 0.1292 corresponds to a chloride concentration of 250 milligrams per liter.

observed data could still be simulated, given the assumptions of the revised conceptual models. If so, results of subsequent predictive modeling could be strengthened by considering multiple cases that encompassed the possible range of variation of certain flow-zone properties determined from field data. This approach was the focus of a paper by Merritt (1991). The four cases considered and their significance are as follows:

- Flow-zone hydraulic conductivity was larger than that estimated from analysis of the aquifer-test data, resolving the discrepancy between calibrated model and literature estimates of hydraulic gradient;

- Flow-zone thickness was almost twice that estimated on the basis of some spinner flowmeter logs, as suggested by other flowmeter logs and some water-quality data;

- The effective porosity of the flow zone was lower than the

total porosity of rock and pores measured by the neutron porosity log; and

- Flow-zone hydraulic conductivity might actually be anisotropic in the horizontal plane, the major flow direction being in the direction of the regional flow gradient and perpendicular to a line drawn between the injection and observation wells.

Excellent calibrations were achieved in all four cases and are illustrated, together with the basic calibration curve, in figure 25. Table 2 lists the assumed physical and hydraulic properties of the aquifer and parametric values used to calibrate each alternative simulation. In terms of the three parameters adjusted to calibrate the simulations, C-2 (increasing the flow-zone thickness to 21 ft) required doubling the molecular diffusivity, decreasing pore velocity by 15 percent, and decreasing the dispersivities by 23 percent; C-3

(decreasing the flow-zone porosity to 20 percent) required increasing the pore velocity by 40 percent, increasing the dispersivities by 23 percent, and decreasing the molecular diffusivity by 70 percent; and C-4 (anisotropic permeability having a 10 to 1 ratio of directional components) required increasing the pore velocity by 40 percent, decreasing the dispersivities by 23 percent, and leaving the molecular diffusivity unchanged.

In case C-1 the horizontal hydraulic conductivity value was increased to 3,200 ft/d, four times the original value determined from the aquifer-test simulation. This implied an injection-zone transmissivity increase to 38,400 [(ft^3/d)/ft^2]ft. The regional hydraulic gradient was decreased to 0.41 ft/mi, close to the value estimated from published literature and one-fourth the value used in the basic calibration (figs. 25A). Regional pore velocity remained the same at 260 ft/yr, and the dispersivity and molecular diffusion values were unchanged. The simulation curve (fig. 25B) is virtually identical to the previous one. This result indicates the absence of any significant degree of buoyancy stratification, which tends to increase with the value of hydraulic conductivity. However, at the prevailing density contrast, the degree of buoyancy stratification was still insignificant even when $K_x=K_y=3,200$ ft/d, though it did increase slightly.

That identical results were achieved with the two sets of hydraulic conductivities and regional gradient estimates meant that each simulation of alternate conceptual models could be considered to actually represent two test cases corresponding to the two regional gradient estimates. The consequent reduction in the number of simulation runs required to test all hypotheses was especially beneficial, considering the large amount of computer time required for each simulation. The basic simulation required 20.5 hours on the PRIME 9955. When K_x and K_y were increased to 3,200 ft/d in simulation C-1, oscillatory behavior occurred in the second and third recoveries. When the maximum time step was reduced to mitigate this undesirable behavior, the computer run time increased to 48.9 hours. Run times also depend on other work being processed by the computer concurrently, but the processing times per time step did not vary much in these simulation runs. Run times for the test cases are listed in table 2, as are the horizontal hydraulic conductivities that would have been used in simulations assuming that the regional gradient was 0.4 ft/mi.

The ellipsoidal planar distributions of injected freshwater at various stages of the ASR cycles in case C-4 are shown in figure 26. The views correspond to the same times and ASR cycle stages as in the isotropic case C (basic simulation) to facilitate comparison with figure 24. At the end of the first injection, potable freshwater has just reached the observation well along the axis of minimum permeability. This would be consistent with the rapid freshening observed in the observation well in the hours following the end of the first injection. Progressive downgradient advection is evident in the second and third cycles. As in the isotropic case, some injected freshwater remains in a mix with native saline water downgradient of the injection well at the end of the 2.5-year third recovery.

Estimates of Potential Recovery Efficiency After Several Cycles

The calibrated simulations were used for estimating the recovery efficiencies that would be achievable by operating a similar well at the Hialeah site for several annual cycles, as would be done if the ASR process were implemented by water utilities as an alternative for augmenting dry-season water supply. Merritt (1985) reported that, given favorable hydrogeologic conditions, recovery efficiency increases rapidly in early repetitions of the ASR cycle, particularly if each recovery is terminated just when withdrawn water exceeds salinity criteria for potability, leaving some injected freshwater in the flow zone in a nonpotable mix with native brackish water.

The SWIP code was used to simulate 10 successive ASR cycles, using the four sets of calibration values given in table 2 for cases C, C-2, C-3, and C-4. Each cycle consisted of 5 months of injection at 150,000 ft^3/d, 3 months of storage, and a maximum of 4 months of recovery at 150,000 ft^3/d. In southern Florida the injection period might correspond to June through October (when ground-water levels are highest), the storage period might correspond to November through January (the early months of the dry season), and the recovery period might correspond to February through May (the later months of the dry season when water shortages periodically occur in the region). The model was coded to stop recovery in each cycle when solute fraction approximately reached a value of 0.1292, corresponding to 250-mg/L chloride concentration. The pumping rate was then changed to zero until the scheduled beginning of the next simulated injection.
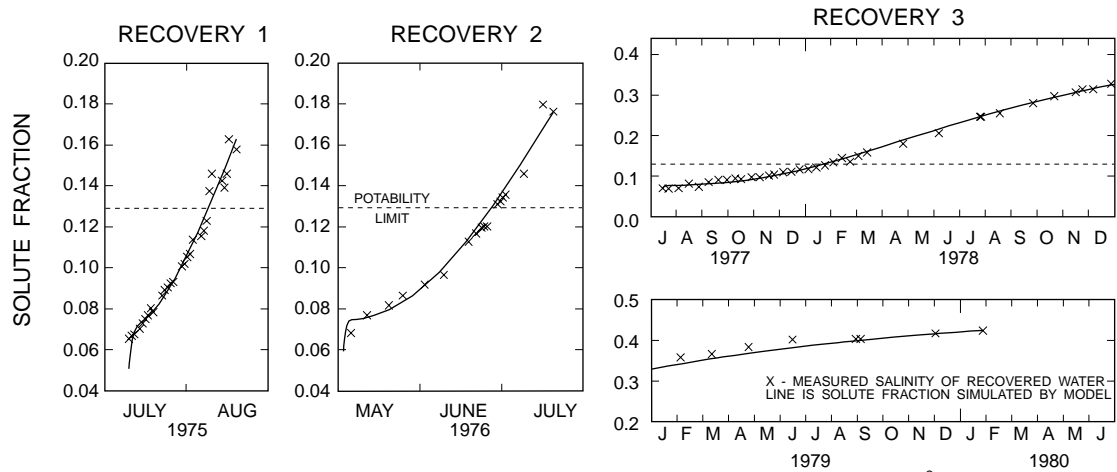
A. Basic simulation, case C: $\alpha_l = 65$ feet $= \alpha_t$, B = 12 feet, P = 35 percent, $D_m = 0.0002$ ft^2/d, VP = 260 ft/yr, $K_x = K_y = 800$ ft/d
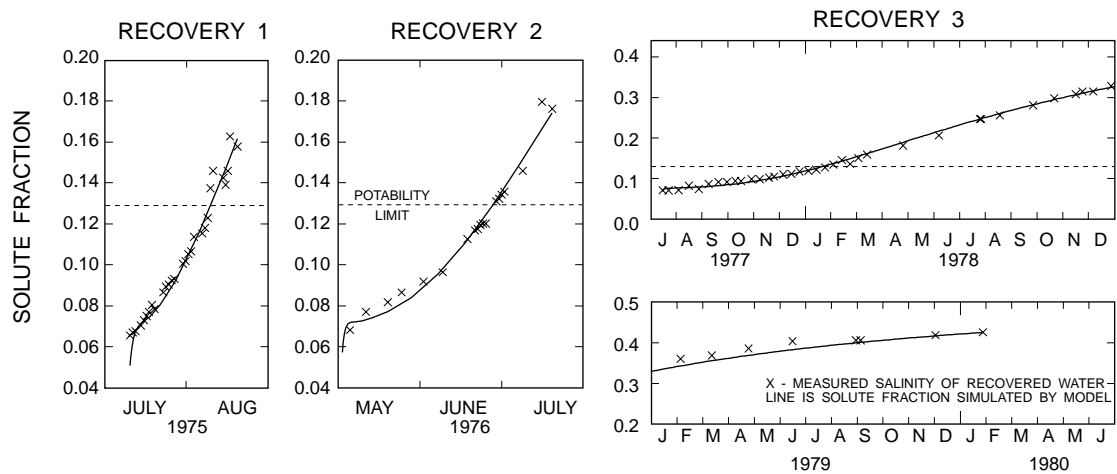
B. Higher hydraulic conductivities, lower regional gradient, case C1: $K_x = K_y = 3,200$ ft/d, VP = 260 ft/d, B = 12 feet, $\alpha_l = 65$ feet $= \alpha_t$, P = 35 percent, $D_m = 0.0002$ ft^2/d
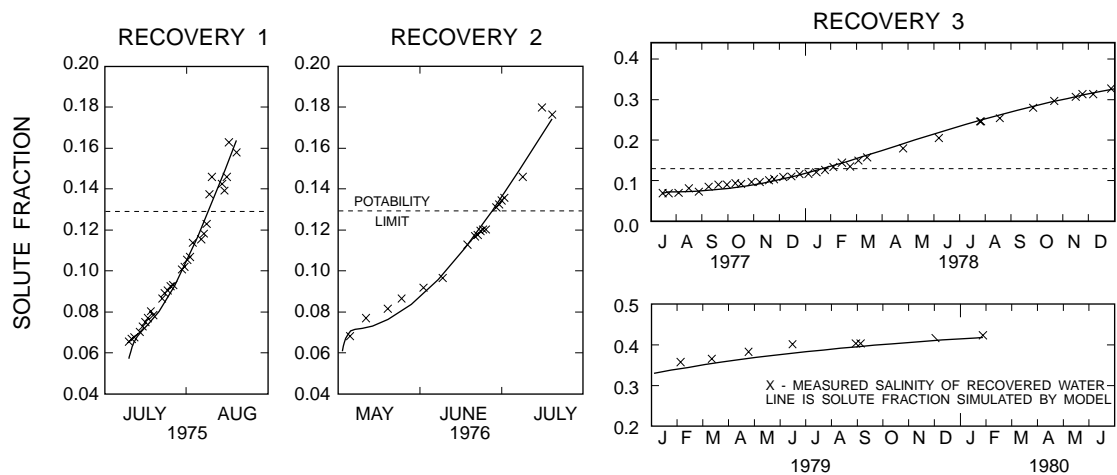
C. Increase flow-zone thickness, case C2: B = 21 feet, $\alpha_l = 50$ feet $= \alpha_t$, VP = 220 ft/yr, $K_x = K_y = 475$ ft/d, P = 35 percent, $D_m = 0.0004$ ft^2/d

Figure 25. Alternative simulations of the salinity of recovered water. P, flow-zone porosity, in percent; α_l, α_t, longitudinal and transverse dispersivities, in feet; B, flow-zone thickness, in feet; VP, aquifer pore velocity, in feet per year (ft/yr); D_m, molecular diffusivity, in feet squared per day (ft^2/d); K_X, K_Y, directional horizontal hydraulic conductivities, in feet per day (ft/d).
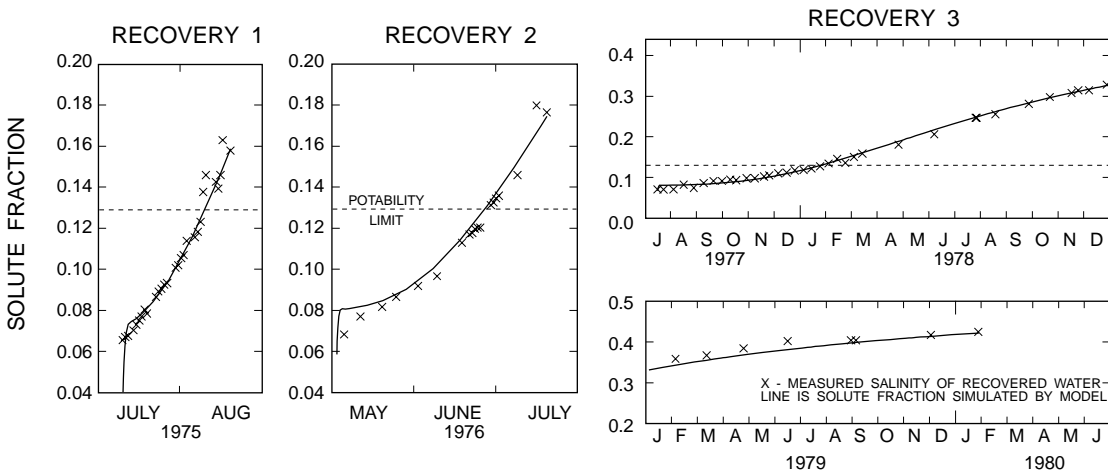
D. Lower flow-zone effective porosity, case C3: P = 20 percent, B = 12 feet, $K_X = K_Y$ = 750 ft/d, D_M = 0.0004 ft^2/d, VP = 364 ft/yr, α_l = 80 feet = α_t
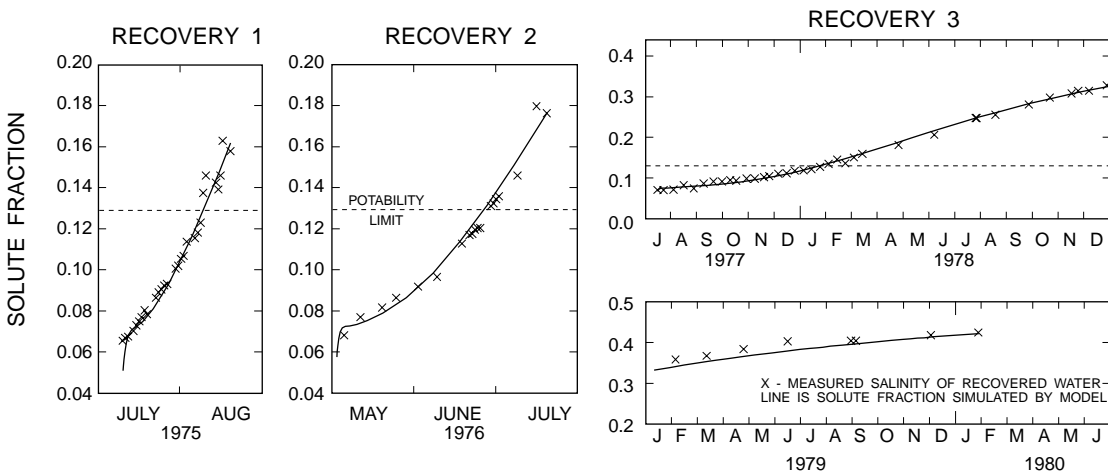
E. Anisotropic horizontal hydraulic conductivity, case C4: K_X = 2,350 ft/d, K_Y = 235 ft/d, B = 12 feet, VP = 364 ft/yr, α_l = 50 feet = α_t, P = 35 percent, D_M = 0.0002 ft^2/d

Figure 25. Alternative simulations of the salinity of recovered water--Continued.

Table 2. Physical and hydraulic properties and parameter values used to calibrate basic and alternative simulations of the freshwater injection, storage, and recovery tests

[Description: 1, basic simulation; 2, increase hydraulic conductivities, decrease regional gradient; 3, increase flow-zone thickness; 4, decrease flow-zone effective porosity; 5, anisotropic permeability. Abbreviations: ft/mi, feet per mile; ft/yr, feet per year; ft^2/d, square feet per day; in^2/lb, (pounds per square inch)$^{-1}$; K_x, K_y, hydraulic conductivities in the *x*- and *y*-coordinate directions, in ft/d; K_{xa}, and K_{ya}, adjusted hydraulic conductivities in the *x*- and *y*- coordinate directions, in ft/d]

Case	Descrip-tion	Flow-zone thickness (feet)	Flow-zone porosity (percent)	Regional gradient (ft/mi)	Regional pore velocity (ft/yr)	Disper-sivity value (feet)	Molecular diffusivity value (ft^2/d)	Rock compress-ibility (in^2/lb)	Hydraulic conductivity (ft/d)				Simulation run time (hours)
									Regional gradient				
									1.6 ft/mi		0.4 ft/mi		
									K_x	K_y	K_{xa}	K_{ya}	
C	**1**	12	35	1.6	260	65	0.0002	0.0000400	800	800	—	—	18.6–20.5
C-1	2	12	35	.4	260	65	.0002	.0000400	—	—	3,200	3,200	48.9
C-2	3	21	35	2.35	220	50	.0004	.0000225	475	475	2,780	2,780	13.3
C-3	4	12	20	1.4	364	80	.00006	.0000750	750	750	2,625	2,625	18.2
C-4	5	12	35	.8	364	50	.0002	.0000100	2,350	235	4,580	458	17.2–17.9
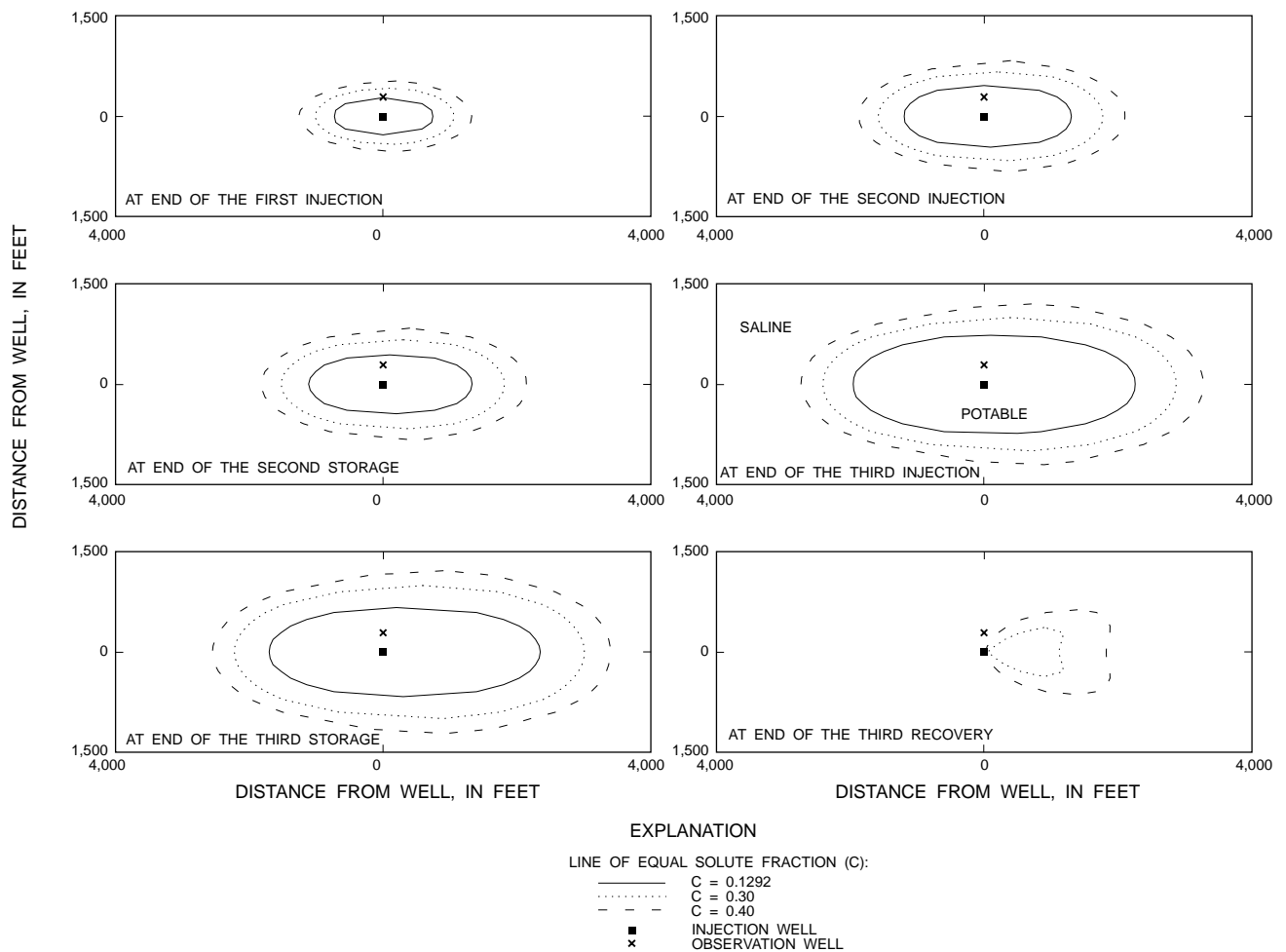
Figure 26. Horizontal distribution of injected freshwater at various stages of the aquifer storage and recovery cycles when permeability is anisotropic. A solute fraction of 0.1292 corresponds to a chloride concentration of 250 milligrams per liter.

Results of the 10 annual cycle simulations for the four cases and for an additional sensitivity analysis (case Ca) are given in the table below (values are recovery efficiency, in percent; dashes indicate not computed). Run C-2 was terminated by a power failure. As these computer runs required between 65 and 80 hours computing time on the PRIME 9955, and results of the run appeared definitive after six cycles, run C-2 was not repeated.

For each set of calibration values (C to C-4), virtually the same limiting recovery efficiency of 67–70 percent for the given schedule and rates was

nearly realized after only four cycles. That the different simulations generally encompassed the likely range of possible values of true aquifer thickness, effective porosity, permeability, and permeability anisotropy enhances confidence in the result of the predictive simulations, which are shown to depend on the replication of observed changes in recovered water salinity in the three disparate ASR cycles rather than on the precise identification of aquifer parameters.

One of the principal limitations on recovery efficiency in these simulations was the high rate of regional flow, which was computed to be 260 ft/yr in

Case	Cycle 1	Cycle 2	Cycle 3	Cycle 4	Cycle 5	Cycle 6	Cycle 7	Cycle 8	Cycle 9	Cycle 10
C	40.6	58.4	63.9	66.3	67.4	68.0	68.3	68.4	68.5	68.55
C-2	41.8	58.4	63.2	65.1	65.9	66.3	—	—	—	—
C-3	42.0	58.1	62.5	64.6	65.7	66.4	66.8	67.0	67.2	67.2
C-4	40.1	58.9	65.1	67.8	69.1	69.7	70.1	70.2	70.3	70.3
Ca	45.1	67.9	76.3	>80.0	—	—	—	—	—	—

simulation C. The deleterious effect of downgradient advection is illustrated by simulation Ca, a sensitivity analysis in which the regional pore velocity was assumed to be much smaller (13 ft/yr). Substantially higher recovery efficiencies were realized, ranging from 45 percent in the first cycle to 76 percent in the third cycle. The maximum recovery efficiency possible in these simulations was 80 percent because injection was for 5 months, and recovery at the same rate was limited to 4 months. After 4 months of pumping potable water in the fourth cycle, the chloride concentration of the recovered water remained below the cutoff limit (250 mg/L), and indications were that recovery efficiency could have approached 90 percent in later cycles if a greater withdrawal rate had been specified.

Simulation of Observation-Well Data

Part of the data collected at the observation-well site during the injection and recovery cycles was considered earlier in describing the thickness and hydraulic properties of the injection zone. Generally, water-quality and pressure data from the observation well, though clearly showing qualitative changes caused by the injection and recovery process, fail to unambiguously support the conceptual model of flow and transport used as a basis for simulating water-quality changes during recovery.

A comparison of water-quality and pressure data measured at the observation well with solute fractions and pressures simulated at this location by the calibrated models described in the previous sections is helpful in (1) illustrating the similarities and dissimilarities between measurements and model computations, and (2) evaluating the accuracy of simulations of observed water-quality changes at specific locations in aquifers with solution porosity when the transport of fluids occurs near those locations.

Salinity Data

A simulation of salinity changes measured in the flow zone at the location of the observation well, 289 ft from the injection well, required a revision of the previously described simulation procedures. Because the injection rate varied as a result of wellbore clogging, there was an accompanying variation in the rate of freshwater movement toward the observation well that determined the water-quality changes occurring at the well. Therefore, valid synthetic times could not be assigned to observation-well samples, as was done for recovered water-quality data, and the transport of freshwater toward the observation well could not be accurately simulated using average rates. To provide the desired accuracy, the injection and recovery time periods were subdivided into shorter periods, during which rates remained approximately uniform. The three injection periods were subdivided into 9, 12, and 25 subperiods with corresponding average well rates. The aborted second injection was also explicitly simulated as a 7-day event. Because withdrawal rates varied less than the injection rates, the three recovery periods were subdivided into three, two, and nine subperiods for assignment of average rates.

The simulations were performed using the four sets of calibration values (C, C-2, C-3, and C-4) representing the basic calibration and three alternative calibrations. Chloride concentration values from the silver monitor (1,020 ft) were converted to solute-fraction values based on interpolated dissolved-solids estimates, as previously described, for comparison with the simulated solute-fraction values. The grid spacing that placed four nodes between the injection-well and observation-well nodes (fig. 19) used for aquifer-test simulations was employed again in these simulations.

Computed solute-fraction values and solute-fraction values based on measured data are shown on plate 2. Comparing the four computed curves, it seems that the 21-ft-thick aquifer simulation (C-2) and the horizontally bipolar anisotropic simulation (C-4), in which the observation well is in the direction of lowest permeability, each show a later arrival time of injected freshwater and a less rapid decrease in salinity at the observation well during the first injection, compared with the basic simulation (C, 12-ft thick horizontally isotropic aquifer, 35 percent flow-zone porosity). The observation-well salinity computed by C-2 and C-4 remains higher than that computed by C during the increase of the first recovery and the decreases of the second and third injections. In the simulation where porosity is decreased to 20 percent in the injection zone (C-3), the computed salinities are lower than when porosity is 35 percent (C), representing an earlier arrival and greater proportion of injected freshwater at the well. All simulations indicate a substantial decrease of computed solute fraction during the 7-day aborted second injection of December 1975. The approximate arrival time of freshwater at the observation well in the first cycle, assuming isotropy, was previously observed to be 7–8 days.

None of the four simulations of observation-well salinity matches the measured salinity data except when nearly 100 percent freshwater surrounded the

observation well. Because large dispersivities (65 ft in simulation C) were used to match chlorides measured during recovery at the injection well, the model portrays the observation-well salinity as beginning a rapid decrease at the start of each injection. Computed curves are smooth and monotonic during each injection. Generally, the measured salinity is higher, undergoes more abrupt changes, and occasionally fluctuates considerably, showing no clear trend, as in the first and second injections. The measured data show the changes predicted by the model in a qualitative sense, but do not validate the simulated salinity changes in a quantitatively precise way. As previously noted, salinity fluctuations between 6 and 8 days could indicate the arrival of part of the injected water at the observation-well location during the three cycles.

Pore-Velocity Computations

In an attempt to resolve previously cited difficulties in explaining observed water-quality changes at the observation well immediately following the first and second injections, the model was used for an analysis of aquifer flow rates immediately following the end of the first injection, after the injection pump had been turned off. The simulation addressed the possibility that a sharp interface existed between injected and native waters near the observation well, and that the interface had nearly reached the observation well when the first injection was stopped. If a slight hydraulic gradient prevailed within the flow zone for a short time thereafter, breakthrough of fresh injected water could occur even after the injection pump was turned off. In addition, continuous pumping of the observation well at 5 gal/min for the automatic sampler/recorder could have influenced a nearby sharp interface to approach the observation well by accentuating or maintaining a lingering hydraulic gradient.

Hydraulic-head values at the observation-well node (22, 12) and the immediately adjacent node (22, 13) on the axis toward the injection well (fig. 19) were used to compute approximate pore velocity at the observation-well location just before and following the end of the first injection. The computation was based on Darcy's equation and on assumptions of 800-ft/d horizontal hydraulic conductivity and 35 percent effective porosity. The hydraulic gradient was estimated as the difference in head between the two nodes, 75 ft apart. Darcian flow estimates are not strictly accurate in environments of varying density (Hickey, 1989) but were considered an adequate

approximation for this analysis, given the low density contrast. When 5-gal/min pumping was specified, the nodal value representing a grid-block head average, and not a wellbore drawdown value, was used for the value of the well node head in the analysis. The subdivision of the first injection period into nine subperiods was used for the analysis to increase the accuracy of the computed flow rates in the aquifer near the observation well at the end of injection.

Assuming no pumping at the observation well, the computed pore velocity between the two nodes just before the end of the first injection was 14.08 ft/d. Fifteen minutes after injection pumping stopped, the simulated pore velocity dropped to 0.9 ft/d. After 24 hours, the pore velocity was 0.03 ft/d. The total distance traveled by water particles during the 24-hour period would have been about 0.05 ft. When the observation well was pumped at 5 gal/min in the simulation, the head simulated at node (22, 12) was about 0.1 ft lower during the first injection. The final injection pore velocity of 14.72 ft/d dropped to 1.55 ft/d 15 minutes after injection ceased, and to 0.67 ft/d after 24 hours. The total 24-hour travel distance was about 0.75 ft. Clearly, these simulations do not provide support for the hypothesis of substantial postinjection movement of a sharp interface between injected and native water. The movement of an interface in 24 hours under influence of the 260 ft/yr regional flow used in the basic calibration (C) would only be 0.71 ft. Furthermore, the direction of regional flow was approximately perpendicular to the radial-flow vector extending from the injection well to the observation well.

Pressure Data

Flow and transport processes between the two wells in the injection zone are further elucidated by comparing observation-well head changes during the ASR cycles with simulated head changes. Head changes at the observation well are determined by the injection-well inflow rate and aquifer characteristics, and are affected by injection-well borehole clogging only indirectly, through the effect on injection rate.

Observed and computed head changes at the observation-well location are shown on plate 2. Observed data are recorded pressures referenced to the preinjection value and converted to heads. The simulations shown are the basic calibration (C), the 21 ft-thick flow-zone calibration (C-2), the 20 percent flow-zone porosity calibration (C-3), and the

10:1 bipolar anisotropic calibration (C-4), each of which used a set of hydraulic parameters that replicated drawdowns observed at the injection well during the aquifer test of February 10, 1975. Hydrographs representing simulations C, C2, and C-3 depict similar head changes at the observation well. The C-2 head change is slightly less than that of simulation C, and the C-3 head change is slightly greater.

In harmony with theory, when anisotropy is assumed (curve C-4), computed head changes at the observation well located in the direction of least permeability are appreciably less than those computed by the isotropic basic calibration (C). The hydraulic response at the observation well is most rapid in the anisotropic case, in which the rock compressibility value was only one-fourth that of the isotropic case (C). A lower value of rock compressibility implies lower storativity and a more rapid transmission of hydraulic stresses through the aquifer.

Comparison of computed head changes with the observed data is difficult because the observed data seem to be affected by instrument calibration shifts and other errors occurring during the three ASR cycles. Unexplained pressure variations were recorded during the second storage period, and average heads during the four major inactive periods show variations of as much as 3 ft. Cessation of pumping water for the automatic sampler after the first cycle can only explain about 0.1 ft of the difference.

Arrival of warmer injected water at the observation well and consequent warming of water in the sampling tube in which pressure was monitored would have caused measured pressures to increase slightly at the wellhead. If the warmest injected water (27 °C) did not cool as it approached the observation well and entered the monitor tubes, the head increase at land surface could have been as much as 1.5 ft.

The observed hydraulic response to changes of stress is even more rapid at the observation well than predicted by the anisotropic model (C-4), lending some credence to the anisotropic hypothesis. Generally, the range of head variation in the second and third cycles is less than predicted by either isotropic or anisotropic models, though the difference is less with the anisotropic model. Possibly, a simulation with an even greater degree of anisotropy and using a smaller rock compressibility value would have better simulated the head data.

A comparison of injection and recovery hydraulic responses at the observation well in each cycle leads to an interesting result. Because the hydraulic response at a point within the aquifer is linearly related to the rate of inflow or outflow at the injection well, the ratio of inflow and outflow rates should be the same as the ratio of corresponding head changes at the observation well. Between August 28 and September 2, 1975, during the first injection, the inflow rate was approximately constant at 455 gal/min, and the head at the observation well was about 4.1 ft higher than the preinjection value. In the initial 14 days of the first recovery, the withdrawal rate averaged 335 gal/min, and the head at the observation well was about 4.8 ft lower than the preinjection value. Measured heads did not vary appreciably during these periods. The ratio of the injection and recovery rates is 1.36, and the ratio of the corresponding head changes is 0.85. This analysis was repeated for selected time intervals in the second and third ASR cycles, when rates were relatively constant. Results are given in the table below. To offset the apparent calibration drift after the first cycle, a head higher by 1.9 ft was accepted as representing a static (non-stress) condition in the second and third cycles.

	Injection			Withdrawal				
Cycle	Time period	Average rate (gallions per minute)	Average head change (feet)	Time period	Average rate (gallions per minute)	Average head change (feet)	Rate ratio	Head ratio
1	Aug. 28, 1975–Sept. 02, 1975	455	4.1	Sept. 10, 1975–Sept. 24, 1975	335	4.8	1.35	0.85
2	Feb. 20, 1976–Feb. 23, 1976	820	6.2	July 01, 1976–July 19, 1976	485	5.5	1.69	1.13
3	Oct. 22, 1976–Oct. 29, 1976	785	7.2	Nov. 04, 1977–Dec. 09, 1977	435	4.6	1.81	1.57

Subject to the difficulty in compensating for calibration errors in the pressure data, the results do not support the description of head changes measured in the observation well as being proportional to the inflow or outflow rate at the injection well. In fact, the head increases during injection seem to be damped in comparison with those observed during withdrawal, suggesting that some process retards flow between well locations during injection, compared with that occurring during withdrawal.

Directionally biased wellbore plugging, in which pores in the less permeable flow direction in an anisotropic aquifer would be plugged to a greater relative extent than in more permeable flow directions, was considered as a possible explanation. However, model simulations designed to test the hypothesis tended to refute rather than confirm it.

The difficulty in simulating observation-well pressure and salinity data illustrates the generalizing nature of porous-media models as applied to problems in secondary-porosity terranes. Simulating the salinity of recovered water merely requires a general representation of the diverse mixing processes occurring within the entire volume of aquifer occupied by injected freshwater. However, simulation of salinity changes at the observation-well location requires the correct representation of flow and mixing processes at all points between the two wells. If these processes differ from the generalizing assumptions of the recovery salinity model, a highly accurate simulation of observation-well data will likely not be achieved. In secondary-porosity media, such local departures from any generalized scenario of flow and mixing processes might be the norm rather than the exception.

SUMMARY

To deal with increasing water demands in a region characterized by seasonal surplus and deficit of water supply and limited reservoir capacity, water-management officials and others in southern Florida have sponsored operational testing of ASR, a water-conservation method in which subsurface formations containing brackish water are used for temporary storage of potable water. As part of a study conducted in cooperation with the SFWMD and the MDWSA, the USGS performed operational ASR tests at the Hialeah Well Field in Dade County.

A well for injecting freshwater and a second well for observing the hydraulic response and water quality were drilled 289 ft apart in late 1974 to depths of 1,105 and 1,064 ft. The injection- and observation-well casings extended to depths of 955 and 953 ft, respectively, so that the uncased part of the injection well was open to consolidated limestone of the intermediate confining unit and the Upper Floridan aquifer assigned to the Tampa Limestone, Suwannee Limestone, Ocala Limestone (if present), and Avon Park Formation. During drilling, a substantial augmentation of flow occurred between 985 and 1,065 ft.

Between July 1975 and January 1980, three ASR cycles were performed. In the first cycle, $41.9{\times}10^6$ gal of freshwater were injected. Recovery began after a 2-day storage period, and a recovery efficiency (volume of potable water recovered, expressed as a percentage of the volume injected) of 32.9 percent was realized. In the second cycle, $85{\times}10^6$ gal were injected and stored for 54 days. Recovery efficiency was 47.8 percent. In the third cycle, $208{\times}10^6$ gal were injected and stored for 181 days. Recovery efficiency was 38.5 percent, less than that of the second cycle. Recovery in all three cycles was by natural artesian flow.

Data acquired during the three ASR cycles include pressure-gage readings at the injection well-head and in two monitor tubes within the observation well. Volumetric data on quantity of inflow and out-flow were regularly obtained during the three cycles. A system of sampling tubes extending to various depths was installed in the open part of the observation well, and water samples were obtained both manually and also, during the first cycle, by means of an automatic sampler/recorder. Before the ASR cycles and at several times during the cycles, water samples from injection and observation wells and from the shallow well used for injection supply were analyzed for major inorganic ions, bacteria, chemical oxygen demand, biochemical oxygen demand, nutrients, total organic carbon, metals, field pH, alkalinity, and specific conductance. The chloride concentration and specific conductance of recovered water were measured frequently. Volumetric readouts from the in-line flow-meter were also recorded at the same time to establish a relation between volume of flow and water quality. Special analyses were made for algal species, nitrate-reducing bacteria, sulfate-reducing bacteria, iron bacteria, dissolved gases, and uranium isotopes.

Plugging of the wellbore occurred during the injections, causing the wellhead pressure to increase and the inflow rate to decrease. Injectivity was

restored by 2- or 3-hour backflushes at the natural artesian flow rate. These backflushes were performed at weekly intervals during the third injection, and well-head pressure and inflow rate remained generally uniform. An X-ray diffraction analysis of the back-flushed sediment showed very fine particles of calcite and iron (not scale).

At Hialeah the top of vertically contiguous consolidated limestone of the Floridan aquifer system is about 975 ft below land surface within the Suwannee Limestone. A shelly interval within the interval from 1,015 to 1,050 ft contains the principal flow zones. Data from an aquifer test at the site were analyzed using various methods, providing transmissivity estimates that range from 8,825 to 12,600 ft^2/d. A slight drawdown was measured in the 840-ft monitor tube during the aquifer test, indicating minor leakage across the confining beds separating it from the injection zone.

Data from spinner flowmeter logs were analyzed to delineate the flow zone by identifying intervals within the injection zone yielding the larger proportions of flow from the well. One such zone was found after analysis of 18 flowmeter logs. The top of the flow zone seemed to be about 1,024 ft below land surface in the injection well. The bottom of the flow zone seemed to be about 1,036 ft below land surface on the basis of some flowmeter log analyses. Temperature and fluid-resistivity logs run during recovery of injected water suggested that minor quantities of freshwater could enter the formation to a depth of about 1,047 ft below land surface. A diameter-compensated neutron porosity log showed porosity to average about 35 percent, there being wide variation in thin, discrete intervals.

Because of its importance for ASR feasibility, injection-zone salinity was the water-quality characteristic of most significance for this study. The chloride and dissolved-solids concentrations of water in the principal flow zone were 1,200 and 2,700 mg/L, respectively. Water from the 840-ft monitor tube had chloride and dissolved-solids concentrations of 1,700–2,300 mg/L and 3,900–5,000 mg/L, respectively, considerably higher than those of the flow zone 180 ft below. The dissolved-solids concentration in relatively impermeable rocks overlying and underlying the flow zone was assumed to be about 6,000 mg/L, and the relatively low salinity of the flow zone was assumed to be the result of flushing from areas of recharge in central Florida, 150 to 200 mi upgradient.

Data from widely scattered locations indicate that permeable strata in the Upper Floridan aquifer are present near erosional surfaces at the tops of the Ocala Limestone, if present, and Avon Park Formation, both of Eocene age. The top strata of Eocene age seems to correspond to a marked contrast in natural gamma activity (high above, in beds containing phosphatic materials, and low below). The chloride concentration of water at this contact increases from less than 900 mg/L at the St. Lucie County ASR site, to 1,200 mg/L in central and northeastern Dade County, and to more than 2,200 mg/L on the island of Key Largo in Monroe County.

A solute-transport code was used for simulating the salinity of water recovered after injection of freshwater. The model is fully three-dimensional, and solution of the equations is by standard finite-difference techniques. Fractional values ranging between 0 and 1 describe the relative concentrations of two miscible fluids in the aquifer. Values of density are associated with the extreme values of solute fraction, and water density within the modeled domain is considered to be a time-varying linear function of solute fraction, temperature, and pressure.

A Cartesian coordinate system was selected for the simulations so that downgradient advection and anisotropy could be represented. Boundaries were 20,000 ft from the injection well at their nearest point, and time-invariant pressure values were specified at the boundaries as an approximation that did not affect simulated freshwater flows during the ASR cycles. Central differencing techniques were used to eliminate first-order numerical dispersion related in degree to grid-cell sizes and the length of time increments.

A series of numerical tests was devised to examine the importance of the vertical component of mechanical dispersion and of molecular diffusion from the confining zones and their effect on recovery efficiency. The original 1979 SWIP code algorithms for vertical dispersion and advective weighting were compared with experimental techniques, and various values were assigned to transverse dispersivity, molecular diffusivity, and a scaling factor for vertical dispersion. The tests showed that when the experimental methods were used to eliminate vertical dispersion across flow-zone boundaries, a significant influence on recovery efficiency is the degree of molecular diffusion from the more saline confining zones. The magnitude of this influence depends upon the degree of vertical dispersion occurring within the

flow zone, which is under user control by use of the scaling factor. When the 1979 methods were used, vertical dispersion across flow-zone boundaries reduced recovery efficiency.

Observed drawdown data from the aquifer test of February 10, 1975, were simulated to derive estimates of hydraulic parameters for use in simulations of recovery chloride increases. Based on the assumption derived from interpretation of geophysical and water-quality data that the flow zone was 12 ft thick, isotropic, and had an effective porosity of about 35 percent, the drawdown data were calibrated by setting values of horizontal hydraulic conductivity equal to 800 ft/d and the value of rock compressibility to 0.0000400 $(lb/in^2)^{-1}$. The calibrated hydraulic parameters were used to derive estimates of composite hydraulic parameters (transmissivity and storage coefficient) for the injection zone. The transmissivity was computed to be 9,600 $[(ft^3/d)/ft^2]$ft, and the equivalent storage coefficient was computed to be 7.8×10^{-5}.

Alternative calibrations of the aquifer-test data were obtained to give consideration to the possibility that assumptions concerning the aquifer physical properties were in error. Alternative assumptions were that (1) the flow zone was 21 ft thick; (2) flow-zone effective porosity was 20 percent; and (3) flow-zone hydraulic conductivity had a 10:1 horizontal anisotropy, the preferred flow direction being at a right angle from a vector pointing from the injection well to the observation well. Each aquifer-test calibration showed excellent agreement with observed data.

The hydraulic parameters determined from the aquifer-test calibration that assumed a 12-ft flow zone having a 35 percent effective porosity were used as part of a simulation of the chloride increases observed during the three recoveries. A simulation was completed by setting the longitudinal and transverse dispersivities equal to 65 ft, by setting the molecular diffusivity equal to 0.0002 ft^2/d, and by assuming a hydraulic gradient in the aquifer of 1.6 ft/mi, about 4 times as large as estimated from regional hydraulic-head measurements. The computed regional pore velocity was 260 ft/yr. When results of simulating the aquifer test were disregarded and hydraulic conductivity values were assumed to be 3,200 ft/d, the literature estimate of 0.4 ft/mi for the regional hydraulic gradient led to a virtually identical simulation. This result was possible because the higher estimate of hydraulic conductivity did not lead to buoyancy stratification in the simulations, given the prevailing low density contrast between injected and native aquifer water.

Sets of hydraulic parameters determined from the three aquifer conceptual models used for alternative calibrations of the aquifer-test data were again used for three additional, and equally accurate, simulations of the recovery salinity data. Each simulation used a unique set of calibration parameters different from the others. Because the conceptual models differed in parameters based on field data that could not be accurately measured, the solution dependence upon possible errors in the accepted estimates of these parameters was evaluated by this procedure.

Given the accuracy with which recovered water salinity was simulated in three disparate ASR cycles, predictive simulations were made with a fair degree of confidence. An arbitrary schedule of injection and withdrawal was specified: five wet-season months of injection at 150,000 ft^3/d, followed by three early dry-season months of storage, and then by a maximum of four late dry-season months of withdrawal at 150,000 ft^3/d. These runs showed recovery efficiency to improve from about 40 percent in the initial cycle to nearly 70 percent in later cycles. The cited figures depend on the specified rates and schedule. The predictive run was repeated with sets of calibration parameters that represented the alternative conceptual models previously described. Each case yielded results similar to those of the basic simulation, lending credence to the predictive application of the model and showing that predictive results depended on the simulation of recovered water salinities rather than on the precise identification of aquifer parameters. When regional pore velocity was substantially reduced, recovery efficiency exceeded 80 percent in the fourth cycle, demonstrating the adverse influence of the large degree of downgradient advection indicated by the calibrated models.

Additional model runs in which the temporal variation in well rates was discretized in greater detail attempted to simulate head and salinity changes at the observation well, given the same four aquifer descriptions used for the simulations of recovered water salinity and the predictive analyses. Although the general trends of the measured data and simulated values are similar, neither the observed head changes nor the salinity changes are accurately matched by the model computations. Most likely, unknown local heterogeneities in aquifer hydraulic properties in the neighborhood of the observation well rendered the generalized design of the model, developed to simulate recovery salinity changes, inappropriate for precise simulations of hydraulic or water-quality changes at an isolated point location, such as that of the observation well.

REFERENCES CITED

Chih Shan Chen, 1965, The regional lithostratigraphic analysis of Paleocene and Eocene rocks of Florida: Florida Geological Survey Bulletin 45, 105 p.

Ehrlich, G.G., Godsy, E.M., Pascale, C.A., and Vecchioli, John, 1979, Chemical changes in an industrial waste liquid during post-injection movement in a limestone aquifer, Pensacola, Florida: Ground Water, v. 17, no. 6, p. 562–573.

Hickey, J.J., 1989, An approach to the field study of hydraulic gradients in variable-salinity ground water: Ground Water, v. 27, no. 4, p. 531–539.

Hoopes, J.A., and Harleman, D.R.F., 1967, Dispersion in radial flow from a recharge well: Journal of Geophysical Research, v. 72, no. 14, p. 3595–3607.

INTERA Environmental Consultants, Inc., 1979, Revision of the documentation for a model for calculating effects of liquid waste disposal in deep saline aquifers: U.S. Geological Survey Water-Resources Investigations Report 79–96, 73 p.

INTERCOMP Resource Development and Engineering, Inc., 1976, A model for calculating effects of liquid waste disposal in deep saline aquifers; Part 1—Development, Part 2—Documentation: U.S. Geological Survey Water-Resources Investigations Report 76–61, 253 p.

Jacob, C.E., 1940, On the flow of water in an elastic artesian aquifer: American Geophysical Union Transactions, pt. 2, p. 574–586.

Jacob, C.E., and Lohman, S.W., 1952, Nonsteady flow to a well of constant drawdown in an extensive aquifer: American Geophysical Union Transactions, v. 33, p. 559–569.

Kipp, K.L., Jr., 1987, HST3D—A computer code for simulation of heat and solute transport in three-dimensional ground-water flow systems: U.S. Geological Survey Water-Resources Investigations Report 86–4095, 517 p.

Kohout, F.A., 1965, A hypothesis concerning cyclic flow of salt water related to geothermal heating in the Floridan aquifer: New York Academy of Sciences Transactions, ser. II, v. 28, no. 2, p. 249–271.

Lantz, R.B., 1971, Quantitative evaluation of numerical diffusion (truncation error): Society of Petroleum Engineers Journal, September 1971, p. 315–320.

Lohman, S.W., 1979, Ground-water hydraulics: U.S. Geological Survey Professional Paper 708, 70 p.

Merritt, M.L., 1985, Subsurface storage of freshwater in south Florida—A digital model analysis of recoverability: U.S. Geological Survey Water-Supply Paper 2261, 44 p.

———1991, Nonunique simulations of the quality of water recovered following injection of freshwater into a brackish aquifer, *in* Proceedings of the Fifth Biennial Symposium on Artificial Recharge of Groundwater—Challenges of the 1990's, Tucson, Ariz., May 29–31, 1991, p. 255–266.

———1993, Aspects of numerical and representational methods related to the finite-difference simulation of advective and dispersive transport of freshwater in a thin brackish aquifer: Journal of Hydrology, 148, p. 61–92.

Merritt, M.L., Meyer, F.W., Sonntag, W.H., and Fitzpatrick, D.J., 1983, Subsurface storage of freshwater in south Florida—a prospectus: U.S. Geological Survey Water-Resources Investigations Report 83–4214, 69 p.

Meyer, F.W., 1989a, Hydrogeology, ground-water movement, and subsurface storage in the Floridan aquifer system in southern Florida: U.S. Geological Survey Professional Paper 1403-G, 59 p.

———1989b, Subsurface storage of liquids in the Floridan aquifer system in southern Florida, 1943–83: U.S. Geological Survey Open-File Report 88–477, 25 p.

Miller, J.A., 1986, Hydrogeologic framework of the Floridan aquifer system in Florida and in parts of Georgia, Alabama, and South Carolina: U.S. Geological Survey Professional Paper 1403-B, 91 p.

Price, H.S., Varga, R.S., and Warren, J.E., 1966, Application of oscillation matrices to diffusion-convection equations: Journal of Mathematics and Physics, no. 45, p. 301–311.

Reeder, H.O., Wood, W.W., Ehrlich, G.G., and Ren Jen Sun, 1976, Artificial recharge through a well in fissured carbonate rock, West St. Paul, Minnesota—Hydrodynamic dispersion and movement of injected water by Ren Jen Sun: U.S. Geological Survey Water-Supply Paper 2004, p. 52–75.

Reilly, T.E., 1990, Simulation of dispersion in layered coastal systems: Journal of Hydrology, 114, p. 211–228.

Scott, T.M., 1988, The lithostratigraphy of the Hawthorn Group (Miocene) of Florida: Florida Geological Survey Bulletin 59, 148 p.

Voss, C.I., 1984, SUTRA—a finite-element simulation model for saturated-unsaturated fluid-density-dependent ground-water flow with energy transport or chemically reactive single-species solute transport: U.S. Geological Survey Water-Resources Investigations Report 84–4369, 409 p.

Voss, C.I., and Souza, W.R., 1987, Variable density flow and solute transport simulation of regional aquifers containing a narrow freshwater-saltwater transition zone: Water Resources Research, v. 23, no. 10, p. 1851–1866.

Wedderburn, L.A., and Knapp, M.S., 1983, Field investigation into the feasibility of storing freshwater in saline parts of the Floridan aquifer system, St. Lucie County, Florida: South Florida Water Management District Technical Publication 83–7, 135 p.

APPENDIXES

APPENDIX A—DRILLING LOG OF INJECTION WELL G-3061 AND OBSERVATION WELL G-3062

Drilling Log of Injection Well G-3061

[Lithology and remarks by W.L. Miller to 970 feet and by F.W. Meyer below 970 feet. S, soft; VS, very soft; M, medium; H, hard; VH, very hard; min/ft, minute per foot; –, no data]

Date in 1974	Depth interval (feet)	Relative drilling hardness	Drilling speed (min/ft)	Lithology and remarks
Oct. 3	0–8	S	0.375	Black top soil, tan, sandy subsoil, light-tan limestone, oolite at about 8 ft.
	12–15	S-M	3.33	Light-tan limestone, solution-riddled, shells, some dark-tan limestone.
	20–23	M	1.66	Limestone-sandstone contact about 19–20 ft, white to light-tan sandstone, fine to medium, limestone fragments. Surface casing (30 in.) set to 19.95 ft below land surface, 13 in. cut off, 25 in. above ground, original length 23.11 ft. Drove 30-in. surface casing down.
Oct. 4	25–30	S	—	Fine to very fine quartz sandstone, shell fragments.
	30–35	S	—	White to light-tan coloration.
	35–40	S	—	
	40–45	S-M	—	Fine sandstone and lenses of limestone, hard zone at 41 ft, shell fragments in limestone, 10 percent limestone in cuttings.
	45–50	S	—	Fine quartz sandstone, some large quartz sand, ream.
	50–55	—	1.0	Limestone at 54 ft, hard rock.
	56–58	H	—	Gray to white limestone, quartz sand, coarse grains.
	60–62	H	3.0	
	62–65	H	—	Limestone, concretions, little sand.
	60–65	H	2.0	Calcareous sandstone, limestone, shells, quartz sand.
	65–68	—	—	Secondary calcite, sandy limestone, a few shells.
	68–70	H	7.0	
	70–75	H	—	More calcite (secondary), hard limestone.
	75–80	H	7.1	Cavernous sandy limestone, fine-grained quartz sand.
	80–82	H	—	Large cavities, lost circulation, very sandy limestone.
	82–88	H	—	No circulation, lost mud, large cavities. Surface casing settled to 3 ft below land surface, 22.03 ft of casing in ground must seal formation and cement in additional surface casing.
Oct. 7	88–90	M	3.0	Calcareous sandstone to limestone, large percentage of quartz sand, medium- to fine-grained, white to tan, cavities.
	90–95	M	3.2	Very sandy limestone, gray to tan, some loss of circulation.
	95–100	M	—	Fort Thompson/Caloosahatchee Marl(?). Soft, dense calcareous sandstone, tan to gray.
	100–105	S	—	Same as above, fast drilling, shells.
	105–108	S	—	Same as above.
	108–110	S	—	Same.
	110–115	S	—	Some green marl in sample, coarse.
	115–120	S	—	Quartz sand.
	120–125	S	—	Green marl, barnacles, large quartz grains, shells.
	125–128	S	—	Same as above, phosphates, shells.
	128–130	S	—	Same as above.
	130–135	S	—	No sample.
	135–140	S	—	Same as above.
	140–145	S	—	Caloosahatchee Marl/Tamiami(?). Some presence of white–green clay, oyster shell, *Ostrea hytensi(?)*.
	145–148	S	—	Some quartz sand, increasing amount of green clay.
	148–150	S	—	No sample.
	150–155	S	—	Green marl, shell, green clay increasing.
	155–160	S	—	No sample.
	160–168	S	—	More green clay balls, phosphates, shells.
	168–170	S	—	No sample.
	170–175	S	—	Green marl, green clay, shells, phosphates.
	175–180	S	—	Hawthorn Formation, large quantity of green clay (first predominant clay).
	180–188	S	—	Eighty-five-percent green clay.
	188–190	M	—	Decrease in clay, green marl, little clay.
	190–195	M	—	Green marl, coarse quartz sand, shell, little clay.
	195–200	M	—	Green marl, little clay, coarse quartz sand.

Date in 1974	Depth interval (feet)	Relative drilling hardness	Drilling speed (min/ft)	Lithology and remarks
Oct. 7	200–208	M	—	Still little or no clay.
	208–210	M	—	No sample.
	210–215	M	0.6	Dense sandstone, green sandy marl, little clay, quartz, medium to coarse.
	215–220	M	—	No sample.
	220–225	M	—	Dense green shale and sandstone, shell fragments, no clay.
	225–228	M	—	Same as above.
	228–235	M	—	Green shale, fine grained to sandy, dense.
	235–240	—	—	Clayey marl, green shale, quartz sand.
	240–248	—	—	Same as above.
Oct. 8				Ream to 48 ft.
Oct. 9				Ream to 72 ft, lost some mud.
Oct. 10				Ream to 95 ft, lost circulation 82–95 ft.
Oct. 11				Ream to 167 ft.
Oct. 14				Ream to 206 ft, hole reamed to 29-in. diameter to depth of 206 ft, will set 200 ft of 24-in. OD casing.
Oct. 15				Back into hole to check depth, only 3 ft short of 206 ft.
Oct. 16				Ten yards cement used to seal casing to a depth of about 201 ft. Shut down for day to allow cement to harden.
Oct. 17				Prepared to resume drilling, opened casing, and drilled bird nest.
Oct. 18				Cemented casing to land surface, took 1 yard additional cement.
Oct. 21				Start 9 7/8-in. pilot hole.
	250–260	S	1.2	Green marl, large percent clay, fine-grained quartz sand.
	260–270	S	—	Same as above.
	270–280	S	—	Green marl, 75–80 percent clay.
	280–290	S	—	Green marl, fine-grained quartz sand, some fragments limestone.
	290–300	M	2.1	Same as above.
	300–310	M	—	Green marl, large amount of very fine sand.
	310–320	M	—	Same as above.
	320–330	M	—	Same.
	330–340	M	—	Same.
	340–347	M	—	Same.
Oct. 22	347–360	S	.46	Fine-grained sand, green clay, 90 percent sand.
	360–370	S	—	No sample has reached surface yet.
	370–380	S	—	Same as above.
	380–390	S	—	Marl, fine sand, marl breaking up and sand too fine to settle, little or no sample can be collected.
	390–400	S	—	No sample.
	400–410	S	—	Hit layer of limestone at 406 ft, sample is fine sand and green clay.
	410–420	M	1.1	Dense clayey sand, green, very fine quartz.
	420–430	M	—	Sandy limestone and green marl, very fine green quartz, increasing limestone.
	430–440	M	—	Limestone, some very fine quartz sand.
	440–450	M	—	Sandy limestone, some green clay.
	450–460	M	—	Same as above.
	460–470	M	—	Same.
	470–480	M	—	Same.
	480–490	M	—	Same.
	490–500	S-M	—	Fine, dense limestone, white, some fine quartz sand.
	500–510	S-M	—	Limestone, breaks into small fragments.
	510–520	S-M	.8	Relatively clean limestone, little sand.

Date in 1974	Depth interval (feet)	Relative drilling hardness	Drilling speed (min/ft)	Lithology and remarks
Oct. 22	520–530	S-M	—	Limestone, soft, fragments crush easily.
	530–540	S-M	—	Same as above.
	540–550	S-M	—	Same.
Oct. 23	550–560	S-M	1.4	Gray lime marl.
	560–570	M	—	Gray and green marl, large amount of gray clay, limestone.
	570–580	S	—	Gray and green marl.
	580–590	S	—	Gray marl (clay)
	590–600	S	—	Same as above.
	600–610	S	—	Same.
	610–620	M	2.1	Gray-green marl, increasing shells, limestone.
	620–630	M	—	Same as above.
Oct. 24	630–647	M	—	White limestone, mostly shells, quartz sand, fine to coarse.
	647–660	S	—	Gray limestone, shelly, some green fragments.
	660–670	S	—	Same as above.
	670–675	S	—	Gray limestone, shelly, probably Tampa Formation.
	675–680	S	—	Gray limestone, shell, tan quartz sand increasing.
	680–685	S	—	Gray limestone, fine quartz sand, clear.
	685–690	S	—	Limestone, shell, echinoid spines, sand (sample of last 40 ft).
	690–695	S	—	Mostly shell fragments, some sand.
	695–700	S	—	Same as above.
	700–705	S	—	Large shell fragments, some sand.
	705–707	S	—	Large shell fragments, echinoid spines, circulating.
	707–715	S	—	Limestone, shelly, clay increasing.
	715–720	S	—	Gray limestone, shell, some gray clay.
	720–725	S	—	Gray limestone, shell, some fine quartz sand.
	725–727	M	—	Gray limestone, gray-green clay increasing, circulating.
	727–735	M	—	Gray limestone, shell, gray clay.
	735–740	H	—	Shell, sand, green clay.
	740–745	H	—	Green limestone, gray limestone, green clay, shell decreasing.
	745–747	H	—	Same as above, circulating.
	747–755	H	—	Gray limestone, not much clay, little shell.
	755–760	H	—	Same as above.
	760–765	H	—	Gray limestone, dense, breaks into small fragments.
	765–767	H	—	Same as above, circulating.
	767–775	M	—	Softer gray limestone, some shell, little sand.
	775–780	S	—	Gray limestone, no shell or sand.
	780–785	S	—	Same as above.
	785–787	—	—	Same as above, circulating.
Oct. 25	787–795	M	—	Gray limestone, some shell.
	795–800	M	—	Same as above, some dark-green fragments.
	800–805	M	—	Same as above, large amount of mollusks.
	805–807	M	—	Same as above, circulating.
	807–815	M	—	Some green clay in gray limestone.
	815–820	M	—	Clay increasing in gray limestone.
	820–825	M	—	Large amount of gray clay in shell limestone.
	825–827	S	—	Gray-green clay, stringer of limestone at 826 ft, circulating.
	827–835	—	—	Gray clay and tan limestone.
	835–840	—	—	Tan limestone.
	840–845	—	—	Same as above.
	845–847	—	—	Same as above, circulating.
	847–855	S	—	Fine-grained tan limestone.
	855–860	S	—	Tan limestone, crushes easily.
	860–865	S	—	Same as above, some green clay.
	865–867	S	—	Large amount of light-green clay and tan limestone, circulating.
	867–875	M	—	Gray-green clay and large amount of gray limestone.
	875–880	M	—	Gray limestone, soft, crushes easily, little clay.
	880–885	M	—	Soft gray limestone.
	885–887	M	—	Same as above and gray clay, circulating.

Date in 1974	Depth interval (feet)	Relative drilling hardness	Drilling speed (min/ft)	Lithology and remarks
Oct. 28	887–895	M	—	Very sandy green marl, very fine quartz sand.
	895–900	M	9.0	Sandy green marl, little sample because most of green clay is breaking up in mud, drilling mud has changed from gray to green color, limestone fragments increasing.
	905–907	M	—	Same as above, circulating.
	907–915	M	—	Sandy green marl, phosphates in sample.
	915–920	M	—	Lime chips, green marl, forams, phosphate.
	920–925	M	—	Same as above.
	925–927	M	—	Same.
	927–930	M	—	Same.
Oct. 29	930–935	M	9.0	Green marl, forams, shell.
	935–940	M	—	Same as above, more green clay.
	940–945	M	—	Same as above.
	945–947	M	—	Lighter colored green clay, shell, phosphate, softer material.
	947–955	S	5.0	Green marl, limestone at 954 ft.
	955–960	S	3.0	Green clay, some lime, fine quartz sand.
	960–965	S	—	No sample.
	965–967	S	—	Green clay, mostly shell, mollusks, tan fossiliferous limestone.
	967–970	S	—	Tan to gray limestone, fossiliferous. Will set casing at about 970 ft (F.W. Meyer), removed all drill pipe from hole.
Oct. 30				Reaming hole to 22.5 in. at 258 ft.
Oct. 31				Reaming hole to 22.5 in. at 389 ft.
Nov. 4				Reaming hole at 436 ft.
Nov. 5				Reaming hole at 460 ft.
Nov. 22				Cemented 14-in. casing at 955.28 ft below top of 24-in. casing.
Dec. 2				Obtained gamma log from 0 to ±940 ft. On bottom with 11 7/8-in. bit, top of cement at 946 ft. First sign of returns, 25-minute lag in cuttings from cement plug.
	946–955	H	3.63	
	955–965	H-S	3.50	Slight flow. Hard to 957 ft; soft at 957 ft.
	965–970	H	1.80	Soft streaks.
	970–975	H	1.60	Limestone, gray, silty, tiny black specks, soft streaks.
	975–980	H	1.20	Same as above, *Miogypsina* sp., soft streaks.
	980–985	S	1.60	Limestone, gray-white, fossils *Operculinoides* sp. and papillate(?). Laps. Flow estimated at 10 gal/min, hard streaks.
Dec. 3				Collected 1 pint water sample, T=73.0 °F; slight H_2S. Hole filled back to about 970 ft.
	970–985	—	—	Drilling out filled-in hole. First sign of returns. 25-minute lag in cuttings. Water sample collected.
	985–990	H	10.4	Very hard streaks.
	990–995	M	3.4	Limestone, gray, sand as above, very hard streaks, 985–990 ft.
	995–1,000	S	1.4	
	1,000–1,005	S	1.4	Limestone, cream-tan, fossils of *Operculinoides* sp., and gray limestone as above.
	1,005–1,010	S	2.0	
	1,010–1,015	S	1.8	Same as above, more forams and some shell fragments.
	1,015–1,020	S	1.6	Permeability increases here.
	1,020–1,025	S	1.8	Limestone, tan-gray, some shell but many forams, barnacles.
	1,025–1,030	S	1.8	Noticeable increase in flow. Coarse fragments of echinoids and ribbed mollusks.
	1,030–1,035	S	3.4	Hard streaks, 1,032–1,035 ft. Limestone, tan-gray, coarse fragments of mollusks.
	1,035–1,040	S	1.2	Increase in flow.
	1,040–1,045	S	1.0	Limestone, cream, soft, porous, fossiliferous, miliolids.
	1,045–1,050	S	1.4	

Date in 1974	Depth interval (feet)	Relative drilling hardness	Drilling speed (min/ft)	Lithology and remarks
Dec. 3	1,050–1,055	VS	.6	Same as above, some gray shale.
	1,055–1,060	S	1.4	
	1,060–1,065	S	.6	Same as above, many *Dictyoconus* sp., Avon Park Formation.
	1,065–1,070	S	1.2	
	1,070–1,075	S	.8	
	1,075–1,080	—	.6	
	1,080–1,085	—	.4	Limestone, tan, many *Dictyoconus* sp. Terminated circulation, coming out of hole.
Nov. 4				Barbara Howie collected water samples for extended complete analysis (bacteria, standard complete, chemical oxygen demand, biochemical oxygen demand, nutrients, total organic carbon, metals, field pH, alkalinity, specific conductance, chloride). F.W. Meyer and W.A. Long logged hole (electric, caliper, gamma) and found obstruction (cement at 964 ft prevented flowmeter survey). Apparently, a piece of cement wall in overdrill below casing cracked off and lodged across the borehole. Cancel logging by Schlumberger. Jim Kern plans to return December 9 with drilling rig to drill out the cement. Estimated flow about 500–600 gal/min.
Dec. 9				Collected water sample. T=70.3 °F, moderate H_2S, flow about same. Going into hole, on top of cement slab at 964 ft.
	964–1,085	—	—	Drilled 964–1,085 ft, cement now at bottom. Decided to drill another 20 ft below cement, cuttings show greater than 50 percent cement.
	1,085–1,090	S	.6	
	1,090–1,095	S	.6	
	1,095–1,100.5	S	.8	
	1,100–1,105.5	S	1.0	Limestone, tan, microfossils, and much cement.
Dec. 10				Collected 1 L water sample. Flow about same, about 600 gal/min. Drillers cleaning up area.
Dec. 11				Construction forms for floor.
Dec. 13				Poured concrete floor.
Dec. 16				Drillers clean up site, remove equipment.
Dec. 17				Pressure measurement.

Drilling Log of Injection Well G-3062

[Lithology and remarks by W.L. Miller to 183 feet and by F.W. Meyer below 183 feet. S, soft; VS, very soft; M, medium; H, hard; VH, very hard; min/ft, minute per foot;. —, no data]

Date	Depth interval (feet)	Relative drilling hardness	Drilling speed (min/ft)	Lithology and remarks
Oct. 11, 1974	0–5	VH	0.21	Fine-grained, white Miami Oolite and gray consolidated sand.
	5–10	S	1.0	Brown limestone and gray consolidated sand; tan limestone, some fossils evident.
	10–15	S	.8	Lost circulation at 13 ft, back at 14 ft.
	15–20	S	.4	White sandstone cemented with calcium carbonate.
	20–25	S	—	Same as above. Adding drill stem. Drill stopped for day for repairs.
Oct. 14, 1974	25–30	S	—	Drilling with 7 7/8-in. bit for pilot hole. Limestone and sand grains cemented with limestone. Large fragments greater than 5 millimeters.
	30–35	S	—	Same as above. Mainly small fragments, 1–5 millimeters.
	35–40	S	—	Bit chatter at 39 ft. Limestone, not as much sand as above.

Date	Depth interval (feet)	Relative drilling hardness	Drilling speed (min/ft)	Lithology and remarks
	40–43	VH	10	Equal amounts of small and large fragments.
	43–45	VH	9.0	Small limestone fragments, more cemented sand than at 35–40 ft.
	45–50	VH	5.0	Small fragments of limestone. Larger fragments of cemented sand grains.
	50–55	S	.8	Same as above.
	55–60	S	2.0	Same.
	60–63	VS	.67	Same.
	63–65	S	1.5	Same.
	65–70	S	2.0	Same.
	70–75	S	1.6	Same as above. Lost circulation at 72 ft, back at 73 ft.
	75–80	S	2.0	Very hard at 80 ft, bit chattering.
	80–85	H	—	Lost circulation at 81 ft, mixing mud.
	85–90	—	1.4	Pumped drilling mud at a very slow rate. No circulation.
	90–95	S	1.0	
	95–100	S	.4	No sampling from 80 to 100 ft.
	100–105	—	—	Gray sand cemented with limestone, many shell fragments. Upon reaching 103 ft, pumped at a faster rate and achieved circulation.
	105–110	VS	.5	
	110–115	VS	.3	Same as at 100–105 ft.
	115–120	VS	.4	Lost circulation between 117–118 ft.
	120–123	VS	.33	Grayish-white marl, sand grains, limestone and shell fragments.
	125–130	VS	1.0	Same as above.
	130–135	VS	.4	Same as above, but grayer.
	135–140	VS	.2	
	140–145	VS	—	Lost circulation at 143 ft.
	145–150	VS	.2	
	150–155	VS	.2	
	155–160	VS	.2	
	160–163	VS	.33	No circulation from 143 to 163 ft.
	163–165	VS	—	
	165–170	VS	.2	
	170–175	VS	.3	
	175–180	VS	.1	
	180–183	VS	.17	No samples from 143 to 183 ft. Started to pick up circulation at 183 ft. Letting hole set overnight.
Oct. 15, 1974	183–185	—	2.5	Shell, dark-gray, very coarse quartz sand, some green clay. Much aquagel. Losing returns.
	185–190	—	1.0	Shell, dark-gray to white, fine to very coarse quartz sand, some gray sandstone, phosphorite, cf. barnacles.
	190–203	VS	2.6	Still losing returns; shell as above.
	203–208	VS	1.0	Some hard streaks. Added rod, lost returns. Sand, light-gray, fine.
	208–215	S	1.4	Hard streaks. No returns. Removed drill pipe to add reaming bits. Start reaming 7 7/8-in. hole to 22 3/4 in. No lag.
Oct. 16, 1974				7 7/8-in. pilot hole reamed to 187 ft (22 3/4-in. diameter), rain stopped drilling.

Date	Depth interval (feet)	Relative drilling hardness	Drilling speed (min/ft)	Lithology and remarks
Oct. 17, 1974				200-ft level reached. Preparing to set 14-in. casing. Total casing 200.52 ft.
Oct. 18, 1974				Cemented casing to 200 ft, used 390 bags (17 yards).
Oct. 21, 1974				Temperature log of 150 ft of cased, cemented hole. Gamma log to 150 ft.
Oct. 22, 1974				Drilled 7 7/8-in. pilot hole to 460 ft. Caught own samples, no log kept.
Oct. 23, 1974				Pilot hole to 740 ft. No log kept.
Oct. 24, 1974				Began to go back into hole. Bridged at ±240 ft. On bottom at 740 ft. Circulating new mud.
	740–764	S	0.416	Shell, white to gray, cf. mollusks, white sticky clay, little hard dark-green sandy clay.
	764–769	S	.6	Shell, white to gray, cf. mollusks, white sticky clay, little hard, dark-green, sandy clay.
	769–774	S	1.4	Same as above.
	774–779	S	1.8	Same as above. Shell is bluish.
	779–784	S	.4	Limestone, white to gray, soft, shelly, sticky white clay and hard dark-green sandy clay concretions resembling casts of worm burrows.
	784–789	S	.6	Same as above; casts of small snails.
	789–794	S	.8	Same as above; snail casts, shark teeth, and light-green clay.
	794–799	S	1.25	Same as above; light-green sandy clay.
	799–804	S	1.0	Same as above.
	804–809	S	1.8	Limestone, white, soft, shelly, white calcareous clay and dark-green sandy clay concretions.
	809–814	S	1.8	Same as above.
	814–817	S	3.8	Clay, white, sticky, shelly, and limestone as above.
	819–824	S	3.0	Clay, white, some shell, and stringers of limestone. Some flat branching Bryozoa.
	824–829	S	.8	Limestone, tan to white, soft, some shell.
	829–834	S	.4	Same as above.
	834–839	S	.6	Same.
	839–844	S	2.0	Limestone, tan to white, soft, clayey, some shell (less than at 824 ft).
	844–849	S	1.0	Limestone, tan, soft, porous, clayey, some shell.
	849–854	S	.6	Same as above.
	854–859	S	1.4	Same as above; some hard streaks.
	859–864	S	2.6	Limestone, tan, soft, clayey, and some green clay.
	864–869	S	1.25	Same as above; shell.
	869–874	S	.6	Same as above; light-green "slipperly" clay.
	874–879	S	1.25	Shell, mollusks, and soft light-green to tan clay.
	879–884	S	1.4	Clay, light-green, "slippery," and pieces of hard dark-green calcareous clay or limestone, some shell as at 804 ft.
	884–889	S	3.0	Clay, light-green, sticky, and tan shelly limestone.
	889–894	S	3.6	Same as above.
	894–899	S	2.4	Same as above.
	899–904	S	3.4	Clay, dark-green, slightly sandy (very fine quartz) and large mollusks.
Oct. 25, 1974				Driller has bit stuck at 884 ft.
Oct. 29, 1974				Driller retrieved 7 7/8-in. bit.
Oct. 30, 1974				Driller repairing equipment.
Oct. 31, 1974				Driller reaming 7 7/8-in. hole to 13.5 in.
Nov. 14, 1974				6 5/8-in. OD steel casing on bottom, free and clear, 953 ft deep.

Date	Depth interval (feet)	Relative drilling hardness	Drilling speed (min/ft)	Lithology and remarks
Nov. 19, 1974				5 7/8-in. bit on bottom and circulating. On float shoe, soft cement.
	953–958	—	1.8	Drilling out cement plug.
	958–961	—	3.3	Pieces of cement and the float shoe. Well is flowing from drill pipe.
	961–966	—	1.6	
	966–971	S	1.0	
	971–976	S	.8	
	976–984	S	.8	Tan to gray shell, sand, and dark-green shale. Duplicate sample shows tan fossiliferous limestone.
	984–989	S	.6	(?) Suwannee Limestone; *Miogypsina* sp. cf.
	989–994	S	1.6	Hard streak at 989 ft. Limestone, tan, many forams cf. *Miogypsina*.
	994–999	S	.4	Soft with hard streaks.
	999–1,004	VS	.6	Same as above.
	1,004–1,009	VS	.8	
	1,009–1,014	VS	.4	Same as above.
	1,014–1,019	VS	.2	
	1,019–1,024	VS	.2	Same as above; some blue-gray limestone.
	1,024–1,029	VS	.2	
	1,029–1,034	VS	1.0	
	1,034–1,044	VS	3.3	Medium to hard at 1,039 ft.
	1,044–1,049	S	.2	Flow about 200 gal/min estimated. Slight H_2S odor.
	1,049–1,054	S	.2	Tan limestone, fossiliferous, Avon Park fauna noted.
	1,054–1,059	S	.4	
	1,059–1,064	VS	.4	Limestone, tan, fossiliferous. Many *Dictyconus* and *Coskinolinus*, few *Lepidocyclinus* and *Operculinoides* sp. Water sample analyzed by Miami Water Department. Decided to terminate drilling at 1,064 ft. All drill pipe and collars out of hole. Flow increased to estimated 250 gal/min.
Nov. 20, 1974				Water samples collected by D.J. McKenzie for complete analysis. Q=240 gal/min.
Nov. 17, 1974				Pressure gage measurement.
Feb. 6, 1975				Measured flow with 4- and 5-in. orifices.
Feb. 10, 1975				Flow tests. Monitoring well Q=250 gal/min for 100 minutes.
Feb. 24, 1975				Obstruction at 983.7 ft. Original total depth is 1,064 ft. Filled into ±1,054 ft. "Clean out" needed. Rig in place and drill stems stacked. No apparent obstruction at 983.7 ft. Bottomed at 1,058 ft. Clean out to 1,064.83 ft (total depth). Pulled off well and capped. Let run overnight. Rig will leave tomorrow.

APPENDIX B—LITHOLOGIC DESCRIPTION OF ROCK SAMPLES FROM INJECTION WELL G-3061 AND OBSERVATION WELL G-3062

Lithologic Description of Rock Samples from Injection Well G-3061

[Description is by R.T. Mooney, Florida Geological Survey]

Depth interval (feet)	Description
0–5	Sand; unconsolidated quartz; pale-yellowish-brown (10 YR 6/2); grains are primarily subangular to subrounded, clear, clean quartz; very fine to fine sand size, fair sorting; above 25 percent brown-black organic-looking materials (peat?); traces (1 percent) of limestone; small gastropod shell.
8–11	Limestone, very pale orange (10 YR 8/2); evidence of solution activity; some very fine quartz grains in the limestone; trace of white clay; few shell fragments and shell molds.
12–15	Primarily limestone as above; beginning of an unconsolidated sand layer; clear, very fine sand, moderately sorted, subangular to subrounded quartz grains; also much fine sand size, limestone pieces.
20–25	Sand; unconsolidated quartz; white (N 9); very clean, clear, subangular to subrounded; very fine to fine sand grains with fair sorting; some pieces of limestone as above; piece of crab claw; few abraded shell fragments.
25–50	Same as above.
51–53	Sandstone; pinkish-gray (5 YR 8/1); calcareous cement; sand grains are primarily quartz, subangular to subrounded, fine to very fine sand size; some calcite grains are present; some pieces of limestone with evidence of solution activity is also present; few shell fragments.
55–105	Same as above; varying from a calcareous sandstone to a sandy limestone in different sample intervals, increasing shell fragments.
105–110	Same as above, increasing shell fragments.
110–115	Shell bed; pinkish-gray (5 YR 8/1) to medium-gray (N 5); many warm, abraded, gray and white shell fragments; also pieces of limestone and sand with sandstone from above; few rounded sand-size phosphorite grains.
115–145	Same as above; traces of a white clay.
150–155	Shell bed as above; beginning of a very light olive-gray (5 Y 7/1) clay.
160–175	Same as above.
175–180	Clay, yellowish-gray (5 Y 7/2); fine sand-size, rounded, quartz grains in the clay; calcareous; some large quartz and phosphorite grains, rounded; many shell fragments, bryozoan; trace of limestone.
180–188	Same as above; less shell fragments.
188–190	Mixture of shell bed, worn abraded pelecypod shells, and clear quartz sandstone with a calcareous clay matrix.
190–195	Sandstone as above, yellowish-gray (5 Y 7/2); trace of shell fragments and limestone.
195–200	Same as above.
200–208	Much sandstone as above; beginning of a yellow-gray, slightly calcareous clay; trace of shell fragments.
208–215	Clay as above; some sandstone as above; trace of shell fragments.
220–225	Clay as above; decreasing sandstone and shell fragments.
225–228	Clay as above; same sandstone and sandy limestone.

Depth interval (feet)	Description
228–235	Clay, pale-olive (10 Y 6/2); marly when wet, calcareous; trace of sandstone and limestone; few shell fragments; bryozoan, echinoid spine.
235–240	Same as above.
240–248	Clay, medium-olive (10 Y 5/2); very sandy, calcareous; some shell fragments and limestone pieces; bryozoan.
250–260	Same as above.
260–270	Clay, medium-olive (10 Y 5/2); very sandy, calcareous; trace of sandy limestone.
270–280	Same as above; trace of shell fragments.
280–290	Same as above; some phosphate.
290–300	Same as above; decreasing in sand.
300–310	Same as 260–270 ft; some phosphate.
310–327	Same as 300–310 ft.
330–347	Same as above; much quartz sand (fine to medium).
347–360	Sand, unconsolidated, clear quartz and phosphorite, fine to medium, moderately sorted, subrounded.
360–390	Same as above; trace of clay, some zircon(?) present, *Globigerina ruber.*
390–410	Unconsolidated sand as above, yellowish-gray (5 Y 7/2), change of color may be due to an increase of clay.
410–420	Same as 390–410 ft; slight increase in clay and larger grains phosphorite.
420–430	Same as above; beginning of a white limestone.
430–440	Same as above.
440–450	Same as above; increase in clay content.
450–460	Clay, yellowish-gray (5 Y 8/1), very sandy, phosphorite, trace of limestone, *Rubulus.*
460–470	Limestone, yellowish-gray (5 Y 8/1); much sand and clay, phosphorite, echinoid spine.
470–480	Same as above; slightly less clay, trace of sand and phosphorite.
480–490	Same as above.
490–500	Primarily limestone as above; increase in clay and sand (very fine) content, trace of very fine phosphorite.
500–510	Limestone, yellowish-gray (5 Y 8/1); yellowish-gray clay; phosphorite; some shell fragments.
510–550	Same as above.
550–560	Limestone as above; about 50 percent, except broken into larger granule-size fragments; about 40 percent clean quartz sand, subangular to subrounded, fine to medium sand size; some polished phosphorite grains; rest of sample is composed of traces of shell fragments, dolomite, and chert(?).
560–570	Limestone, yellowish-gray (5 Y 8/1); granule-size fragments covered with a yellowish-gray calcareous clay; some quartz sand, pieces of "proto" sandstone composed of quart sand grains with a clay matrix; traces of chert; unknown hard black material (possibly phosphorite), some of it in a honeycomb pattern.
570–580	Clay, yellowish-gray (5 Y 8/1); calcareous; pieces of limestone, shell fragments, dolomite, phosphorite from above.
580–630	Clay as above.

Depth interval (feet)	Description
630–647	Limestone, white (N 9) to yellowish-gray (5 Y 8/1); covered with white clay; many shell fragments; some calcite crystals, fine.
647–705	Limestone as above; decreasing clay; many shell fragments.
705–725	Same as above.
725–727	Clay, yellowish-gray (5 Y 8/1); calcareous; silt to very fine sand size phosphorite (few coarse-size grains); many limestone and shell fragments; some quartz sand.
727–747	Same as above; trace of a light-olive gray (5 Y 6/1) clay; gradually turning into a limestone with high amount of clay.
747–755	Limestone; very light yellowish-gray (5 Y 9/1); seems to be a calcilutite to a very fine calcarenite; white clay; very fine calcite crystals; few shell fragments.
755–760	Same as above.
760–787	Same as above.
787–795	Primarily as above; beginning of a clay, light-olive-gray (5 Y 6/1); clay has a high percentage of quartz sand within it; in some cases it seems to be a "proto" sandstone composed of fine sand grains in a clay matrix.
795–820	Largely as above with an increasing clay covering on the limestone.
820–825	Limestone, yellowish-gray (5 Y 8/1); soft; much yellowish-gray calcareous clay; shell fragments; traces of quartz sand grains weakly cemented with clay matrix.
825–827	Clay, yellow-gray (5 Y 8/1); calcareous; many white limestone fragments, soft; shell fragments.
827–835	Clay as above.
835–875	Same as above.
875–880	Primarily clay as above; increasing limestone and shell fragments.
880–885	Shell hash; pinkish-gray (5 YR 8/1) to yellowish-gray (5 Y 8/1); many shell fragments, primarily pelecypod; limestone fragments with very fine phosphorite grains within it; trace of white clay.
885–887	Shell bed as above, but with much more clay; covers everything.
887–895	Sand, unconsolidated, yellowish-gray (5 Y 8/1); composed of calcite, quartz and phosphorite grains; silt to fine sand size; some clay material; forams, *Rubulus*(?), *Amphistegina*(?) (very small).
895–900	Same as above.
900–905	Sand, very light olive-gray (5 Y 7/1); primarily sand-size limestone fragments and silt to very fine quartz and phosphorite grains; much clay; traces of light-olive-gray (5 Y 6/1) clay; shell fragments.
905–907	Same as above.
907–915	Sand, yellowish-gray (5 Y 8/1); primarily fine sand-size quartz and calcite grains; many pieces of light-olive-gray (5 Y 6/1) clay; silt-size phosphorite(?) grains within the clay; shell fragments.
915–920	Same as above; much light-olive-gray (5 Y 6/1) clay; 50 percent of sample.
920–927	Sand as in sample 907–915 ft; traces of light-olive-gray (5 Y 6/1) clay.

Depth interval (feet)	Description
927–930	Clay, light-gray (N 7) and yellowish-gray (5 Y 8/1); much quartz and calcite sand; shell fragments; traces of phosphorite and dolomite(?).
930–945	Same as above.
945–947	Primarily as above; pieces of chert.
947–955	Sand, white to a light-olive-gray (5 Y 6/1); composed of rounded phosphorite, quartz and calcite grains, fine to medium sand size, much light-gray (N 7) clay; chert and dolomite; shell fragments.
955–960	Clay, light-olive-gray (5 Y 6/1); sample contains much quartz, phosphorite, and calcite sand; chert; shell fragments.
960–965	Clay, white (N 9); very fine black specks (possibly phosphorite) in the clay; much unknown gray material (drilling contamination?); much limonite rust from drill stem.
965–975	White clay as above; less unknown gray material.
965–967	Light-olive-gray clay as in sample 955–960 feet; many shell fragments.
967–970	Same as above; pieces of white limestone.
975–985	Limestone, white (N 9); also pieces of buff white limestone and clay; everything is covered with clay; shell fragments; forams *Operculinoides*(?), abraded *Heterostegina*(?), *Miogypsina* sp.
985–995	White limestone as above; no clay; abraded *Heterostegina*; few shell fragments.
995–1,005	Limestone, pinkish-gray (5 YR 8/1); seems to be a calcarenite, possibly bioclastic; *Operculinoides* sp., *Lepidocyclinus*(?).
1,005–1,015	Same as above.
1,015–1,025	Limestone, light-gray (N 7) and pinkish-gray (5 YR 8/1); many pieces from calcarenite above; many worn and abraded shell fragments and forams; pieces of gray dolomite and rounded phosphorite; echinoid spines; also some white limestone with black specks from above.
1,025–1,035	Same as above, but larger fragments.
1,035–1,045	Limestone, pinkish-gray (5 YR 8/1); bioclastic calcarenite; pieces of gray dolomite(?); few shell fragments; pelecypod, gastropod.
1,045–1,055	Lithology as above, but small fragments; *Dictyoconus cookei*, *Textularia*.
1,055–1,065	Same as above; *Dictyoconus cookei*(?).
1,065–1,085	Limestone; white (N 9) to pinkish-gray (5 YR 8/1); seems to be a bioclastic calcarenite; some evidence of recrystallization; *Dictyoconus cookei*.
1,085–1,105	Same as above.

Lithologic Description of Rock Samples from Injection Well G-3062

[Description is by R.T. Mooney, Florida Geological Survey]

Depth interval (feet)	Description
0–5	Limestone, pinkish-gray (5 YR 8/1); about 1 percent quartz sand grains in the limestone; evidence of solution activity.
5–55	Limestone as above; slightly higher percentage of quartz.
55–60	Sandstone, pinkish-gray (5 YR 8/1); calcareous matrix (almost a very sandy limestone); sandy grains are very fine to fine, subangular to subrounded, primarily quartz with some heavy minerals (darker, honey-colored grains); trace of shell fragments.
60–63	Largely sandstone as above; also pieces of a sandy limestone; traces of a white clay; traces of shell fragments.
63–65	Same as above; slightly increasing limestone.
65–70	Limestone, very light gray (N 8); quartz sand in the limestone (varying percentages); much sandstone as above; traces of shell fragments and white clay.
70–75	Same as above.
75–80	Same as above.
80–100	No sample.
100–105	Shell bed, white (N 9) and medium-gray (N 5); many broken, worn, and abraded pelecypod and gastropod shells; medium to coarse, rounded, polished quartz and phosphorite sand grains; pieces of limestone and sandstone as above.
110–115	Same as above.
120–123	Same as above.
125–130	Primarily as above; white clay on the cuttings; some fine sand-size limestone grains.
130–135	Same as above.
135–183	No sample.
183–190	Clay, light-olive-gray (5 Y 6/1); many very fine to fine quartz and calcite sand grains; some shell fragments from above; few medium sand-size, polished quartz and phosphorite grains as above.
190–203	Limestone, white (N 9) to greenish-gray (5 GY 6/1); large amount of calcareous clay and very fine quartz sand; shell fragments; phosphorite; traces of a calcareous sandstone.
203–208	Sand, unconsolidated; light-gray (N 7); primarily very fine to fine, clear quartz grains, angular to subrounded, some polished phosphorite and heavy mineral grains; some greenish-gray-clay from above; shell fragments and traces of limestone.
220–225	Clay; many pieces of limestone, shell fragments, and drill pipe rust all covered with a gray-greenish clay.
225–230	Same as above.
230–235	Clay, light-olive-gray (5 Y 6/1); calcareous; pieces of limestone, shell fragments, etc., from above; traces of fine quartz sand.
235–240	Same as above; minor phosphorite.

Depth interval (feet)	Description
240–245	Clay, olive-gray (5 Y 4/1) (slightly marly when wet); minor very fine quartz sand in the clay, minor phosphorite, limestone fragments from above.
245–270	Clay as above; increasing very fine quartz sand.
270–275	Clay as above; slight color change to about medium-olive-gray (5 Y 5/1).
275–290	Same as above.
290–295	Clay (5 GY 6/1), greenish-gray, very fine clear quartz, sandy; minor phosphate, traces of limestone and shell fragments.
295–300	Same as above.
300–305	Same as above.
305–310	Same as above.
310–315	Same as above.
315–320	Same as above; peat; *Amphistegina*(?).
320–325	Primarily as above; increasing limestone.
325–330	Same as above.
330–405	No samples.
405–410	Limestone, yellowish-gray (5 Y 8/1); covered with a grayish clay; soft limestone; trace of shell fragments; phosphorite.
410–415	Same as above; echinoid spine.
415–420	Same as above.
420–425	Same as above; increasing clay.
425–430	Limestone, yellowish-gray (5 Y 8/1); clay covering the limestone; minor phosphorite; shell fragments.
430–435	Same as above.
435–440	Limestone as above; increasing clay (about 40 percent clay).
440–445	Primarily clay-covered limestone as above; minor phosphorite; beginning of a white limestone bed.
445–450	Same as above.
450–455	White limestone as above; increasing clay; minor quartz in the limestone.
455–460	Same as above; decrease in clay.
460–465	Same as above; increasing quartz and phosphorite; shell fragments; echinoid spine.
465–470	Same as above; less quartz.
470–475	Same as above; increasing quartz (same as 460–465 ft).
475–480	Same as above; less quartz.

APPENDIX B—LITHOLOGIC DESCRIPTION OF ROCKS SAMPLES FROM INJECTION WELL G-3061 AND OBSERVATION WELL G-3062—Continued

Depth interval (feet)	Description
480–485	Same as above.
485–490	Limestone, white (N 9); seems to be a calcilutite; minor phosphate in limestone; trace of clay; some shell fragments.
490–495	Same as above.
495–500	Same as above.
500–505	Same as above.
505–510	Same as above.
510–515	Same as above.
515–520	Same as above; some shell molds in the limestone.
520–525	Same as above.
525–530	Same as above.
530–535	Same as above; slight increase in clay.
535–540	Same as above; trace of peat.
540–545	Clay, yellowish-gray (5 Y 8/1); calcareous; phosphorite in clay; about 40 percent limestone as above; trace of shell fragments.
545–550	Limestone as in 530–535 ft; about 20 percent clay (micrite?).
555–560	Micrite limestone as above; minor phosphorite.
560–565	Same as above.
565–570	Same as above.
570–575	Same as above.
575–580	Same as above.
580–585	Same as above.
585–590	Same as above; echinoid spine; decrease in phosphorite.
590–595	Same as above.
595–600	Same as above; trace of shell fragments.
600–605	Same as above; increase in shell fragments.
605–610	Same as above.
610–615	Same as above.
615–620	Same as above.
620–625	Same as above.
625–630	Same as above.

Depth interval (feet)	Description
630–635	Same as above.
635–640	Same as above.
640–645	Primarily as above; beginning of a consolidated, hard, white limestone, fossiliferous.
645–650	Same as above with increase of the fossiliferous hard limestone.
650–655	Same as above; shell fragments.
655–660	Same as above.
660–665	Same as above.
665–670	Limestone, white (N 9); fossiliferous, some of the micritic limestone; shell fragments.
670–675	Same as above; evidence of secondary calcite; echinoid spines.
675–680	Same as above.
680–685	Same as above.
685–690	Same as above.
690–695	Same as above.
695–700	Same as above.
700–705	Same as above.
705–710	Same as above.
710–715	Same as above.
715–720	Same as above.
720–725	Clay, yellowish-gray (5 Y 8/1); calcareous; silt-size phosphorite; about 40 percent limestone as above; shell fragments; trace of sand-size quartz.
725–730	Same as above.
730–735	Same as above; slightly decreasing clay.
735–740	Same as above.
744–764	Primarily as above; much quartz sand within clay (25 percent); beginning of a light-brown dolomitic limestone(?); shark tooth, shell fragments.
764–769	Limestone, white (N 9); much quartzitic clay as above; some dolomitic(?) limestone as above.
769–774	Same as above; white seems to be fossiliferous.
774–779	Same as above; phosphorite.
779–784	Same as above.
784–789	Same as above.

Depth interval (feet)	Description
789–794	Same as above; less clay.
794–799	Same as above.
799–804	Limestone, white (N 9); fossiliferous, some quartzitic clay as above; minor phosphorite.
804–809	Same as above; increase in calcareous, white clay (micrite?).
809–814	Same as above.
814–819	Micrite, yellowish-gray (5 Y 8/1); trace of quartzitic clay as above.
819–824	Same as above; increase in micrite clay.
824–829	Same as above; phosphorite.
829–834	Same as above.
834–839	Same as above; trace of quartz (some granules).
839–844	Same as above; increase in sand-size quartz.
844–849	Same as above; trace of phosphorite.
849–854	Same as above.
854–859	Same as above; beginning of a white fossiliferous limestone.
859–864	Limestone, white (N 9) covered with a calcareous white clay; shell fragments.
864–869	Same as above; increase in calcareous clay gives slight color change to yellowish-gray (5 Y 8/1).
869–874	Same as above; trace of quartz sand, echinoid spine.
874–879	Same as above.
879–884	Same as above.
884–889	Same as above; increasing shell fragments; trace of phosphorite, very fine.
889–894	Same as above; beginning of a gray phosphatic clay; increase in shell fragments.
894–899	Clay, white-olive-gray (5 Y 6/1), very fine phosphorite in clay, shell fragments, coarse sand-size quartz grains; some limestone as above.
899–904	Clay as above.
953–984	Limestone, yellowish-gray (5 Y 8/1); covered with a light clay, seems to be fossiliferous (forams); *Miogypsin*a, *Camerina*(?).
961–984	*Operculinoides*, *Heterostegina*.
984–994	Limestone, pinkish-gray (5 YR 8/1); covered with calcareous clay-size particles; minor phosphate; shell fragments; *Miogypsina*, *Camerina*.
994–1,004	Same as above; *Miogypsina*, *Camerina*.
1,004–1,014	Same as above.

Depth interval (feet)	Description
1,014–1,024	Same as above.
1,024–1,034	Dolomite, light-gray (N 7); moldic; microcrystalline; limestone as above (but bigger cuttings); less clay; quartz in limestone; minor phosphorite.
1,034–1,044	Same as above; limestone seems to be bioclastic in part.
1,044–1,054	Limestone, pinkish-gray (5 YR 8/1); fossiliferous; 35 percent dolomite as above; phosphorite; *Cermina*.
1,054–1,064	Limestone as above; less dolomite; more forams *Camerina*, *Amphistegina*.

APPENDIX C—VOLUME AND RATE DATA FROM INJECTION AND RECOVERY CYCLES AND QUALITY OF RECOVERED WATER

Time of measurement		Days from beginning of data	Cumulative volume readout on flowmeter (gallons)	Flow rate (gallons per minute)	Chemical concentrations in recovered water		Change of activity
Date	Hour				Chloride (milligrams per liter)	Specific conductance (microsiemens per centimeter)	
Aug. 1975							
17	1500		14,463				Begin injection 1
17	1610		16,110	-176			
18	803	1	115,795	-782			
18	1630	1	168,400	-776			
19	1435	2	302,440	-757			
21	706	4	543,540	-742			
21	1600	4	596,300	-739			
22	920	5	706,920	-796			
22	1535	5	736,510	-590			
23	1040	6	838,400	-666			
23	1610	6	875,590	-843			
24	755	7	964,650	-705			
24	1613	7	1,010,850	-694			
25	849	8	1,102,650	-689			
25	1456	8	1,136,245	-685			
28	738	11	1,470,180	-643			
28	1437	11	1,515,390	-807			
28	1618	11	1,524,900	-704			
29	747	12	1,602,050	-621			
30	742	13	1,722,930	-630			
31	725	14	1,841,560	-624			
Aug. 1975							
01	734	15	1,956,440	-593			
04	735	18	2,279,790	-560			
05	739	19	2,387,740	-559			
06	734	20	2,493,900	-553			
07	727	21	2,599,140	-549			
08	734	22	2,707,300	-559			
11	733	25	3,011,430	-527			
12	730	26	3,111,680	-522			
13	740	27	3,210,995	-512			
14	740	28	3,307,820	-503			
15	734	29	3,407,640	-521			
18	736	32	3,704,050	-513			
19	1600	33	3,834,570	-502			
20	741	34	3,895,860	-487			
21	749	35	3,994,380	-509			
22	748	36	4,088,880	-491			
25	735	39	4,366,030	-481			
26	814	40	4,450,440	-427			
27	811	41	4,550,850	-523			
28	756	42	4,638,030	-458			
29	740	43	4,726,000	-462			

Time of measurement		Days from beginning of data	Cumulative volume readout on flowmeter (gallons)	Flow rate (gallons per minute)	Chemical concentrations in recovered water		Change of activity
Date	Hour				Chloride (milligrams per liter)	Specific conductance (microsiemens per centimeter)	
Sept. 1975							
02	800	47	5,074,400	-451			
03	759	48	5,150,450	-395			
04	744	49	5,245,300	-498			
05	750	50	5,332,120	-449			
08	746	53	5,585,730	-440			
08	1145	53	5,599,050	-417			
08	1157	53	5,600,032	-612			
10	1318	55	5,600,033				Begin backflow I
11	1253	56	5,664,050	338	66	650	
12	1241	57	5,728,500	338	68	650	
14	1020	59	5,851,400	336	76	680	
15	1100	60	5,918,500	339	84	720	
16	1030	61	5,981,700	335	90	760	
17	730	62	6,038,100	335	96	760	
18	820	63	6,105,400	338	106	800	
19	715	64	6,166,500	332	100	800	
22	825	67	6,362,460	334	124	870	
23	750	68	6,425,800	337	132	920	
24	815	69	6,491,500	335	136	900	
25	825	70	6,554,640	326	142	930	
26	855	71	6,619,000	328	144	950	
29	615	74	6,816,700	356	166	1,035	
30	820	75	6,873,600	272	270	1,040	
Oct. 1975							
01	830	76	6,938,000	332	180	1,075	
02	820	77	7,000,700	328	184	1,100	
03	840	78	7,065,200	330	205	1,150	
06	910	81	7,256,200	328	210	1,230	
07	900	82	7,319,200	330	218	1,215	
08	825	83	7,381,200	330	232	1,250	
09	840	84	7,443,480	320	275	1,280	
10	750	85	7,504,500	328	300	1,310	
10	1350	85	7,526,100	449			
10	1730	85	7,536,900	367			
14	815	89	7,738,500	290	290	1,435	
15	830	90	7,794,900	290	280	1,450	
16	900	91	7,840,200	231	300	1,450	
17	755	92	7,892,700	286	350	1,580	
20	755	95	8,068,100	304	335	1,620	
20	930	95	8,072,100	315			
24	1048	99	8,072,100				Pump test
24	1055	99	8,072,900	-855			
24	1130	99	8,077,100	-898			Meter burned out

Time of measurement		Days from beginning of data	Cumulative volume readout on flowmeter (gallons)	Flow rate (gallons per minute)	Chemical concentrations in recovered water		Change of activity
Date	Hour				Chloride (milligrams per liter)	Specific conductance (microsiemens per centimeter)	
Nov. 1975							
07	900	113	8,082,396	-2			
Dec. 1975							
08	730	114	8,082,400				Pump test
08	917	144	8,085,542	-220			
10	1034	146	8,085,542				Injection
10	1108	146	8,090,960	-1,192			
11	931	147	8,239,930	-830			
16	1154	152	9,091,650	-868			
17	1100	153	9,270,200	-964			Pump failure
Jan. 1976							
05	1400	172	9,270,200				Begin injection II
06	900	173	9,419,450	-979			
07	920	174	9,606,920	-961			
08	730	175	9,771,860	-928			
12	800	179	10,448,360	-874			
13	830	180	10,615,100	-849			
14	830	181	10,777,270	-842			
15	830	182	10,936,960	-830			
16	830	183	11,089,260	-791			
16	1330	183	11,120,700	-784			
19	830	186	11,541,830	-784			
20	715	187	11,685,000	-785			
21	715	188	11,831,560	-761			
22	700	189	11,975,900	-758			
23	800	190	12,131,900	-778			
26	800	193	12,552,400	-728			
27	830	194	12,700,800	-755			
28	700	195	12,831,100	-722			
29	800	196	12,961,550	-651			
30	800	197	13,109,820	-770			
Feb. 1976							
02	815	200	13,497,200	-668			
02	849	200	13,500,470	-719			
02	904	200	13,502,465	995			End backflush
03	734	201	13,661,600	-882			
04	730	202	13,826,700	-860			
05	800	203	14,005,300	-909			
06	830	204	14,168,600	-831			
09	700	207	14,628,100	-813			
10	800	208	14,785,400	-784			
11	815	209	14,936,100	-775			
12	815	210	15,084,100	-769			
13	750	211	15,227,100	-756			
13	839	211	15,233,568	-987			End backflush
13	1203	211	15,250,920	-636			

| Time of measurement | | Days from beginning of data | Cumulative volume readout on flowmeter (gallons) | Flow rate (gallons per minute) | Chemical concentrations in recovered water | | Change of activity |
Date	Hour				Chloride (milligrams per liter)	Specific conductance (microsiemens per centimeter)	
Feb. 1976							
17	800	215	16,906,200	-888			
18	800	216	16,072,200	-862			
19	800	217	16,231,100	-825			
20	830	218	16,392,200	-820			
23	830	221	16,865,600	-820			
24	900	222	17,021,400	-793			
25	800	223	17,172,900	-821			
26	800	224	17,318,700	-757			
27	935	225	17,472,200	-748			
27	1025	225	17,478,800	987			End backflush
Mar. 1976							
01	800	228	17,976,100	-891			
02	1015	229	18,153,600	-843			
03	800	230	18,305,500	-871			
04	830	231	18,468,300	-828			
05	800	232	18,623,500	-823			
08	800	235	19,090,100	-808			
08	900	235	19,098,020	987			End backflush
10	830	237	19,436,600	-889			
10	850	237	19,436,900	-112			
May 1976							
03	1312	291	19,436,900				Begin backflow II
06	800	294	19,709,100	508	70	670	
12	800	300	20,281,200	495	96	760	
19	955	307	20,946,900	488			
20	1150	308	21,046,900	481	110	810	
25	845	313	21,537,500	523	124	860	
25	1240	313	21,551,900	458			
June 1976							
02	1000	321	22,294,800	489	140	940	
09	900	328	22,969,900	504	154	990	
15	730	334	23,541,900	500			
18	1330	337	23,854,700	497	202	1,170	
21	745	340	24,115,500	495	214	1,200	
22	800	341	24,212,300	498	216	1,220	
23	800	342	24,308,600	500	222	1,240	
24	800	343	24,402,500	488	224	1,200	
25	800	344	24/496,300	487	224		
28	800	347	24,780,200	492			
29	800	348	24,874,200	488	256	1,450	
30	800	349	24,968,900	492	260	1,450	

Time of measurement		Days from beginning of data	Cumulative volume readout on flowmeter (gallons)	Flow rate (gallons per minute)	Chemical concentrations in recovered water		Change of activity
Date	Hour				Chloride (milligrams per liter)	Specific conductance (microsiemens per centimeter)	
July 1976							
01	640	350	25,058,200	491	266	1,400	
02	800	351	25,157,300	488	270	1,350	
09	735	358	25,810,000	486	300	1,550	
16	1145	365	26,483,200	488	400	1,850	
19	1050	368	26,760,400	486			
20	958	369	26,850,100	483	390	1,860	
21	1015	370	26,850,100				Injection test
21	1035	370	26,852,700	-972			
23	800	372	27,160,200	-844			Begin injection III
30	1100	379	28,191,400	-752			
Aug. 1976							
06	930	386	29,117,000	-693			
06	1230	386	29,117,600	25			End backflush
13	830	393	30,162,100	-794			
13	935	393	30,179,200	-1,968			
13	1135	393	30,191,200	748			End backflush
20	700	400	31,274,500	-826			
20	800	400	31,285,300	-1,346			
20	1000	400	31,297,300	748			End backflush
27	830	407	32,748,500	-1,087			
27	900	407	32,760,500	2,992			End backflush
Sept. 1976							
02	1130	413	33,713,100	-811			
03	1400	414	33,898,600	-873			
03	1705	414	33,906,600	323			End backflush
10	800	421	34,983,600	-845			
10	1000	421	34,995,600	748			End backflush
17	900	428	36,122,500	-841			
17	1010	428	36,131,100	-919			
17	1210	428	36,143,100	748			End backflush
24	900	435	37,229,600	-822			
24	1015	435	37,234,400	-479			
24	1215	435	37,246,400	748			End backflush
Oct. 1976							
01	1300	442	38,358,650	-822			
01	1500	442	38,370,650	748			End backflush
08	1000	499	39,353,000	-751			
08	1300	449	39,365,000	499			End backflush
15	700	456	40,314,700	-731			
15	1000	456	40,326,700	499			End backflush
22	800	463	41,359,250	-776			
22	1100	463	41,371,250	499			End backflush
29	1000	470	42,425,860	-787			
29	1300	470	42,437,860	499			End backflush

| Time of measurement | | Days from beginning of data | Cumulative volume readout on flowmeter (gallons) | Flow rate (gallons per minute) | Chemical concentrations in recovered water | | Change of activity |
Date	Hour				Chloride (milligrams per liter)	Specific conductance (microsiemens per centimeter)	
Nov. 1976							
05	845	477	43,478,970	-793			
05	1145	477	43,490,970	499			End backflush
12	900	484	44,509,900	-769			
12	1200	484	44,521,900	499			End backflush
19	845	491	45,548,870	-777			
19	1145	491	45,560,870	499			End backflush
26	700	498	46,579,800	-778			
26	1000	498	46,591,800	499			End backflush
Dec. 1976							
03	720	505	47,605,300	-764			
10	800	512	48,694,700	-805			
10	1100	512	48,706,700	499			End backflush
17	700	519	50,197,560	-1,133			
17	1000	519	50,209,560	499			End backflush
23	730	525	51,108,225	-792			
23	1030	525	51,120,225	499			End backflush
30	645	532	52,148,800	-781			
Jan. 1977							
07	1157	540	53,184,700	-655			
07	1500	540	53,196,700	491			End backflush
14	650	547	54,126,700	-725			
18	1230	551	54,661,017	-655			
24	1016	557	54,661,020				
Feb. 1977							
18	911	732	54,661,020				Begin backflow III
22	1034	736	55,071,210	525	78	700	
29	820	743	55,768,230	525	80	730	
Aug. 1977							
05	845	750	56,482,350	529	113	780	
12	1000	757	57,173,970	509	90	830	
19	1030	764	57,862,000	509	125	860	
26	900	771	58,552,870	517	140	885	
Sept. 1977							
02	1200	778	59,135,200	425	140	895	
09	730	785	59,722,900	448	150	935	
14	723	790	60,122,700	416	146	940	
23	1500	799	60,842,250	401	160	950	
Oct. 1977							
01	1600	807	61,420,780	374	160	1,000	
07	1500	813	62,059,150	557	172	1,080	
03	827	819	62,417,200	325	180	1,090	
21	911	827	63,055,100	413	196	1,080	
28	1300	834	63,628,550	416	200	1,200	

APPENDIX C—VOLUME AND RATE DATA FROM INJECTION AND RECOVERY CYCLES AND QUALITY OF RECOVERED WATER—Continued

Time of measurement		Days from beginning of data	Cumulative volume readout on flowmeter (gallons)	Flow rate (gallons per minute)	Chemical concentrations in recovered water		Change of activity
Date	Hour				Chloride (milligrams per liter)	Specific conductance (microsiemens per centimeter)	
Nov. 1977							
04	1300	841	64,206,250	429	217	1,200	
11	1400	848	64,803,950	441	220	1,340	
18	1100	855	65,364,850	424	230	1,250	
25	1000	862	65,953,570	440	246	1,320	
Dec. 1977							
02	1200	869	66,640,150	430	268		
09	1400	876	67,142,750	442	300	1,300	
16	1200	883	67,713,650	429	272		
23	1200	890	68,305,850	439	315	1,400	
30	1200	897	68,894,250	437	340	1,450	
Jan. 1978							
30	1000	928	71,412,025	423	405	1,825	
Mar. 1978							
03	1450	960	73,875,850	397	480	2,160	
Apr. 1978							
13	1307	1,001	76,762,950	366	600	2,450	
14	1200	1,002	76,823,500	330	600	2,450	
May 1978							
05	1045	1,023	78,135,800	325	625	2,550	
June 1978							
12	1050	1,061	80,460,400	318	700	3,000	
July 1978							
07	841	1,086	81,920,860	305	750	3,100	
Aug. 1978							
02	1045	1,112	83,429,220	300	780	3,300	
10	1030	1,120	83,888,600	299	800	3,240	
24	800	1,134	84,649,770	285	800	3,300	
Sept. 1978							
16	1300	1,157	85,878,700	275	840	3,400	
Oct. 1978							
31	1215	1,202	88,244,700	273	925	3,625	
Dec. 1978							
14	1050	1,246	90,398,500	255	950	3,800	
Feb. 1979							
27	1100	1,321	92,972,300	178	1,000	4,050	
Apr. 1979							
12	1230	1,365	96,029,400	360	1,055	4,120	
18	1300	1,371	96,308,800	241			
July 1979							
17	835	1,461	100,433,500	239	1,060		
18	835	1,462	100,479,700	240			
24	1215	1,468	100,769,500	245	1,060	4,260	
Nov. 1979							
15	1330	1,582	105,941,600	236			
16	1030	1,583	105,980,300	230	1,100	4,350	
Jan. 1980							
28	1051	1,656	109,283,100	235	1,120	4,290	
30	1000	1,658	109,373,100	238			

APPENDIX D—WATER-QUALITY DATA OBTAINED DURING WELL CONSTRUCTION AND THE SUBSEQUENT INJECTION AND RECOVERY CYCLES AT THE HIALEAH SITE

Bacteriological Analyses for Nitrogen-, Sulfate-, and Iron-Reducing Bacteria

[Nitrate, nitrate agar (14 days); sulfate, sulfate API media (14 weeks); iron, sphaerotilus agar; OW, observation well; SW, supply well; IW, injection well; —, no data]

Source	Date	Activity	Nitrate-reducing bacteria[1]	Sulfate-reducing bacteria[1]	Iron-reducing bacteria[2]	Microscopic iron bacteria[2]
OW	April 16, 1975	Preinjection background in injection zone	90	70	—	—
SW	July 22, 1975	Supply water for first injection	70	<30	—	—
OW	Aug. 04, 1975	Monitor zone, after 18 days of first injection	40	150	—	—
IW	Sept. 16, 1975	Recovered water, 6 days into first recovery	40	<30	—	—
	Sept. 23, 1975	13 days into first recovery	210	200	—	—
	Sept. 30, 1975	20 days into first recovery	110	200	—	—
	Oct. 15, 1975	35 days into first recovery				
	Mar. 04, 1976	Sampling supply water at injection wellhead during second injection	150	<30	—	—
	May 25, 1976	Recovered water, 22 days into second recovery	280	200	—	—
	July 18, 1977	Recovered water, first day of third backflow	<30	<30	<30	2

[1]MPN (most probable number) per 100 milliliters; MPN is based on multiple counts of bacteria colonies.
[2]Negative; considerable iron rust present.

Dissolved-Gas Analyses

[Analyses by D.H. Fisher, U.S. Geological Survey, written commun. (1975, 1977). ASR, aquifer storage and recovery; IW, injection well; OW, observation well;. —, no data]

Source	Date	Nitrogen	Oxygen	Argon	Methane	Carbon dioxide	Test status
			Pressures, in atmospheres, of Dissolved Gases at Sampling Temperature				
IW	Aug. 04, 1975	5.34	0.34	0.036	0.019	0.021	After 18 days of first injection (supply well water)[1]
	Sept. 16, 1975	.87	<.0001	.0104	.022	.0124	6 days into first recovery
	Sept. 30, 1975	.89	<.0005	—	.019	.0103	20 days into first recovery[2]
	Oct. 15, 1975	.99	<.0004	—	.017	.0088	35 days into first recovery[2]
OW	Apr. 24, 1975	1.05	<.001	.013	.0005	.0010	Background conditions in injection zone prior to ASR cycles
	Aug. 04, 1975	4.96	.61	.036	.007	.0047	After 18 days of first injection[1]
	Jan. 18, 1977	.89	<.002	—	.033	.019	Near end (after 181 days) of third injection
			Concentrations, in milligrams per liter				
IW	Aug. 04, 1975	99	14	2.1	.40	31	After 18 days of first injection (supply well water)
	Sept. 16, 1975	16	<.005	.61	.47	18	6 days into first recovery
	Sept. 30, 1975	17	<.02	—	.40	15	20 days into first recovery
	Oct. 15, 1975	19	<.02	—	.36	13	35 days into first recovery
OW	Apr. 24, 1975	21.4	<.05	.82	.012	1.7	Background conditions in injection zone prior to ASR cycles
	Aug. 04, 1975	96	26	2.17	.15	7.3	After 18 days of first injection
	Jan. 18, 1977	17	<.05	—	.72	29	Near end (after 181 days) of third injection

[1]High nitrogen pressures indicate atmospheric contamination (leaky stopcock or faulty sampling;, methane and carbon dioxide analyses should be relatively accurate; H_2S will have been oxidized.

[2]Argon added to the inner tube of the sampler.

Chemical Analyses of Water Samples

[mg/L, milligrams per liter; JTU, Jackson turbidity units; NTU, nephelometric turbidity units; Pt-Co, platinum cobalt units; µS/cm, microsiemens per centimeter; µg/L, micrograms per liter; mL, milliliter; g/mL, grams per milliliter, tons/acre-ft, tons per acre-feet; NO_2+NO_3, nitrate plus nitrite; ND, not detected; —, no data]

Well	Date	Time	Sampling depth (feet)	Tempera-ture (degrees Celsius)	Agency analyzing sample (code number)	Tur-bidity (JTU)	Tur-bidity (NTU)	Color (Pt-Co)	Specific conduc-tance (µS/cm)	Dissolved oxygen (mg/L)	Biochemical oxygen demand, 5 day (mg/L)
					During Construction						
G-3062	Nov. 20, 1974	0730	1,060	21.5	—	2	—	4	4,200	—	—
G-3061	Dec. 04, 1974	0900	1,090	21.5	—	1	—	5	4,750	—	0.9
					During First Injection						
G-3061	July 22, 1975	1000	1,110	25.5	—	6	—	55	665	—	.2
S-3000	July 22, 1975	1000	106	25.5	—	6	—	55	665	—	.2
G-3062	Aug. 04, 1975	1230	1,020	24.0	—	3	—	0	5,600	0.8	—
					During First Recovery						
G-3061	Sept. 16, 1975	0900	1,110	26.0	—	10	—	43	760	1.0	.9
	Sept. 23, 1975	0900	1,110	26.0	—	8	—	40	907	—	.5
	Sept. 30, 1975	0900	1,110	25.0	—	10	—	65	1,020	.4	.6
	Oct. 15, 1975	0930	1,110	25.0	—	10	—	10	1,460	.7	.6
					During Second Injection						
G-3061	Mar. 04, 1976	0900	1,110	26.0	—	3	—	50	657	—	—
S-3000	Mar. 04, 1976	0900	106	26.0	—	3	—	50	657	—	—
					During Second Recovery						
G-3061	May 30, 1976	1530	1,110	25.0	—	7	—	70	645	—	—
	May 25, 1976	1030	1,110	24.5	—	8	—	60	860	—	.7
	July 19, 1976	1200	1,110	24.0	—	10	—	20	1,860	—	1.3
G-3062	July 19, 1976	1210	840	26.5	—	—	—	0	8,200	—	—
	July 19, 1976	1215	957	24.5	—	—	—	0	3,110	—	—
	July 19, 1976	1220	978	25.0	—	—	—	0	3,100	—	—
	July 19, 1976	1225	999	25.0	—	—	—	0	2,860	—	—
	July 19, 1976	1230	1,020	25.0	—	—	—	0	2,630	—	—
	July 19, 1976	1235	1,040	25.0	—	—	—	0	2,960	—	—
	July 19, 1976	1240	1,060	25.5	—	—	—	5	3,370	—	—
					During Third Injection						
G-3061	Jan. 18, 1977	0800	1,110	25.0	—	2	—	40	660	—	—
S-3000	Jan. 18, 1977	0800	106	25.0	—	2	—	40	660	—	—
G-3062	Jan. 18, 1977	0830	1,060	23.5	—	30	—	0	1,060	—	—
	Jan. 18, 1977	0900	1,040	23.5	—	2	—	0	720	—	—
	Jan. 18, 1977	0930	1,020	23.5	—	2	—	0	700	—	—
	Jan. 18, 1977	0945	999	23.5	—	2	—	0	960	—	—
	Jan. 18, 1977	1000	978	23.5	—	2	—	0	1,100	—	—
	Jan. 18, 1977	1045	957	23.5	—	3	—	0	1,300	—	—
	Jan. 18, 1977	1115	840	23.0	—	4	—	0	6,020	—	—

Well	Date	Time	Sampling depth (feet)	Tempera-ature (degrees Celsius)	Agency analyzing sample (code number)	Tur-bidity (JTU)	Tur-bidity (NTU)	Color (Pt-Co)	Specific conduc-tance (µS/cm)	Dissolved oxygen (mg/L)	Biochemical oxygen demand, 5 day (mg/L)
					During Third Recovery						
G-3061	July 18, 1977	0930	1,110	26.0	—	5	—	90	708	—	—
	July 17, 1979	0930	—	22.5	80,010	—	2.0	5	3,900	—	—
G-3062	July 17, 1979	1005	957	24.0	80,010	—	1.0	5	4,260	—	—
	July 17, 1979	1025	978	24.0	80,010	—	1.0	0	4,020	—	—
	July 17, 1979	1040	1,020	24.0	80,010	—	1.0	3	4,020	—	—
	July 17, 1979	1055	999	24.0	80,010	—	1.0	1	4,070	—	—
	July 17, 1979	1108	1,040	—	80,010	—	1.0	0	4,180	—	—
	July 17, 1979	1130	1,060	24.0	80,010	—	1.0	0	4,180	—	—
	July 18, 1979	0830	840	26.5	80,010	—	1.0	2	7,300	—	—

Well	Date	Chem-ical oxygen demand (mg/L)	pH, field (units)	Dis-solved carbon dioxide (mg/L as CO_2)	Alka-linity, field (mg/L as $CaCO_3$)	Acidity (mg/L as $CaCO_3$)	Bicar-bon-ate, field (mg/L as HCO_3)	Car-bonate, field (mg/L as CO_3)	Solids, residue at 105 degrees Celsius, total (mg/L)	Solids, volatile igni-tion, total (mg/L)	Oil and grease (mg/L)	Total nitro-gen (mg/L as N)	Total organic nitro-gen (mg/L as N)
						During Construction							
G-3062	Nov. 20, 1974	30	7.7	5.1	131	—	160	—	—	—	—	0.42	0.0
G-3061	Dec. 04, 1974	59	7.9	3.1	125	—	150	0	—	—	—	.45	.0
						During First Injection							
G-3061	July 22, 1975	—	7.2	29	240	—	290	0	—	—	0	1.3	.71
S-3000	July 22, 1975	—	7.2	29	240	—	290	0	—	—	0	1.3	.71
G-3062	Aug. 04, 1975	42	7.8	5.5	177	5	220	0	—	—	10	.70	.21
						During First Recovery							
G-3061	Sept. 16, 1975	22	7.1	46	288	29	350	0	—	—	0	1.2	.72
	Sept. 23, 1975	24	7.3	23	237	50	290	0	556	—	0	1.1	.60
	Sept. 30, 1975	37	7.1	42	262	40	320	0	651	—	0	1.1	.64
	Oct. 15, 1975	31	7.3	25	249	40	300	0	935	—	0	1.0	.47
						During Second Injection							
G-3061	Mar. 04, 1976	46	6.8	76	246	142	300	0	398	136	0	1.5	.87
S-3000	Mar. 04, 1976	46	6.8	76	246	142	300	0	398	136	0	1.5	.87
						During Second Recovery							
G-3061	May 03, 1976	—	7.4	18	237	—	290	0	—	—	—	1.4	.86
	May 25, 1976	26	7.1	43	269	55	330	0	522	143	0	1.5	1.0
	July 19, 1976	28	7.2	31	256	—	310	0	—	—	0	.80	.24
G-3062	July 19, 1976	—	6.8	38	125	—	150	0	—	—	—	—	—
	July 19, 1976	—	7.3	20	207	—	250	0	—	—	—	—	—
	July 19, 1976	—	7.2	29	239	—	290	0	—	—	—	—	—
	July 19, 1976	—	7.5	13	203	—	250	0	—	—	—	—	—
	July 19, 1976	—	6.8	71	233	—	280	0	—	—	—	—	—
	July 19, 1976	—	7.4	18	230	—	280	0	—	—	—	—	—
	July 19, 1976	—	7.6	11	223	—	270	0	—	—	—	—	—

Well	Date	Chemical oxygen demand (mg/L)	pH, field (units)	Dissolved carbon dioxide (mg/L as CO₂)	Alkalinity, field (mg/L as CaCO₃)	Acidity (mg/L as CaCO₃)	Bicarbonate, field (mg/L as HCO₃)	Carbonate, field (mg/L as CO₃)	Solids, residue at 105 degrees Celsius, total (mg/L)	Solids, volatile ignition, total (mg/L)	Oil and grease (mg/L)	Total nitrogen (mg/L as N)	Total organic nitrogen (mg/L as N)
During Third Injection
G-3061	Jan. 18, 1977	—	7.2	28	227	—	280	0	—	—	—	1.2	.60
S-3000	Jan. 18, 1977	—	7.2	28	227	—	280	0	—	—	—	1.2	.60
G-3062	Jan. 18, 1977	—	7.2	36	295	—	360	0	—	—	—	.79	.30
	Jan. 18, 1977	—	7.2	36	289	—	350	0	—	—	—	.82	.30
	Jan. 18, 1977	—	7.2	36	262	—	360	0	—	—	—	.97	.37
	Jan. 18, 1977	—	7.2	40	325	—	400	0	—	—	—	.97	.43
	Jan. 18, 1977	—	7.2	39	315	—	380	0	—	—	—	.97	.47
	Jan. 18, 1977	—	7.2	32	259	—	320	0	—	—	—	.72	.34
	Jan. 18, 1977	—	8.5	1.1	174	—	190	12	—	—	—	.81	.15
During Third Recovery
G-3061	July 18, 1977	40	7.2	28	230	—	280	0	—	—	—	1.4	.74
	July 17, 1979	—	7.7	5.6	140	—	180	0	—	—	—	1.1	.72
G-3062	July 17, 1979	—	7.7	5.6	140	—	180	0	—	—	—	1.1	.66
	July 17, 1979	—	7.7	5.4	140	—	170	0	—	—	—	1.1	.72
	July 17, 1979	—	7.7	5.1	130	—	160	0	—	—	—	.86	.50
	July 17, 1979	—	7.6	6.4	130	—	160	0	—	—	—	.87	.48
	July 17, 1979	—	7.8	4.1	130	—	160	0	—	—	—	.96	.57
	July 17, 1979	—	8.1	2.0	130	—	160	0	—	—	—	.96	.55
	July 18, 1979	—	8.6	.9	180	—	180	20	—	—	—	1.9	1.0

Well	Date	Dissolved organic nitrogen (mg/L as N)	Dissolved ammonia nitrogen (mg/L as N)	Total ammonia nitrogen (mg/L as N)	Dissolved nitrite nitrogen (mg/L as N)	Total nitrite nitrogen (mg/L as N)	Dissolved nitrate nitrogen (mg/L as N)	Total nitrate nitrogen (mg/L as N)	Dissolved ammonia + organic nitrogen (mg/L as N)	Total ammonia + organic nitrogen (mg/L as N)	Total NO₂+NO₃ nitrogen (mg/L as N)	Dissolved NO₂+NO₃ nitrogen (mg/L as N)
During Construction
G-3062	Nov. 20, 1974	—	—	0.42	—	<0.01	—	0.00	—	0.42	<0.10	—
G-3061	Dec. 04, 1974	—	—	.45	—	<.01	—	.00	—	.45	<.10	—
During First Injection
G-3061	July 22, 1975	—	—	.50	—	<.01	—	.14	—	1.2	.14	—
S-3000	July 22, 1975	—	—	.50	—	<.01	—	.14	—	1.2	.14	—
G-3062	Aug. 04, 1975	—	—	.47	—	.01	—	.01	—	.68	.02	—
During First Recovery
G-3061	Sept. 16, 1975	—	—	.49	—	<.01	—	.00	—	1.2	<.10	—
	Sept. 23, 1975	—	—	.51	—	<.01	—	.00	—	1.1	<.10	—
	Sept. 30, 1975	—	—	.48	—	<.01	—	.03	—	1.1	.03	—
	Oct. 15, 1975	—	—	.55	—	<.01	—	.03	—	1.0	.03	—
During Second Injection
G-3061	Mar. 04, 1976	0.78	0.57	.58	0.01	.01	0.00	.01	1.3	1.5	.02	0.01
S-3000	Mar. 04, 1976	.78	.57	.58	.01	.01	.00	.01	1.3	1.5	.02	.01

Well	Date	Dissolved organic nitrogen (mg/L as N)	Dissolved ammonia nitrogen (mg/L as N)	Total ammonia nitrogen (mg/L as N)	Dissolved nitrite nitrogen (mg/L as N)	Total nitrite nitrogen (mg/L as N)	Dissolved nitrate nitrogen (mg/L as N)	Total nitrate nitrogen (mg/L as N)	Dissolved ammonia + organic nitrogen (mg/L as N)	Total ammonia + organic nitrogen (mg/L as N)	Total NO_2+NO_3 nitrogen (mg/L as N)	Dissolved NO_2+NO_3 nitrogen (mg/L as N)
During Second Recovery												
G-3061	May 03, 1976	—	—	.54	—	<.01	—	.01	—	1.4	.01	—
	May 25, 1976	1.0	.50	.50	.01	<.01	.01	.01	1.5	1.5	.01	.10
	July 19, 1976	—	—	.56	—	<.01	—	.00	—	.80	<.10	—
G-3062	July 19, 1976	—	—	—	—	—	—	—	—	—	—	—
	July 19, 1976	—	—	—	—	—	—	—	—	—	—	—
	July 19, 1976	—	—	—	—	—	—	—	—	—	—	—
	July 19, 1976	—	—	—	—	—	—	—	—	—	—	—
	July 19, 1976	—	—	—	—	—	—	—	—	—	—	—
	July 19, 1976	—	—	—	—	—	—	—	—	—	—	—
	July 19, 1976	—	—	—	—	—	—	—	—	—	—	—
During Third Injection												
G-3061	Jan. 18, 1977	—	—	.60	—	<.01	—	.05	—	1.2	.05	—
S-3000	Jan. 18, 1977	—	—	.60	—	<.01	—	.05	—	1.2	.05	—
G-3062	Jan. 18, 1977	—	—	.48	—	.01	—	.00	—	.78	.01	—
	Jan. 18, 1977	—	—	.52	—	<.01	—	.00	—	.82	<.10	—
	Jan. 18, 1977	—	—	.60	—	<.01	—	.00	—	.97	<.10	—
	Jan. 18, 1977	—	—	.54	—	<.01	—	.00	—	.97	<.10	—
	Jan. 18, 1977	—	—	.50	—	<.01	—	.00	—	.97	<.10	—
	Jan. 18, 1977	—	—	.38	—	<.01	—	.00	—	.72	<.10	—
	Jan. 18, 1977	—	—	.66	—	<.01	—	.00	—	.81	<.10	—
During Third Recovery												
G-3061	July 18, 1977	—	—	.68	—	<.01	—	.00	—	1.4	<.10	—
	July 17, 1979	—	—	.38	—	<.01	—	.00	—	1.1	<.10	—
G-3062	July 17, 1979	—	—	.45	—	<.01	—	.01	—	1.1	.01	—
	July 17, 1979	—	—	.39	—	<.01	—	.01	—	1.1	.01	—
	July 17, 1979	—	—	.35	—	<.01	—	.01	—	.85	.01	—
	July 17, 1979	—	—	.38	—	<.01	—	.01	—	.86	.01	—
	July 17, 1979	—	—	.38	—	<.01	—	.01	—	.95	.01	—
	July 17, 1979	—	—	.40	—	<.01	—	.01	—	.95	.01	—
	July 18, 1979	—	—	.86	—	<.01	—	.01	—	1.9	.01	—

Well	Date	Dissolved ortho phosphate (mg/L as PO_4)	Total phosphorus (mg/L as P)	Dissolved phosphorus (mg/L as P)	Dissolved ortho phosphorus (mg/L as P)	Total organic carbon (mg/L as C)	Dissolved organic carbon (mg/L as C)	Total cyanide (mg/L as Cn)	Total hardness (mg/L as $CaCO_3$)	Total noncarbonate hardness, field (mg/L as $CaCO_3$)	Dissolved calcium (mg/L as Ca)	Dissolved magnesium (mg/L as Mg)
During Construction												
G-3062	Nov. 20, 1974	—	0.01	—	—	3	—	—	660	530	100	100
G-3061	Dec. 04, 1974	—	.01	—	—	5	—	—	740	620	100	120
During First Injection												
G-3061	July 22, 1975	—	.03	—	—	12	—	0.01	260	18	89	8.4
S-3000	July 22, 1975	—	.03	—	—	12	—	.01	260	18	89	8.4
G-3062	Aug. 04, 1975	—	.01	—	—	2	—	.00	580	440	84	88

Well	Date	Dissolved ortho phosphate (mg/L as PO$_4$)	Total phosphorus (mg/L as P)	Dissolved phosphorus (mg/L as P)	Dissolved ortho phosphorus (mg/L as P)	Total organic carbon (mg/L as C)	Dissolved organic carbon (mg/L as C)	Total cyanide (mg/L as Cn)	Total hardness (mg/L as CaCO$_3$)	Total noncarbonate hardness, field (mg/L as CaCO$_3$)	Dissolved calcium (mg/L as Ca)	Dissolved magnesium (mg/L as Mg)
					During First Recovery							
G-3061	Sept. 16, 1975	—	.03	—	—	8	7	.00	280	40	92	12
	Sept. 23, 1975	—	.01	—	—	8	8	.00	300	66	91	18
	Sept. 30, 1975	—	.02	—	—	9	8	.00	310	70	88	21
	Oct. 15, 1975	—	.01	—	—	13	8	.00	360	130	89	32
					During Second Injection							
G-3061	Mar. 04/, 1976	0.09	.03	0.03	0.03	15	14	.00	260	30	90	8.4
S-3000	Mar. 04, 1976	.09	.03	.03	.03	15	14	.00	260	30	90	8.4
					During Second Recovery							
G-3061	May 03, 1976	—	.03	—	—	11	9	—	250	3	84	8.4
	May 25, 1976	.00	.01	.01	<.01	11	11	.00	280	58	84	17
	July 19, 1976	—	.01	—	—	7	7	.00	400	0	87	42
G-3062	July 19, 1976	—	—	—	—	—	—	—	520	390	40	100
	July 19, 1976	—	—	—	—	—	—	—	540	330	81	79
	July 19, 1976	—	—	—	—	—	—	—	540	300	81	80
	July 19, 1976	—	—	—	—	—	—	—	510	310	78	74
	July 19, 1976	—	—	—	—	—	—	—	490	260	78	70
	July 19, 1976	—	—	—	—	—	—	—	530	300	76	80
	July 19, 1976	—	—	—	—	—	—	—	550	330	77	86
					During Third Injection							
G-3061	Jan. 18, 1977	—	.02	—	—	16	—	—	250	26	87	8.4
S-3000	Jan. 18, 1977	—	.02	—	—	16	—	—	250	26	87	8.4
G-3061	Jan. 18, 1977	—	.01	—	—	7	—	—	320	25	73	31
	Jan. 18, 1977	—	.01	—	—	7	—	—	270	0	73	19
	Jan. 18, 1977	—	.01	—	—	11	—	—	260	0	79	15
	Jan. 18, 1977	—	.01	—	—	10	—	—	280	0	78	21
	Jan. 18, 1977	—	.01	—	—	8	—	—	340	25	69	40
	Jan. 18, 1977	—	.01	—	—	6	—	—	300	41	77	25
	Jan. 18, 1977	—	.01	—	—	3	—	—	630	460	51	120
					During Third Recovery							
G-3061	July 18, 1977	—	.02	—	—	27	—	—	250	22	86	8.8
	July 17, 1979	—	.01	—	—	14	—	—	630	490	83	100
G-3062	July 17, 1979	—	.01	—	—	3	—	—	670	520	82	110
	July 17, 1979	—	.01	—	—	11	—	—	640	500	88	100
	July 17, 1979	—	.01	—	—	10	—	—	640	510	88	100
	July 17, 1979	—	.01	—	—	8	—	—	630	500	84	100
	July 17, 1979	—	.01	—	—	17	—	—	680	550	88	110
	July 17, 1979	—	.01	—	—	12	—	—	680	550	87	110
	July 18, 1979	—	.01	—	—	5	—	—	680	500	71	120

Well	Date	Dissolved sodium (mg/L as Na)	Sodium adsorption ratio	Sodium percentage	Dissolved sodium + potassium (mg/L as Na)	Dissolved potassium (mg/L as K)	Dissolved chloride (mg/L as Cl)	Dissolved sulfate (mg/L as SO$_4$)	Dissolved fluoride (mg/L as F)	Dissolved silica (mg/L as SiO$_2$)	Dissolved arsenic (µg/L as As)	Total suspended arsenic (µg/L as As)
					During Construction							
G-3062	Nov. 20, 1974	700	12	68	—	32	1,200	480	1.2	14	—	—
G-3061	Dec. 04, 1974	700	11	66	—	35	1,200	500	1.1	14	—	—
					During First Injection							
G-3061	July 22, 1975	43	1	26	—	2.2	68	10	.3	7.2	2	<1
S-3000	July 22, 1975	43	1	26	—	2.2	68	10	.3	7.2	2	<1
G-3062	Aug. 04, 1975	640	12	69	—	34	1,300	410	1.3	16	<1	<1
					During First Recovery							
G-3061	Sept. 16, 1975	54	1	29	—	2.4	89	20	.4	7.6	1	<1
	Sept. 23, 1975	76	2	35	—	3.3	120	35	.7	8.0	1	<1
	Sept. 30, 1975	100	2	41	—	3.8	170	46	.5	8.5	<1	<1
	Oct. 15, 1975	180	4	52	—	7.0	280	100	.9	9.2	<1	1
					During Second Injection							
G-3061	Mar. 04, 1976	40	1	25	—	1.7	65	7.1	.4	7.3	2	<1
S-3000	Mar. 04, 1976	40	1	25	—	1.7	65	7.1	.4	7.3	2	<1
					During Second Recovery							
G-3061	May 03, 1976	41	1	27	—	2.0	65	8.0	.3	6.9	—	—
	May 25, 1976	70	2	35	—	2.9	120	27	.5	7.9	<1	<1
	July 19, 1976	230	5	55	—	10	390	140	.8	10	<1	1
G-3062	July 19, 1976	1,600	31	87	—	11	2,300	760	1.7	5.4	—	—
	July 19, 1976	430	8	62	—	27	720	310	1.3	13	—	—
	July 19, 1976	430	8	63	—	22	720	320	1.3	13	—	—
	July 19, 1976	380	7	61	—	20	650	270	1.2	12	—	—
	July 19, 1976	350	7	60	—	19	580	250	1.2	12	—	—
	July 19, 1976	410	8	62	—	22	690	310	1.2	13	—	—
	July 19, 1976	480	9	64	—	27	790	360	1.3	15	—	—
					During Third Injection							
G-3061	Jan. 18, 1977	46	1	28	—	2.1	79	11	.3	7.1	—	—
S-3000	Jan. 18, 1977	46	1	28	—	2.1	79	11	.3	7.1	—	—
G-3062	Jan. 18, 1977	110	3	43	—	6.6	170	80	.9	9.0	—	—
	Jan. 18, 1977	50	1	29	—	3.0	79	21	.9	7.6	—	—
	Jan. 18, 1977	46	1	28	—	2.5	76	13	.7	7.2	—	—
	Jan. 18, 1977	76	2	37	—	4.7	130	46	.8	8.1	—	—
	Jan. 18, 1977	140	3	47	—	4.8	200	140	1.0	11	—	—
	Jan. 18, 1977	100	3	42	—	6.6	170	69	.8	8.6	—	—
	Jan. 18, 1977	1,200	21	79	—	70	1,700	600	2.4	14	—	—
					During Third Recovery							
G-3061	July 18, 1977	48	1	29	—	2.2	79	6.6	.2	7.6	—	—
	July 17, 1979	630	11	68	—	26	990	430	1.0	12	—	—
G-3062	July 17, 1979	700	12	69	—	31	1,100	460	1.2	15	—	—
	July 17, 1979	650	11	68	680	28	1,100	440	1.2	13	—	—
	July 17, 1979	640	11	68	—	27	1,000	440	1.2	13	—	—
	July 17, 1979	640	11	68	—	26	1,000	440	1.2	13	—	—
	July 17, 1979	680	11	68	—	28	1,100	460	1.2	13	—	—
	July 17, 1979	680	11	68	—	28	1,100	460	1.2	13	—	—
	July 18, 1979	1,700	29	83	—	64	2,100	780	1.9	23	—	—

Well	Date	Total arsenic (µg/L as As)	Dissolved barium (µg/L as Ba)	Total recoverable barium (µg/L as Ba)	Dissolved boron (µg/L as B)	Total recoverable boron (µg/L as B)	Dissolved cadmium (µg/L as Cd)	Suspended recoverable cadmium (µg/L as Cd)	Total recoverable cadmium (µg/L as Cd)	Dissolved chromium (µg/L as Cr)	Suspended recoverable chromium (µg/L as Cr)	Dissolved hexavalent chromium (µg/L as Cr)
					During Construction							
G-3062	Nov. 20, 1974	<1	—	—	—	—	—	—	5	—	—	0
G-3061	Dec. 04, 1974	<1	—	—	—	—	—	—	5	—	—	0
					During First Injection							
G-3061	July 22, 1975	2	<100	—	70	—	ND	0	ND	ND	<10	—
S-3000	July 22, 1975	2	<100	—	70	—	ND	0	ND	ND	<10	—
G-3062	Aug. 04, 1975	<1	<100	—	480	—	<2.0	0	<2	ND	<10	—
					During First Recovery							
G-3061	Sept. 16, 1975	1	<100	—	70	—	ND	0	ND	ND	<10	—
	Sept. 23, 1975	1	<100	—	90	—	ND	0	ND	ND	10	—
	Sept. 30, 1975	<1	10	—	110	—	ND	0	ND	ND	10	—
	Oct. 15, 1975	1	<100	—	170	—	ND	0	ND	ND	<10	—
					During Second Injection							
G-3061	Mar. 04, 1976	2	<100	—	80	—	ND	2	2	<20	10	—
S-3000	Mar. 04, 1976	2	<100	—	80	—	ND	2	2	<20	10	—
					During Second Recovery							
G-3061	May 03, 1976	—	—	—	—	—	—	—	—	—	—	—
	May 25, 1976	<1	<100	—	110	—	<2.0	0	<2	ND	<10	—
	July 19, 1976	1	<100	<100	190	410	ND	1	<2	ND	20	—
G-3062	July 19, 1976	—	—	—	—	—	—	—	—	—	—	—
	July 19, 1976	—	—	—	—	—	—	—	—	—	—	—
	July 19, 1976	—	—	—	—	—	—	—	—	—	—	—
	July 19, 1976	—	—	—	—	—	—	—	—	—	—	—
	July 19, 1976	—	—	—	—	—	—	—	—	—	—	—
	July 19, 1976	—	—	—	—	—	—	—	—	—	—	—
	July 19, 1976	—	—	—	—	—	—	—	—	—	—	—
					During Third Injection							
G-3061	Jan. 18, 1977	—	—	<100	—	—	—	—	—	—	—	—
S-3000	Jan. 18, 1977	—	—	<100	—	—	—	—	—	—	—	—
G-3062	Jan. 18, 1977	—	—	—	—	—	—	—	—	—	—	—
	Jan. 18, 1977	—	—	—	—	—	—	—	—	—	—	—
	Jan. 18, 1977	—	—	—	—	—	—	—	—	—	—	—
	Jan. 18, 1977	—	—	—	—	—	—	—	—	—	—	—
	Jan. 18, 1977	—	—	—	—	—	—	—	—	—	—	—
	Jan. 18, 1977	—	—	—	—	—	—	—	—	—	—	—
	Jan. 18, 1977	—	—	—	—	—	—	—	—	—	—	—
					During Third Recovery							
G-3061	July 18, 1977	—	—	—	—	—	—	—	—	—	—	—
	July 17, 1979	—	—	—	—	—	—	—	—	—	—	—
G-3062	July 17, 1979	—	—	—	—	—	—	—	—	—	—	—
	July 17, 1979	—	—	—	—	—	—	—	—	—	—	—
	July 17, 1979	—	—	—	—	—	—	—	—	—	—	—
	July 17, 1979	—	—	—	—	—	—	—	—	—	—	—
	July 17, 1979	—	—	—	—	—	—	—	—	—	—	—
	July 17, 1979	—	—	—	—	—	—	—	—	—	—	—
	July 18, 1979	—	—	—	—	—	—	—	—	—	—	—

Well	Date	Total recoverable chromium (μg/L as Cr)	Dissolved copper (μg/L as Cu)	Suspended recoverable copper (μg/L as Cu)	Total recoverable copper (μg/L as Cu)	Suspended recoverable iron (μg/L as Fe)	Total recoverable iron (μg/L as Fe)	Dissolved iron (μg/L as Fe)	Dissolved lead (μg/L as Pb)	Suspended recoverable lead (μg/L as Pb)	Total recoverable lead (μg/L as Pb)	Suspended recoverable manganese (μg/L as Mn)
During Construction												
G-3062	Nov. 20, 1974	<20	—	—	<2	—	—	—	—	—	3	—
G-3061	Dec. 04, 1974	20	—	—	ND	—	—	—	—	—	ND	—
During First Injection												
G-3061	July 22, 1975	<20	<20	0	<20	—	810	760	ND	4	4	20
S-3000	July 22, 1975	<20	<20	0	<20	—	810	760	ND	4	4	20
G-3062	Aug. 04, 1975	<20	ND	1	<2	—	110	100	7	3	10	6
During First Recovery												
G-3061	Sept. 16, 1975	<20	ND	1	<2	—	1,900	1,900	<2	3	4	10
	Sept. 23, 1975	<20	2	1	3	—	1,700	1,700	6	2	8	10
	Sept. 30, 1975	<20	2	2	4	—	1,700	1,600	2	4	6	20
	Oct. 15, 1975	<20	ND	5	5	—	1,600	1,600	11	0	11	0
During Second Injection												
G-3061	Mar. 04, 1976	20	3	0	3	—	930	870	7	8	15	0
S-3000	Mar. 04, 1976	20	3	0	3	—	930	870	7	8	15	0
During Second Recovery												
G-3061	May 03, 1976	—	—	—	—	—	—	—	—	—	—	—
	May 25, 1976	<20	ND	6	6	—	2,000	1,800	18	18	36	10
	July 19, 1976	20	ND	2	2	—	1,300	1,200	4	0	4	10
G-3062	July 19, 1976	—	—	—	—	—	—	—	—	—	—	—
	July 19, 1976	—	—	—	—	—	—	—	—	—	—	—
	July 19, 1976	—	—	—	—	—	—	—	—	—	—	—
	July 19, 1976	—	—	—	—	—	—	—	—	—	—	—
	July 19, 1976	—	—	—	—	—	—	—	—	—	—	—
	July 19, 1976	—	—	—	—	—	—	—	—	—	—	—
	July 19, 1976	—	—	—	—	—	—	—	—	—	—	—
During Third Injection												
G-3061	Jan. 18, 1977	—	—	—	—	—	—	830	—	—	—	—
S-3000	Jan. 18, 1977	—	—	—	—	—	—	830	—	—	—	—
G-3062	Jan. 18, 1977	—	—	—	—	—	—	—	—	—	—	—
	Jan. 18, 1977	—	—	—	—	—	—	—	—	—	—	—
	Jan. 18, 1977	—	—	—	—	—	—	—	—	—	—	—
	Jan. 18, 1977	—	—	—	—	—	—	—	—	—	—	—
	Jan. 18, 1977	—	—	—	—	—	—	—	—	—	—	—
	Jan. 18, 1977	—	—	—	—	—	—	—	—	—	—	—
	Jan. 18, 1977	—	—	—	—	—	—	—	—	—	—	—
During Third Recovery												
G-3061	July 18, 1977	—	—	—	—	—	—	2,200	—	—	—	—
	July 17, 1979	—	—	—	—	110	210	100	—	—	—	—
G-3062	July 17, 1979	—	—	—	—	110	150	40	—	—	—	—
	July 17, 1979	—	—	—	—	60	110	50	—	—	—	—
	July 17, 1979	—	—	—	—	70	110	40	—	—	—	—
	July 17, 1979	—	—	—	—	70	110	40	—	—	—	—
	July 17, 1979	—	—	—	—	40	80	40	—	—	—	—
	July 17, 1979	—	—	—	—	280	350	70	—	—	—	—
	July 18, 1979	—	—	—	—	80	150	70	—	—	—	—

APPENDIX D—WATER-QUALITY DATA OBTAINED DURING WELL CONSTRUCTION AND THE SUBSEQUENT INJECTION AND RECOVERY CYCLES AT THE HIALEAH SITE—Continued

Well	Date	Total recoverable manganese (μg/L as Mn)	Dissolved manganese (μg/L as Mn)	Dissolved molybdenum (μg/L as Mo)	Dissolved nickel (μg/L as Ni)	Suspended recoverable nickel (μg/L as Ni)	Total recoverable nickel (μg/L as Ni)	Dissolved silver (μg/L as Ag)	Total recoverable silver (μg/L as Ag)	Dissolved strontium (μg/L as Sr)	Dissolved zinc (μg/L as Zn)	Suspended recoverable zinc (μg/L as Zn)
					During Construction							
G-3062	Nov. 20, 1974	—	—	—	—	—	—	—	—	—	—	—
G-3061	Dec. 04, 1974	—	—	—	—	—	—	—	—	—	—	—
					During First Injection							
G-3061	July 22, 1975	20	<10	2	ND	4	4	ND	—	940	<20	0
S-3000	July 22, 1975	20	<10	2	ND	4	4	ND	—	940	<20	0
G-3062	Aug. 04, 1975	<10	4	<1	ND	—	ND	ND	—	7,800	<20	20
					During First Recovery							
G-3061	Sept. 16, 1975	30	20	<1	ND	0	ND	ND	—	1,000	4	20
	Sept. 23, 1975	30	20	<1	ND	0	ND	—	—	1,600	20	0
	Sept. 30, 1975	30	<10	<1	ND	3	3	—	—	2,000	40	30
	Oct. 15, 1975	30	30	<1	ND	5	5	—	—	4,500	20	0
					During Second Injection							
G-3061	Mar. 04, 1976	<10	<10	<1	2	0	2	—	—	780	<20	30
S-3000	Mar. 04, 1976	<10	<10	<1	2	0	2	—	—	780	<20	30
					During Second Recovery							
G-3061	May 03, 1976	—	—	—	—	—	—	—	—	960	—	—
	May 25, 1976	<10	<10	<1	ND	10	10	—	—	1,400	ND	30
	July 19, 1976	20	<10	<1	ND	4	4	ND	ND	4,400	<20	50
G-3062	July 19, 1976	—	—	—	—	—	—	—	—	3,700	—	—
	July 19, 1976	—	—	—	—	—	—	—	—	7,800	—	—
	July 19, 1976	—	—	—	—	—	—	—	—	8,300	—	—
	July 19, 1976	—	—	—	—	—	—	—	—	8,000	—	—
	July 19, 1976	—	—	—	—	—	—	—	—	8,200	—	—
	July 19, 1976	—	—	—	—	—	—	—	—	7,900	—	—
	July 19, 1976	—	—	—	—	—	—	—	—	7,200	—	—
					During Third Injection							
G-3061	Jan. 18, 1977	—	—	—	—	—	—	—	—	900	—	—
S-3000	Jan. 18, 1977	—	—	—	—	—	—	—	—	900	—	—
G-3062	Jan. 18, 1977	—	—	—	—	—	—	—	—	5,100	—	—
	Jan. 18, 1977	—	—	—	—	—	—	—	—	4,500	—	—
	Jan. 18, 1977	—	—	—	—	—	—	—	—	2,800	—	—
	Jan. 18, 1977	—	—	—	—	—	—	—	—	3,100	—	—
	Jan. 18, 1977	—	—	—	—	—	—	—	—	3,700	—	—
	Jan. 18, 1977	—	—	—	—	—	—	—	—	3,200	—	—
	Jan. 18, 1977	—	—	—	—	—	—	—	—	4,400	—	—
					During Third Recovery							
G-3061	July 18, 1977	—	—	—	—	—	—	—	—	1,000	—	—
	July 17, 1979	—	—	—	—	—	—	—	—	9,000	—	—
G-3062	July 17, 1979	—	—	—	—	—	—	—	—	9,000	—	—
	July 17, 1979	—	—	—	—	—	—	—	—	10,000	—	—
	July 17, 1979	—	—	—	—	—	—	—	—	10,000	—	—
	July 17, 1979	—	—	—	—	—	—	—	—	10,000	—	—
	July 17, 1979	—	—	—	—	—	—	—	—	10,000	—	—
	July 17, 1979	—	—	—	—	—	—	—	—	10,000	—	—
	July 18, 1979	—	—	—	—	—	—	—	—	8,000	—	—

Well	Date	Total recoverable zinc (µg/L as Zn)	Total recoverable aluminum (µg/L as Al)	Dissolved aluminum (µg/L as Al)	Suspended recoverable aluminum (µg/L as Al)	Dissolved selenium (µg/L as Se)	Total suspended selenium (µg/L as Se)	Total selenium (µg/L as Se)	Coliforms per 100 mL			Total phenols (µg/L)
									Total coliform	Fecal coliform	Fecal streptococci	
During Construction												
G-3062	Nov. 20, 1974	ND	--	--	--	--	--	--	<2	<2	<2	--
G-3061	Dec. 04, 1974	100	--	--	--	--	--	--	<2	<1	<1	--
During First Injection												
G-3061	July 22, 1975	<20	30	<100	30	<1	0	<1	<2	<1	<1	0
S-3000	July 22, 1975	<20	30	<100	30	<1	0	<1	<2	<1	<1	0
G-3062	Aug. 04, 1975	30	20	9	10	<1	0	<1	--	--	--	0
During First Recovery												
G-3061	Sept. 16, 1975	20	<100	<100	0	<1	0	<1	<1	<1	<2	2
	Sept. 23, 1975	20	60	30	30	<1	0	<1	<1	<1	<2	0
	Sept. 30, 1975	70	10	<100	10	<1	0	<1	--	--	--	1
	Oct. 15, 1975	20	50	20	30	<1	0	<1	--	--	--	1
During Second Injection												
G-3061	Mar. 04, 1976	40	10	10	0	<1	0	<1	--	--	--	1
S-3000	Mar. 04, 1976	40	10	10	0	<1	0	<1	--	--	--	1
During Second Recovery												
G-3061	May 03, 1976	--	--	--	--	--	--	--	--	--	--	--
	May 25, 1976	30	10	10	0	<1	--	2	--	--	--	1
	July 19, 1976	60	50	20	30	<1	0	<1	<1	<1	<1	4
G-3062	July 19, 1976	--	--	--	--	--	--	--	--	--	--	--
	July 19, 1976	--	--	--	--	--	--	--	--	--	--	--
	July 19, 1976	--	--	--	--	--	--	--	--	--	--	--
	July 19, 1976	--	--	--	--	--	--	--	--	--	--	--
	July 19, 1976	--	--	--	--	--	--	--	--	--	--	--
	July 19, 1976	--	--	--	--	--	--	--	--	--	--	--
	July 19, 1976	--	--	--	--	--	--	--	--	--	--	--
During Third Injection												
G-3061	Jan. 18, 1977	--	--	--	--	--	--	--	--	--	--	0
S-3000	Jan. 18, 1977	--	--	--	--	--	--	--	--	--	--	0
G-3062	Jan. 18, 1977	--	--	--	--	--	--	--	--	--	--	--
	Jan. 18, 1977	--	--	--	--	--	--	--	--	--	--	--
	Jan. 18, 1977	--	--	--	--	--	--	--	--	--	--	--
	Jan. 18, 1977	--	--	--	--	--	--	--	--	--	--	--
	Jan. 18, 1977	--	--	--	--	--	--	--	--	--	--	--
	Jan. 18, 1977	--	--	--	--	--	--	--	--	--	--	--
	Jan. 18, 1977	--	--	--	--	--	--	--	--	--	--	--
During Third Recovery												
G-3061	July 18, 1977	--	--	--	--	--	--	--	--	--	--	--
	July 17, 1979	--	--	--	--	--	--	--	--	--	--	--
G-3062	July 17, 1979	--	--	--	--	--	--	--	--	--	--	--
	July 17, 1979	--	--	--	--	--	--	--	--	--	--	--
	July 17, 1979	--	--	--	--	--	--	--	--	--	--	--
	July 17, 1979	--	--	--	--	--	--	--	--	--	--	--
	July 17, 1979	--	--	--	--	--	--	--	--	--	--	--
	July 17, 1979	--	--	--	--	--	--	--	--	--	--	--
	July 18, 1979	--	--	--	--	--	--	--	--	--	--	--

Well	Date	Methylene blue active substance (mg/L)	Total polychlorinated naphthalenes (µg/L)	Total aldrin (µg/L)	Total lindane (µg/L)	Total chlordane (µg/L)	Total DDD (µg/L)	Total DDE (µg/L)	Total DDT (µg/L)	Total dieldrin (µg/L)	Endrin water unfiltered (µg/L)	Total ethion (µg/L)
					During Construction							
G-3062	Nov. 20, 1974	—	—	—	—	—	—	—	—	—	—	—
G-3061	Dec. 04, 1974	—	—	—	—	—	—	—	—	—	—	—
					During First Injection							
G-3061	July 22, 1975	0.0	—	0.0	0.0	0	0.0	0.0	0.0	0.0	0.0	—
S-3000	July 22, 1975	.0	—	.0	.0	0	.0	.0	.0	.0	.0	—
G-3062	Aug. 04, 1975	.1	0.0	.0	.0	0	.0	.0	.0	.0	.0	—
					During First Recovery							
G-3061	Sept. 16, 1975	.0	—	—	—	—	—	—	—	—	—	—
	Sept. 23, 1975	.0	—	—	—	—	—	—	—	—	—	—
	Sept. 30, 1975	.2	—	—	—	—	—	—	—	—	—	—
	Oct. 15, 1975	.0	—	—	—	—	—	—	—	—	—	—
					During Second Injection							
G-3061	Mar. 04, 1976	.0	—	—	—	—	—	—	—	—	—	—
S-3000	Mar. 04, 1976	.0	—	—	—	—	—	—	—	—	—	—
					During Second Recovery							
G-3061	May 03, 1976	—	—	—	—	—	—	—	—	—	—	—
	May 25, 1976	.1	.0	.0	.0	0	.0	.0	.0	.0	.0	—
	July 19, 1976	.1	.0	.0	.0	0	.0	.0	.0	.0	.0	0.0
G-3062	July 19, 1976	—	—	—	—	—	—	—	—	—	—	—
	July 19, 1976	—	—	—	—	—	—	—	—	—	—	—
	July 19, 1976	—	—	—	—	—	—	—	—	—	—	—
	July 19, 1976	—	—	—	—	—	—	—	—	—	—	—
	July 19, 1976	—	—	—	—	—	—	—	—	—	—	—
	July 19, 1976	—	—	—	—	—	—	—	—	—	—	—
	July 19, 1976	—	—	—	—	—	—	—	—	—	—	—
					During Third Injection							
G-3061	Jan. 18, 1977	.1	—	—	—	—	—	—	—	—	—	—
S-3000	Jan. 18, 1977	.1	—	—	—	—	—	—	—	—	—	—
G-3062	Jan. 18, 1977	—	—	—	—	—	—	—	—	—	—	—
	Jan. 18, 1977	—	—	—	—	—	—	—	—	—	—	—
	Jan. 18, 1977	—	—	—	—	—	—	—	—	—	—	—
	Jan. 18, 1977	—	—	—	—	—	—	—	—	—	—	—
	Jan. 18, 1977	—	—	—	—	—	—	—	—	—	—	—
	Jan. 18, 1977	—	—	—	—	—	—	—	—	—	—	—
	Jan. 18, 1977	—	—	—	—	—	—	—	—	—	—	—
					During Third Recovery							
G-3061	July 18, 1977	—	—	—	—	—	—	—	—	—	—	—
	July 17, 1979	—	—	—	—	—	—	—	—	—	—	—
G-3062	July 17, 1979	—	—	—	—	—	—	—	—	—	—	—
	July 17, 1979	—	—	—	—	—	—	—	—	—	—	—
	July 17, 1979	—	—	—	—	—	—	—	—	—	—	—
	July 17, 1979	—	—	—	—	—	—	—	—	—	—	—
	July 17, 1979	—	—	—	—	—	—	—	—	—	—	—
	July 17, 1979	—	—	—	—	—	—	—	—	—	—	—
	July 18, 1979	—	—	—	—	—	—	—	—	—	—	—

Well	Date	Total toxaphene (µg/L)	Total heptachloride (µg/L)	Total heptachloride epoxide (µg/L)	Total polychloride biphenyls (µg/L)	Total malathion (µg/L)	Total parathion (µg/L)	Total diazinon (µg/L)	Total methyl parathion (µg/L)	Total 2,4-D (µg/L)	Total 2,4,5-T (µg/L)	Total silvex (µg/L)
During Construction												
G-3062	Nov. 20, 1974	—	—	—	—	—	—	—	—	—	—	—
G-3061	Dec. 04, 1974	—	—	—	—	—	—	—	—	—	—	—
During First Injection												
G-3061	July 22, 1975	0	0.0	0.0	0	—	—	—	—	0.0	0.0	0.0
S-3000	July 22, 1975	0	.0	.0	0	—	—	—	—	.0	.0	.0
G-3062	Aug. 04, 1975	0	.0	.0	0	—	—	—	—	.0	.0	.0
During First Recovery												
G-3061	Sept. 16, 1975	—	—	—	—	—	—	—	—	—	—	—
	Sept. 23, 1975	—	—	—	—	—	—	—	—	—	—	—
	Sept. 30, 1975	—	—	—	—	—	—	—	—	—	—	—
	Oct. 15, 1975	—	—	—	—	—	—	—	—	—	—	—
During Second Injection												
G-3061	Mar. 04, 1976	—	—	—	—	—	—	—	—	—	—	—
S-3000	Mar. 04, 1976	—	—	—	—	—	—	—	—	—	—	—
During Second Recovery												
G-3061	May 03, 1976	—	—	—	—	—	—	—	—	—	—	—
	May 25, 1976	0	.0	.0	0	—	—	—	—	.0	.0	.0
	July 19, 1976	0	.0	.0	0	0.0	0.0	0.0	0.0	.0	.0	.0
G-3062	July 19, 1976	—	—	—	—	—	—	—	—	—	—	—
	July 19, 1976	—	—	—	—	—	—	—	—	—	—	—
	July 19, 1976	—	—	—	—	—	—	—	—	—	—	—
	July 19, 1976	—	—	—	—	—	—	—	—	—	—	—
	July 19, 1976	—	—	—	—	—	—	—	—	—	—	—
	July 19, 1976	—	—	—	—	—	—	—	—	—	—	—
	July 19, 1976	—	—	—	—	—	—	—	—	—	—	—
During Third Injection												
G-3061	Jan. 18, 1977	—	—	—	—	—	—	—	—	—	—	—
S-3000	Jan. 18, 1977	—	—	—	—	—	—	—	—	—	—	—
G-3062	Jan. 18, 1977	—	—	—	—	—	—	—	—	—	—	—
	Jan. 18, 1977	—	—	—	—	—	—	—	—	—	—	—
	Jan. 18, 1977	—	—	—	—	—	—	—	—	—	—	—
	Jan. 18, 1977	—	—	—	—	—	—	—	—	—	—	—
	Jan. 18, 1977	—	—	—	—	—	—	—	—	—	—	—
	Jan. 18, 1977	—	—	—	—	—	—	—	—	—	—	—
	Jan. 18, 1977	—	—	—	—	—	—	—	—	—	—	—
During Third Recovery												
G-3061	July 18, 1977	—	—	—	—	—	—	—	—	—	—	—
	July 17, 1979	—	—	—	—	—	—	—	—	—	—	—
G-3062	July 17, 1979	—	—	—	—	—	—	—	—	—	—	—
	July 17, 1979	—	—	—	—	—	—	—	—	—	—	—
	July 17, 1979	—	—	—	—	—	—	—	—	—	—	—
	July 17, 1979	—	—	—	—	—	—	—	—	—	—	—
	July 17, 1979	—	—	—	—	—	—	—	—	—	—	—
	July 17, 1979	—	—	—	—	—	—	—	—	—	—	—
	July 18, 1979	—	—	—	—	—	—	—	—	—	—	—

Well	Date	Total trithion (µg/L)	Total methyl trithion (µg/L)	Total suspended solids, residue at 110 degrees Celsius	Dissolved solids, residue at 180 degrees Celsius	Dissolved solids, sum of constituents (mg/L)	Dissolved solids (tons/acre-ft)	Total ortho phosphorus (mg/L as P)	Density (g/mL at 20 degrees Celsius)	Acidity (mg/L as H)	Dissolved ammonia nitrogen (mg/L as NH$_4$)	Dissolved nitrate nitrogen (mg/L as NO$_3$)
					During Construction							
G-3062	Nov. 20, 1974	—	—	0	2,830	2,710	3.85	0.01	—	—	—	—
G-3061	Dec. 04, 1974	—	—	0	2,920	2,740	3.97	0.01	—	—	—	—
					During First Injection							
G-3061	July 22, 1975	—	—	—	408	373	.55	.03	0.999	—	—	—
S-3000	July 22, 1975	—	—	—	408	373	.55	.03	.999	—	—	—
G-3062	Aug. 04, 1975	—	—	—	2,450	2,660	3.33	.01	—	0.1	—	—
					During First Recovery							
G-3061	Sept. 16, 1975	—	—	1	440	453	.60	.02	—	.6	—	—
	Sept. 23, 1975	—	—	—	540	498	.73	<.01	—	1.0	—	—
	Sept. 30, 1975	—	—	1	646	599	.88	.02	—	.8	—	—
	Oct. 15, 1975	—	—	2	892	854	1.21	.01	—	.8	—	—
					During Second Injection							
G-3061	Mar. 04, 1976	—	—	1	400	370	.54	.03	—	2.9	0.73	0.0
S-3000	Mar. 04, 1976	—	—	1	400	370	.54	.03	—	2.9	.73	.0
					During Second Recovery							
G-3061	May 03, 1976	—	—	—	399	359	.54	.02	—	—	—	—
	May 25, 1976	—	—	1	520	495	.71	.01	—	1.1	.64	.0
	July 19, 1976	0.0	0.0	—	1,080	1,070	1.47	.01	—	—	—	—
G-3062	July 19, 1976	—	—	—	4,880	4,900	6.64	—	—	—	—	—
	July 19, 1976	—	—	—	1,830	1,790	2.49	—	—	—	—	—
	July 19, 1976	—	—	—	1,830	1,820	2.49	—	—	—	—	—
	July 19, 1976	—	—	—	1,690	1,620	2.30	—	—	—	—	—
	July 19, 1976	—	—	—	1,560	1,510	2.12	—	—	—	—	—
	July 19, 1976	—	—	—	1,770	1,750	2.41	—	—	—	—	—
	July 19, 1976	—	—	—	2,010	1,980	2.73	—	—	—	—	—
					During Third Injection							
G-3061	Jan. 18, 1977	—	—	—	409	379	.56	.02	—	—	—	—
S-3000	Jan. 18, 1977	—	—	—	409	379	.56	.02	—	—	—	—
G-3062	Jan. 18, 1977	—	—	—	633	633	.86	<.01	—	—	—	—
	Jan. 18, 1977	—	—	—	410	431	.56	<.01	—	—	—	—
	Jan. 18, 1977	—	—	—	412	419	.56	<.01	—	—	—	—
	Jan. 18, 1977	—	—	—	518	562	.70	<.01	—	—	—	—
	Jan. 18, 1977	—	—	—	755	798	1.03	<.01	—	—	—	—
	Jan. 18, 1977	—	—	—	604	616	.82	<.01	—	—	—	—
	Jan. 18, 1977	—	—	—	3,780	3,870	5.14	<.01	—	—	—	—
					During Third Recovery							
G-3061	July 18, 1977	—	—	13	378	378	.51	.02	—	—	—	—
	July 17, 1979	—	—	—	2,640	2,370	3.59	.01	—	—	—	—
G-3062	July 17, 1979	—	—	—	2,900	2,590	3.94	.01	—	—	—	—
	July 17, 1979	—	—	—	2,680	2,510	3.64	.01	—	—	—	—
	July 17, 1979	—	—	—	2,670	2,400	3.63	.01	—	—	—	—
	July 17, 1979	—	—	—	2,550	2,390	3.47	.01	—	—	—	—
	July 17, 1979	—	—	—	2,760	2,570	3.75	.01	—	—	—	—
	July 17, 1979	—	—	—	2,750	2,570	3.74	<.01	—	—	—	—
	July 18, 1979	—	—	—	4,730	4,980	6.53	<.01	—	—	—	—

Well	Date	Dissolved nitrite nitrogen (mg/L as NO$_2$)	Total hydrogen sulfide (mg/L as H$_2$S)	Total nitrogen (mg/L as NO$_3$)	Dissolved mercury (µg/L as Hg)	Suspended recoverable mercury (µg/L as Hg)	Total recoverable mercury (µg/L as Hg)	Elevation of land surface datum (feet above sea level)	Total depth of well (feet)	Specific gravity	Depth to top of sample interval (feet)	Depth to bottom of sample interval (feet)
				During Construction								
G-3062	Nov. 20, 1974	—	4.2	1.9	—	—	—	5.4	1,064	1.000	—	—
G-3061	Dec. 04, 1974	—	—	2.0	—	—	—	8.4	1,105	—	955	1,110
				During First Injection								
G-3061	July 22, 1975	—	—	6.0	<0.5	0	<0.5	8.4	1,105	.999	—	—
S-3000	July 22, 1975	—	—	6.0	<.5	0	<.5	—	106	.999	—	—
G-3062	Aug. 04, 1975	—	4.0	3.1	<.5	0	<.5	5.4	1,064	1.002	—	—
				During First Recovery								
G-3061	Sept. 16, 1975	—	3.0	5.4	<.5	0	<.5	8.4	1,105	1.001	—	—
	Sept. 23, 1975	—	3.2	4.9	<.5	.1	<.5	8.4	1,105	—	—	—
	Sept. 30, 1975	—	3.2	5.1	<.5	0	<.5	8.4	1,105	1.001	—	—
	Oct. 15, 1975	—	3.7	4.6	<.5	0	<.5	8.4	1,105	1.003	—	—
				During Second Injection								
G-3061	Mar. 04, 1976	0.03	.0	6.5	<.5	0	<.5	8.4	1,105	1.000	—	—
S-3000	Mar. 04, 1976	.03	.0	6.5	<.5	0	<.5	—	106	1.000	—	—
				During Second Recovery								
G-3061	May 03, 1976	—	—	6.2	—	—	—	8.4	1,105	—	—	—
	May 25, 1976	.00	7.7	6.7	<.5	0	<.5	8.4	1,105	1.001	—	—
	July 19, 1976	—	7.2	3.5	<.5	.5	.5	8.4	1,105	1.001	—	—
G-3062	July 19, 1976	—	—	—	—	—	—	5.4	1,064	—	—	—
	July 19, 1976	—	—	—	—	—	—	5.4	1,064	—	—	—
	July 19, 1976	—	—	—	—	—	—	5.4	1,064	—	—	—
	July 19, 1976	—	—	—	—	—	—	5.4	1,064	—	—	—
	July 19, 1976	—	—	—	—	—	—	5.4	1,064	—	—	—
	July 19, 1976	—	—	—	—	—	—	5.4	1,064	—	—	—
	July 19, 1976	—	—	—	—	—	—	5.4	1,064	—	—	—
				During Third Injection								
G-3061	Jan. 18, 1977	—	0	5.5	—	—	—	8.4	1,105	—	—	—
S-3000	Jan. 18, 1977	—	0	5.5	—	—	—	8.4	106	—	—	—
G-3062	Jan. 18, 1977	—	5.4	3.5	—	—	—	5.4	1,064	—	—	—
	Jan. 18, 1977	—	6.4	3.6	—	—	—	5.4	1,064	—	—	—
	Jan. 18, 1977	—	3.5	4.3	—	—	—	5.4	1,064	—	—	—
	Jan. 18, 1977	—	4.2	4.3	—	—	—	5.4	1,064	—	—	—
	Jan. 18, 1977	—	4.8	4.3	—	—	—	5.4	1,064	—	—	—
	Jan. 18, 1977	—	1.6	3.2	—	—	—	5.4	1,064	—	—	—
	Jan. 18, 1977	—	2.2	3.6	—	—	—	5.4	1,064	—	—	—
				During Third Recovery								
G-3061	July 18, 1977	—	—	6.3	—	—	—	8.4	1,105	1.000	—	—
	July 17, 1979	—	—	4.9	—	—	—	8.4	1,105	—	—	—
G-3062	July 17, 1979	—	—	5.0	—	—	—	5.4	1,064	—	—	—
	July 17, 1979	—	—	5.0	—	—	—	5.4	1,064	—	—	—
	July 17, 1979	—	—	3.8	—	—	—	5.4	1,064	—	—	—
	July 17, 1979	—	—	3.9	—	—	—	5.4	1,064	—	—	—
	July 17, 1979	—	—	4.2	—	—	—	5.4	1,064	—	—	—
	July 17, 1979	—	—	4.2	—	—	—	5.4	1,064	—	—	—
	July 18, 1979	—	—	8.3	—	—	—	5.4	1,064	—	—	—

SELECTED SERIES OF U.S. GEOLOGICAL SURVEY PUBLICATIONS

Periodicals

Earthquakes & Volcanoes (issued bimonthly).
Preliminary Determination of Epicenters (issued monthly).

Technical Books and Reports

Professional Papers are mainly comprehensive scientific reports of wide and lasting interest and importance to professional scientists and engineers. Included are reports on the results of resource studies and of topographic, hydrologic, and geologic investigations. They also include collections of related papers addressing different aspects of a single scientific topic.

Bulletins contain significant data and interpretations that are of lasting scientific interest but are generally more limited in scope or geographic coverage than Professional Papers. They include the results of resource studies and of geologic and topographic investigations, as well as collections of short papers related to a specific topic.

Water-Supply Papers are comprehensive reports that present significant interpretive results of hydrologic investigations of wide interest to professional geologists, hydrologists, and engineers. The series covers investigations in all phases of hydrology, including hydrogeology, availability of water, quality of water, and use of water.

Circulars present administrative information or important scientific information of wide popular interest in a format designed for distribution at no cost to the public. Information is usually of short-term interest.

Water-Resources Investigations Reports are papers of an interpretive nature made available to the public outside the formal USGS publications series. Copies are reproduced on request unlike formal USGS publications, and they are also available for public inspection at depositories indicated in USGS catalogs.

Open-File Reports include unpublished manuscript reports, maps, and other material that are made available for public consultation at depositories. They are a nonpermanent form of publication that may be cited in other publications as sources of information.

Maps

Geologic Quadrangle Maps are multicolor geologic maps on topographic bases in 7.5- or 15-minute quadrangle formats (scales mainly 1:24,000 or 1:62,500) showing bedrock, surficial, or engineering geology. Maps generally include brief texts; some maps include structure and columnar sections only.

Geophysical Investigations Maps are on topographic or planimetric bases at various scales; they show results of surveys using geophysical techniques, such as gravity, magnetic, seismic, or radioactivity, which reflect subsurface structures that are of economic or geologic significance. Many maps include correlations with the geology.

Miscellaneous Investigations Series Maps are on planimetric or topographic bases of regular and irregular areas at various scales; they present a wide variety of format and subject matter. The series also includes 7.5-minute quadrangle photogeologic maps on planimetric bases that show geology as interpreted from aerial photographs. Series also includes maps of Mars and the Moon.

Cost Investigations Maps are geologic maps on topographic or planimetric bases at various scales showing bedrock or surficial geology, stratigraphy, and structural relations in certain coal-resource areas.

Oil and Gas Investigations Charts show stratigraphic information for certain oil and gas fields and other areas having petroleum potential.

Miscellaneous Field Studies Maps are multicolor or black-and-white maps on topographic or planimetric bases for quadrangle or irregular areas at various scales. Pre-1971 maps show bedrock geology in relation to specific mining or mineral-deposit problems; post-1971 maps are primarily black-and-white maps on various subjects such as environmental studies or wilderness mineral investigations.

Hydrologic Investigations Atlases are multicolored or black-and-white maps on topographic or planimetric bases presenting a wide range of geohydrologic data of both regular and irregular areas; principal scale is 1:24,000, and regional studies are at 1:250,000 scale or smaller.

Catalogs

Permanent catalogs, as well as some others, giving comprehensive listings of U.S. Geological Survey publications are available under the conditions indicated below from the U.S. Geological Survey, Map Distribution, Box 25286, Bldg. 810, Federal Center, Denver, CO 80225. (See latest Price and Availability List.)

"Publications of the Geological Survey, 1879–1961" may be purchased by mail and over the counter in paperback book form and as a set of microfiche.

"Publications of the Geological Survey, 1962–1970" may be purchased by mail and over the counter in paperback book form and as a set of microfiche.

"Publications of the U.S. Geological Survey, 1971–1981" may be purchased by mail and over the counter in paperback book form (two volumes, publications listing and index) and as a set of microfiche.

Supplements for 1982, 1983, 1984, 1985, 1986, and for subsequent years since the last permanent catalog may be purchased by mail and over the counter in paperback book form.

State catalogs, "List of U.S. Geological Survey Geologic and Water-Supply Reports and Maps For (State)," may be purchased by mail and over the counter in paperback booklet form only.

"Price and Availability List of U.S. Geological Survey Publications," issued annually, is available free of charge in paperback booklet form only.

Selected copies of a monthly catalog "New Publications of the U.S. Geological Survey" are available free of charge by mail or may be obtained over the counter in paperback booklet form only. Those wishing a free subscription to the monthly catalog "New Publications of the U.S. Geological Survey" should write to the U.S. Geological Survey, 582 National Center, Reston, VA 22092.

Note.—Prices of Government publications listed in older catalogs, announcements, and publications may be incorrect. Therefore, the prices charged may differ from the prices in catalogs, announcements, and publications.